

UNIVERSITÀ
DEGLI STUDI
FIRENZE

Università degli Studi di Firenze
Dipartimento di Ingegneria dell'Informazione (DINFO)
Corso di Dottorato in Ingegneria dell'Informazione
Curriculum: Telecommunication (ING-INF/03)

Advanced Position Fixing and Dead Reckoning Techniques: Cooperative GPS Positioning and Context-aware Pedestrian Dead Reckoning

Candidate
Alessio Martinelli

Supervisors
Prof. Enrico Del Re

Dr. Simone Morosi

PhD Coordinator
Prof. Luigi Chisci

ciclo XXIX, 2014-2016

Università degli Studi di Firenze, Dipartimento di Ingegneria dell'Informazione (DINFO).

Thesis submitted in partial fulfillment of the requirements for the degree of Doctor of Philosophy in Information Engineering. Copyright © 2017 by Alessio Martinelli.

Acknowledgments

I would like to thank my supervisors, Dr. Simone Morosi and Prof. Enrico Del Re, for their guidance and expertise. I would also like to thank my present and past colleagues at the Signal Processing and Communications Laboratory (LESC): Eng. Marco Dolfi, Dr. Massimiliano Biagini, Dr. Pierpaolo Piunti, Dr. Sara Jayousi, and Dr. Renato Pucci, for their support and motivation. Special thanks to my friend and colleague, Eng. Patrizio Marcocci, for his generous and precious support during this work.
I would also like to thank Dr Pauld Groves for his outstanding support and kind hospitality during my visiting period at the Department of Civil, Environmental and Geomatic Engineering of the University College London (UCL). I am grateful to Han Gao for his collaboration during my stay at UCL.
Finally, huge thanks to my wonderful girlfriend, Claudia del Tongo, for been amazing, and to my parents, Flora Carlini and Ennio Martinelli, and brother Maurizio Martinelli, for their love and support over the years.

Contents

Contents **v**

1 Introduction **1**
1.1 The objectives 2
1.2 Contributions 2

2 Position Fixing **5**
2.1 Introduction 5
2.2 Radio Positioning Configurations and Methods 6
2.2.1 Self-Positioning and Remote Positioning 6
2.2.2 Relative Positioning 6
2.2.3 Ranging 6
2.2.4 Angular Positioning 11
2.2.5 Proximity 11
2.2.6 Pattern Matching 12
2.3 Global Navigation Satellite Systems 14
2.3.1 Global Positioning System 14
2.3.2 GLONASS 15
2.3.3 Beidou 16
2.3.4 Galileo 17
2.4 Environmental Feature matching 18
2.4.1 Map Matching 19
2.4.2 Terrain-referenced Navigation 19
2.4.3 Image-based Navigation 20

3 Global Positioning System **21**
3.1 Introduction . . . 21
3.2 GPS Modernization . . . 22
3.3 GPS Positioning Method . . . 23
3.4 GPS Signals . . . 25
3.4.1 Carrier Frequencies on L-band . . . 25
3.4.2 PRN Codes . . . 27
3.4.3 Navigation Data . . . 28
3.5 Code Phase Measurements . . . 29
3.6 GPS Time . . . 31
3.7 Coordinate Frames . . . 31
3.7.1 Earth-Centered Inertial Frame . . . 32
3.7.2 Earth-Centered Earth-Fixed Frame . . . 32
3.7.3 Local Navigation Frame . . . 32
3.7.4 World Geodetic System 1984 . . . 33
3.8 Error Sources and Models . . . 35
3.8.1 User Range Error and Dilution of Precision . . . 35
3.9 GPS Receiver . . . 37
3.10 Differential and Assisted GPS . . . 40
3.10.1 Differential GPS . . . 40
3.10.2 Assisted GPS . . . 40

4 Peer-to-Peer Cooperation for GPS Positioning **43**
4.1 Introduction . . . 43
4.2 Cooperative positioning: state of the art . . . 45
4.3 P2P GPS Cooperative Positioning Algorithm . . . 47
4.4 Acquisition procedure: Sensitivity vs Complexity trade-off . . . 51
4.4.1 Stand-alone Positioning . . . 52
4.4.2 Peer-to-Peer Cooperative Positioning . . . 53
4.5 Time Synchronization . . . 56
4.6 Experimental Setup . . . 58
4.7 Experimental Result . . . 59
4.7.1 Satellite signal acquisition assessment . . . 59
4.7.2 Computational load assessment in the signal acquisition procedure . . . 67
4.7.3 Performance assessment: position accuracy and Time-to-First Fix . . . 69
4.8 Conclusion . . . 72

5 Dead Reckoning **73**
5.1 Introduction 73
5.2 Distance measurement 74
5.3 Attitude measurement 76
5.4 Height and Depth Measurements 79

6 Probabilistic Context-aware Step Length Estimation for Pedestrian Dead Reckoning **81**
6.1 Introduction 82
6.2 Backgound and Related Work 83
6.3 Proposed method and Dataset 85
6.4 Step Detection 87
6.5 Step mode and Context Classification 93
6.5.1 Feature Extraction 93
6.5.2 Step mode Classification 96
6.5.3 Context Classification 99
6.6 Step Length Estimation 101
6.6.1 Step Length k-parameters Calibration 101
6.6.2 Step Length Estimation Methods 104
6.7 Results and Discussion 109
6.7.1 Step Detection 109
6.7.2 Step Mode and Context Classification 109
6.7.3 Step Length Estimation 111
6.8 Conclusion 112

7 Conclusion **117**

A Publications **121**

Bibliography **123**

Chapter 1

Introduction

Nowadays, always more applications rely on positioning, such as location-based services (LBS), intelligent transportation systems (ITS), constructions, Earth science, machine control, surveillance, mapping, and navigation.
All navigation and positioning techniques are based on one of two fundamental methods: position fixing and dead reckoning. Position fixing aims to determine the position using external information such as signals or environmental features. Alternatively, dead reckoning measures the distance and direction traveled from a previous position to determine the current position.
One of the most popular signal-based positioning system using position fixing, is the Global Position System (GPS). The latter is one of the global navigation satellite systems (GNSS) available nowadays. The behaviour of these systems is remarkable when the line-of-sight between the satellites and the GNSS receiver is not disturbed. In harsh environments, such as dense urban canyons, light shadowing, or more generally when GNSS signals cannot be received with a sufficiently high signal-to-noise ratio (SNR) due to obstructions, the performance of GNSS declines.
Pedestrian navigation is one of the most challenging applications of navigation technology. Pedestrian dead reckoning is a promising solution for pedestrian navigation. It uses the signal that has been collected by sensors to detect steps and to estimate the step lengths. Step detection and step length estimation algorithms work relatively well when walking in a straight line; however, real paths include turns, sidesteps, stairs, variations in speed, and various actions performed by the subject. These all affect the step detection and the step length estimation, and must be considered to provide

an accurate estimate of the distance traveled during daily activities as well as laboratory tests.
Chapter 2 gives an overview of the position fixing techniques. Chapter 3 focuses on the GPS system and its main characteristics. Chapter 4 presents a peer-to-peer cooperative GPS positioning technique together with its performance assessment. Chapter 5 gives an overview of dead reckoning navigation. Chapter 6 proposes a weighted context-based step length estimation technique as a part of a pedestrian dead reckoning system, which comprises step detection, step mode classification, and context classification. Chapter 7 presents the conclusion of this thesis.

1.1 The objectives

This thesis involves both position fixing and dead reckoning methods, and defines an advanced technique for each one of these. In particular, a peer-to-peer cooperative GPS positioning technique is proposed to improve the performance of the GPS receiver, and a context-aware pedestrian dead reckoning system is presented to improve the pedestrian navigation solution.
The first objective of this thesis is to determine an acceptable position solution determined by the GPS receiver in light-indoor environments.
The second goal of this thesis is to speed up the position solution determination that is carried out by the GPS receiver in outdoor environments.
The third objective of this thesis is to improve the pedestrian dead reckoning navigation solution, by adopting effective techniques for step detection and step mode classification.
The fourth goal of this thesis is to improve the pedestrian dead reckoning navigation solution, by using a probabilistic approach for the step length estimation.

1.2 Contributions

The main contributions of this thesis are the following:

- Analysis and assessment of a peer-to-peer cooperative GPS positioning technique, in both outdoor-to-indoor and outdoor-to-outdoor scenarios, in presence of either fine or coarse time synchronization between the aided and aiding receivers.

- Development of a software-defined aided GPS receiver able to operate in a peer-to-peer cooperative configuration in both outdoor-to-indoor and outdoor-to-outdoor scenarios.
- Analysis and assessment of a pedestrian dead reckoning system which comprises the procedures of step detection, step mode classification, context classification, and step length estimation.
- Development of a context-aware pedestrian dead reckoning navigation system, which comprises the step detection, step mode classification, context classification, and step length estimation algorithms.

Chapter 2

Position Fixing

This chapter gives an overview of the position fixing techniques. The radio signal-based positioning techniques and configurations are defined. Afterwards, a brief description of the available and upcoming global navigation satellite systems is reported. Finally, the positoning fixing methods which rely on environmental feature matching are characterized.

2.1 Introduction

Position fixing methods rely on external information such as signals or environmental features to determine the user position [22]. Radio signals are the most frequently used in position fixing, even if other kind of signals such as acoustic [11,30], ultrasounds [25,59], optical [3] and infrared [72] are involved for particular scenarios. The user can infer its position by either estimating the distance from transmitters placed at know position or by matching the received signal power of the observed features with a predefined database which refers to the considered location. Environmental features such as roads, signs, buildings, terrain height, variations in magnetic and gravitational fields may be exploited by the navigation systems to constrain the user position to a particular location. In navigation scenario, position and location may assume different concepts and they are often interchangeable: position usually refers to the quantitative value of the actual position, i.e. user coordinate in a predefined coordinate system, while location mostly refers to the environmental context [22]. The relation between position and

environmental context can be exploited to improve the navigation solution.

2.2 Radio Positioning Configurations and Methods

2.2.1 Self-Positioning and Remote Positioning

Radio Positioning systems can be categorized as self-positioning or remote positioning depending on which device performs the distance measurements, as shown in Fig.2.1. A self positioning system involves a mobile user which determines its position by receiving the ranging signals from the transmitters placed at know position. These systems are suited for navigation applications for which the position information is required by the user whose position is being determined. When dealing with remote positioning systems, the mobile user transmits the ranging signals to the receivers placed at known location. In this case, the user position is computed by a master receiver. These techniques are suited for tracking application when the user position is required to a master unit. A self-positioning system which transmits the position information to a remote unit through a communication channel is named indirect remote-positioning system, while a remote positioning system which transmits the user position to the user itself is named indirect self-positioning system.

2.2.2 Relative Positioning

Relative positioning refers to a configuration in which the users are able to either receive or transmit signals in order to determine the relative positions from each other. The absolute position of the users can be determined by combining relative positioning with self-positioning or remote positioning.

2.2.3 Ranging

Positioning by ranging [22] aims to estimate the user position by measuring the distance from the user to landmarks placed at known location. In particular, the distance can be computed by considering two approaches: the first one is based on the time of flight (TOF), i.e. the time the signal takes to travel from the landmark to the user; the second one is based on the received signal strength (RSS). There are four type of ranging measurements

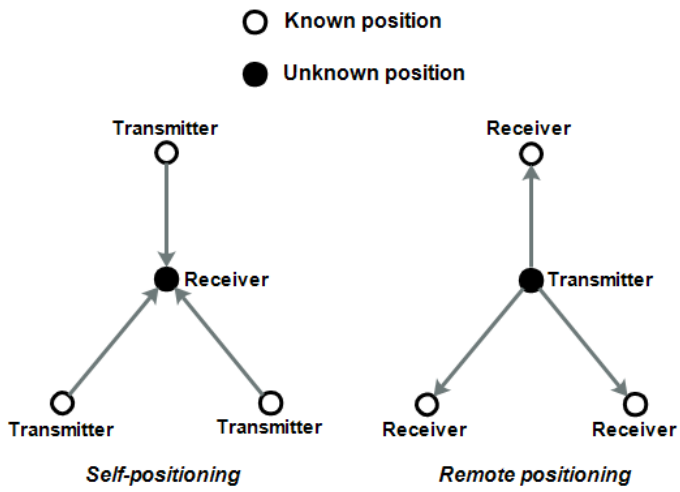


Figure 2.1: self-positioning and remote positioning configurations.

based on TOF principles: time of arrival (TOA), time difference of arrival (TDOA), double-differenced ranging (DDR) and two-way ranging. TOA and RSS ranging methods are described below.

Time of Arrival (TOA): This technique is based on the principle for which the distance between the user and the landmark is directly proporsional to the TOF of the signal. By assuming a self-positioning configuration, the landmark transmits an information packet containing the transmit time stamp to the user, which computes the difference between the receive time stamp and the local generated receive time stamp, as shown in Fig.2.2. The resulting time value is multiplied by the speed of light in vacuum to obtain the ranging estimate:

$$r = \tau * c = (t_R - t_T) * c, \tag{2.1}$$

where c is the speed of light, t_R is the reception time and t_T is the transmission time.
In a 2D scenario, the distance r from the landmark and the user corresponds to a circle equation such as:

$$r^{(k)} = \sqrt{(x^{(k)} - x)^2 + (y^{(k)} - y)^2} = \|\mathbf{x^{(k)}} - \mathbf{x}\|, \tag{2.2}$$

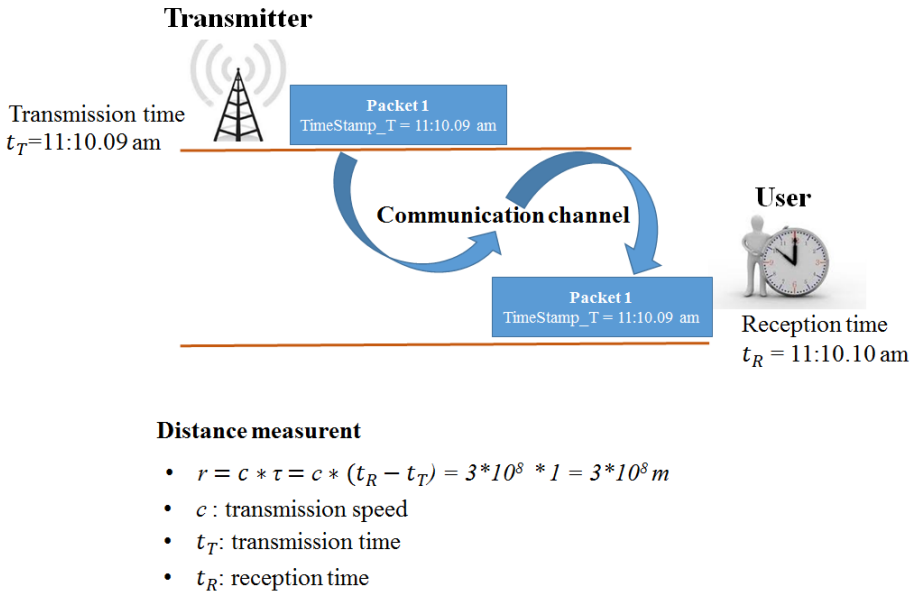


Figure 2.2: range measurements by TOF of the signal.

where $\mathbf{x^{(k)}}$ represents the known $(x^{(k)}, y^{(k)})$ coordinates of the k-th transmitter (landmark), while $\mathbf{x}$ represents the (x, y) coordinates of the user, which is the unknown of the navigation system. In a 2D scenario, the geometric interpretation of the user position is defined by the intersection of the circles generated by the the landmark-user distances. The intersection between two circles generally defines two points, resulting to a position ambiguity, as shown in Fig.2.3. Therefore, three transmitting landmarks are needed to univocally define the user position, as shown in Fig.2.3. However, the ambiguity can be eliminated by knowing some additional information: for example, the previous position or the maximum travelable distance between the previous and the current time can be used to constrain the estimate of the current user position.
Mathematically, the user position can be computed by solving for the system of equations in which each equation represents the ranging measurement in 2.2 and the total number of equations is equals to the number of available landmarks.

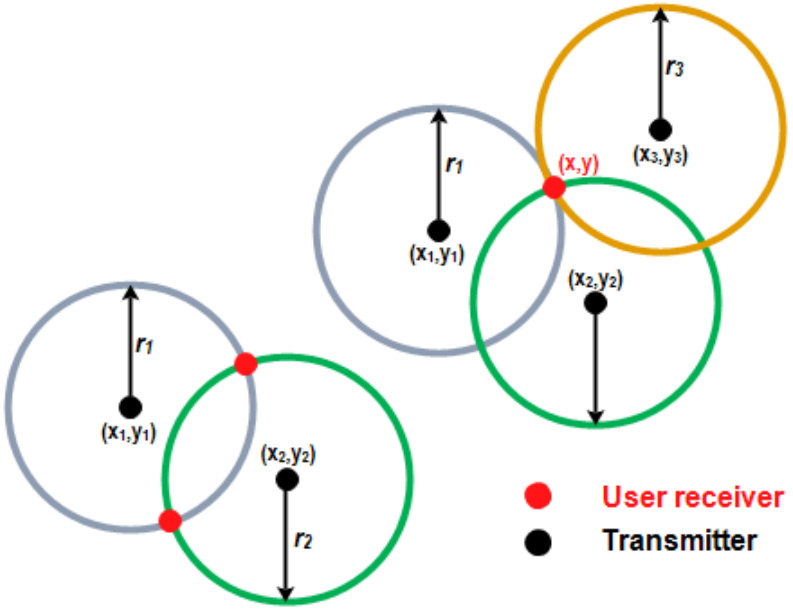


Figure 2.3: geometrical interpretation of the user position.

When dealing with TOF measurements, the time synchronization between the transmitter and the receiver is crucial. Assuming that the transmitters are synchronized with a reference time scale, the time error between the receiver and the transmitter clocks lead the equation 2.2 to be redefined as follows:

$$\rho_c^{(k)} = r^{(k)} + b = \|x^{(k)} - x\| + c * \delta t_R \tag{2.3}$$

where $\rho_c^{(k)}$ is the pseudorange relative to the k-th ranging measurement, b is the receiver clock bias and δt_R is the user time synchronization error which takes into account the time error between the reference time at which the transmitters are synchronized and the user clock. The user clock bias is an additional unknown to be solved together with the user coordinates; this leads to increase the number of transmitters needed to solve for the user position. The ranging measurement based on TOA can be very accurate when the user is located in an open space and the line-of-sight to the transmitters is not obstructed. On the contrary, in harsh environments such as indoor, the line-of-sight between the user and the transmitting landmarks

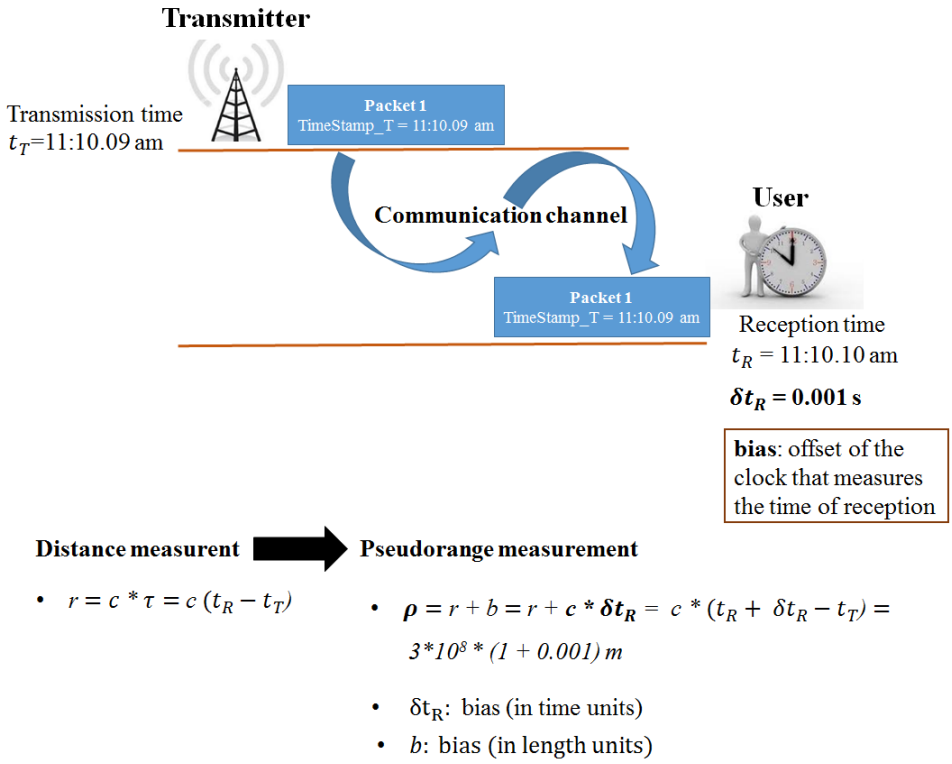


Figure 2.4: pseudorange measurements by TOF of the signal.

is often disturbed and the the multipath effects affect the accuracy of the TOF measurement. Moreover, assuming a self-positioning configuration, the transmitters must be time synchronized.

Recieved Signal Strength (RSS): The power of an electromagnetic wave travelling in free space is attenuated by a factor inversely proportionated to the square of the distance. This concept can be exploited to estimate the distance between a transmitter and a receiver by knowing the transmission power. Unfortunately, the real environment can be much more complicated than free space: obstacles are usually present between the transmitter and the receiver and they can change position over time by leading to

a time-varying communication channel. Furthermore, the receiving antenna can vary its direction over time, e.g. when using smartphone, so leading to a variation in the RSS by the user. For several environment, the signal pathloss can be estimated by empirical models which considers the frequency, the reception environment and the transmitting antenna height [20]. Assuming a self-positioning configuration, once the distance between the receiver and the transmitters have been determined, the user position can be computed solving for the system of ranging equations. The accuracy of the navigation solution based on RSS is typically lower than the one provided by TOF measurements; however, RSS method relieves the receiver to know the signal structure which is needed for the TOF methods and it can relies on signals which are not designed for navigation purposes, avoiding extra hardware for the ranging measurements. Moreover, the time synchronization between transmitters is not need in RSS ranging, while must be present for TOF measurements.

2.2.4 Angular Positioning

Angular positioning, also named as Angle of Arrival (AOA), aims to determine the user position by lines of sight from the user to the landmarks. By assuming a self-positioning, the signals transmitted by landmarks generate lines of position (LOP), as shown in Fig.2.5. The user receiver computes the angle of arrival of the transmitted signal with respect to a reference direction. In a 2D scenario, the user position can be determined by receiving signal from two landmarks and the angles of arrival can be computed with respect to the true north. In AOA positioning, the receiver has to be supplied with particular hardware, that is a directional antenna or arrays of antennas, to be capable of detecting the angle of arrival of the incoming signals. Harsh environments such as indoor can affect the angle of arrival determination due to the multipath effect, leading to a decreasing in the navigation solution performance.

2.2.5 Proximity

Proximity is the simplest form of radio positioning and provides a rough information about the user position. The latter, assuming a self-positioning configuration, is usually assigned to the position of the closest transmitter which position is known. The receiver does not need to know the structure

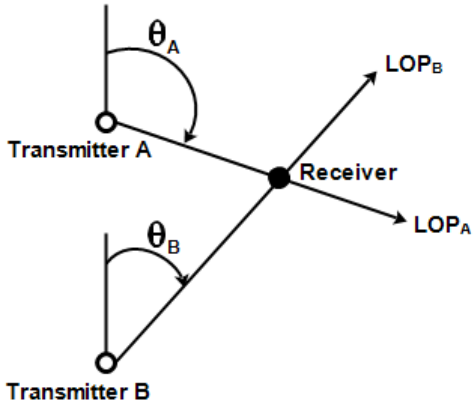


Figure 2.5: position determination by AOA in a 2D scenario.

of the received signals. The proximity approach can exploit signals from many communication technologies such as Wireless LAN, Radio frequency Identinfication (RFID), Bluetooth. Proximity positioning is often used in cellular networks as Cellular identification (Cell-ID) [8]: in this case, the user position is determined depending on the closest base station. A more sophisticated approach relies on the intersection of the coverage area of the transmitters: in this case, the user position is computed as the average of the position of the transmitters, as shown in Fig.2.6. Unfortunately, the transmitter coverage area is not perfectly circular; shadowing and multipath interference can modify the coverage boundaries and affect the navigation solution. Also the receiver antenna does not have a spherical radiation pattern and its rotation can affect the received signal strength.

2.2.6 Pattern Matching

Pattern matching aims to define the user position by comparing the received signal strength (RSS) information. It defines a two-phase procedure: the first one, also named off-line phase, aims to determine a collection of RSS measurements which refer to the location in which the user is supposed to perform the navigation routine. The second one, also named on-line phase, is the actual navigation procedure in which the user receiver compares the RSS measurements with the ones collected during the off-line phase. As the proximity positioning, pattern matching does not need to know the

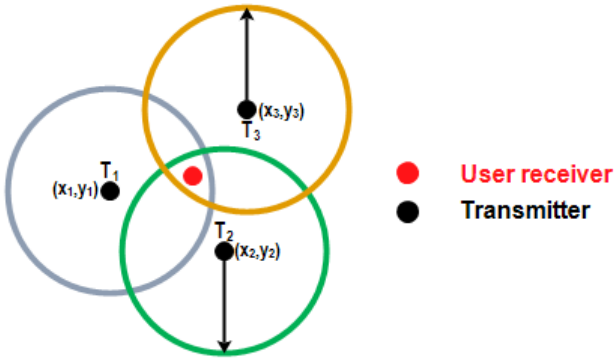


Figure 2.6: proximity positioning by the intersection of the coverage areas of the transmitters.

structure of the signal, but just the RSS, so it can exploit the combination of signals from different technology such as Wifi, Cellular network signal, and Bluetooth. In a self-positioning configuration, the user receiver compares the RSS with the RSS database and defines its position as the one with the closest RSS value. The RSS comparison is usually performed by considering the euclidean distance

$$d_S(x,y) = \sqrt{\frac{1}{m}\sum_{j=1}^{m}[\bar{S}_j - S_{D,j}(x,y)]^2}, \tag{2.4}$$

where (x,y) is the database-referenced candidate position, $\bar{S}_j$ is the RSS by the user receiver, $S_{D,j}(x,y)$ is the RSS at the database-referenced candidate position and m is the number of considered signals. The RSS database can be downloaded or preinstalled by the user receiver when it enters the operation area. The RSS map can vary with time due to time-varying communication channel and the signal availability. Therefore, some reference station can monitor the channel changings to improve the RSS map. When dealing with harsh environment, such as indoor, positioning by map matching usually provides better performance compared to similar positioning techniques such as RSS ranging and proximity.

2.3 Global Navigation Satellite Systems

Global Navigation Satellite System (GNSS) is a navigation system which provide 3D positioning solution by ranging measurements [22, 31, 48]. Satellites orbiting around the earth transmit ranging signals which are processed by a GNSS user receiver which computes the navigation solution, thus GNSS follows a self-positioning configuration. GNSS systems are designed to provide a global coverage and visibility to at least four satellite almost everytime and everywhere. At the moment, two fully operational GNSS systems are available: Global Satellite Positioning (GPS) which is owned and operated by the United states government and the russian GLONASS. Moreover, the upcoming european Galileo is being deployed, while a global version of the chinese Beidou is under development. A brief characterization of the cited GNSS systems is described in 2.3.1, 2.3.2, 2.3.3 and 2.3.4. The architecture of a GNSS system involves three segments: control segment, space segment, and user segment, as depicted in Fig.2.7. The Control Segment consists in a set of stations for monitoring, control and uplink communications with the satellites. The space segments involves the satellites, also known as Space Vehicles (SV), which aims to transmits ranging signals to the user receivers and the monitoring stations. The User segment refers to the user equipment which is the responsible to determine the navigation solution.

2.3.1 Global Positioning System

The United States government started to develop GPS in 1973 as a military GNSS system. The first operation satellites were launched in 1978 and the fully operational system was available in 1994. GPS provides two different positioning service: the standard positioning service (SPS), which is an open access service for civil usage, and the precise positioning pervice (PPS), which is a restricted service for military usage. Since the late 1990s, GPS is undergoing to a modernization process by introducing modern technologies throughout the space and the control segments in order to enhance the overall performance, as illustrated in Fig.2.8. The position solution accuracy depends on the environmental features and the atmosphere conditions; however, real-world data collected in 2014 from the Federal Aviation Administration (FAA) show that high-quality GPS SPS receivers provide an horizontal accuracy better than 3.5 meters [21]. The accuracy of the GPS signal in space is actually the same for both the civilian GPS service and

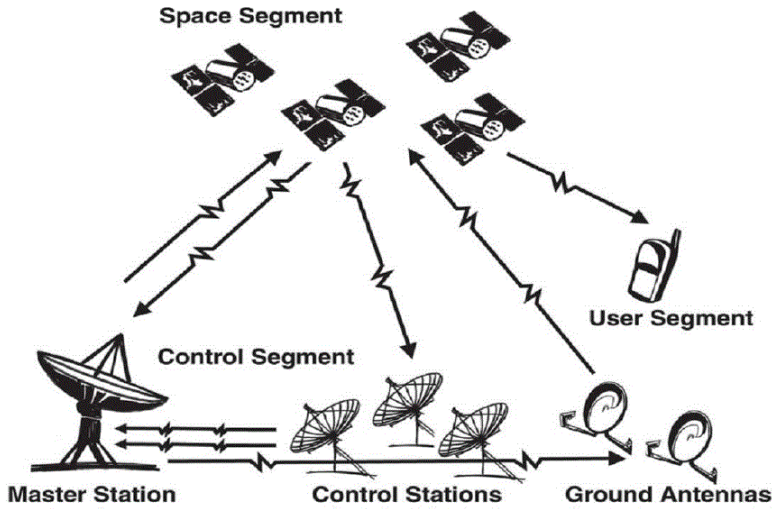


Figure 2.7: illustration of the GNSS segments: control segment, space segment, and user segment.

the military GPS service. However, SPS broadcasts on one frequency, while PPS uses two frequencies to enable ionospheric correction techniques, which allow to reduce the radio degradation caused by the Earth's atmosphere. With less degradation, PPS provides better accuracy than the basic SPS.

2.3.2 GLONASS

GLONASS was developed by USSR in the mid-1970s as a military navigation system, in parallel to GPS. It was designed to provide civil and military services and the first fully operational constellation was achieved in 1995. A Few years later, the number of operational satellites decayed, reaching 6 satellites in 2001. Then, an intense modernization process allowed a global 24-satellite constellation to be fully operational in 2011. The final satellites of the Glonass-K1 generation launched in 2014-2017 also include L3OC signal which is based on code-division multiple access (CDMA) as for the GPS signals. The Glonass-K1 satellite generation is intended to replace the fleet from 2018 until the next generation Glonass-K2 will be validated. The GLONASS satellites untill the Glonass-M generation were based on frequency-division multiple access (FDMA) signals: each satellite was broadcasting at difference

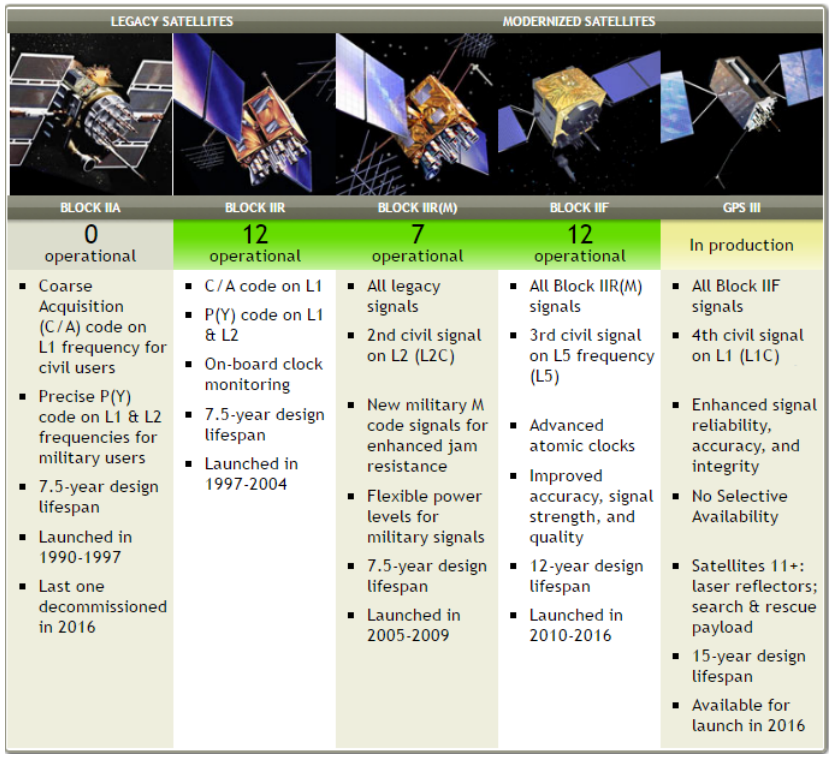


Figure 2.8: modernization process of the GPS space segment [21].

frequencies. From 2011, the Glonass-K1 generation has been designed to be compliant with GPS in terms of signal interoperability. Fig.2.9 described the modernization process at which GLONASS is undergoing.

2.3.3 Beidou

Beidou system is being developed in three phases: the first one has consisted in an experimental regional navigation system. The phase 2, concluded in 2012, has consisted in a restricted number of satellites which provided an open navigation service over China. By 2020, the phase 3 would reach a fully operation constellation of 27 MEO and 5 GEO satellites with a global coverage as GPS, GLONASS and Galileo Systems. In late 2015, China has launched the 20th BeiDou satellite, with a series of tests related to the clock.

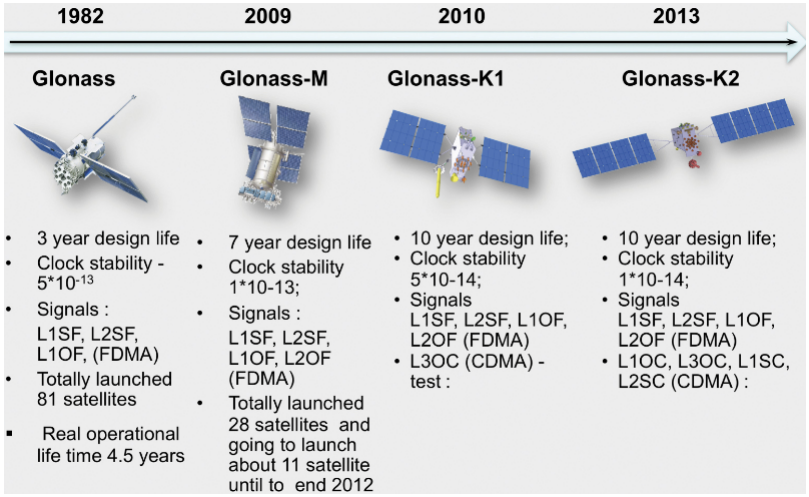


Figure 2.9: modernization process of the GLONASS space segment [52].

The new Phase 3 is currently being undertaken and his last satellite started broadcasting a signal similar to the future GPS L1C.

2.3.4 Galileo

Galileo is the european GNSS developed by European Union (EU) and European Space Agency (ESA) since 1999. It has been designed to mainly focus on civil-commercial purposes and to be fully interoperable with GPS and GLONASS. Galileo is expected to be fully operational by 2020 with 30 satellites constellation (24 operational and 6 active spares). Galileo aims to improve the position accuracy with respect to GPS and GLONASS, to improve the global coverage especially in the high latitude locations, to provide an high signal availability in dense urban area, to provide high reliability and a continuity of service. Galileo will offer five services as described as follows:

- Open service (OS): it points to the mass-market applications such as in-car navigation and mobile phone positioning and it allows a position accuracy down to 1 meter.

- Commercial service (CS): it provided an encrypted communication signals and allows a position accuracy level below 1 meter.

- Public regulated service (PRS): It will be used mostly by government agencies and it will provide a continuous service availability with encrypted communications even if others service will be disabled.

- Search and rescue (SAR): it involves locating and helping people in distress. It allows to send feedback, e.g. relying back to the users an acknowledgement about rescue operation is engaged.

2.4 Environmental Feature matching

Environmental feature matching positioning is based on comparing measured features related to the enviromment with data stored in database, as people do when trying to recognize something that already know. A feature could be something artificial such as roads, buildings, or geophysical such as terrain height, earth's gravitational and magnetic fields [22]. Fig.2.10 illustrates a generic representation of the feature matching position-fixing algorithm. Other navigation systems can be exploited to initialize environmental feature matching techniques and to help in selecting a database subregion depending on the position inizitialization. Dead Reckoning can also exploit feature matching, in order to infer the position change from the variation in feature measurements. Databases can be preinstalled in the feature matching system, downloaded via internet, or download when the system enters a particular area. When dealing with feature matching techniques, an insufficient number of features or a reduced database information can lead to extract ambiguous features or worse to navigation solution errors. Ambiguous features scenario may be treated by considering multiple hypotheses until there is sufficient information to resolve the ambiguity [22]. Environmental feature matching has a central role in Simultaneous Localization and Mapping (SLAM) [6], which exploits dead reckoning navigation solution to determine the environment feature position while it builds the feature database. A refinement of the environmental feature positions and a database information enhancement can be achieved by a multiple revisiting process of the considered feature. Several important environmental feature-matching techniques such as map matching [77], terrain-referenced navigation [13] and image-based navigation [63] are briefly described in 2.4.1, 2.4.2 and 2.4.3, respectively.

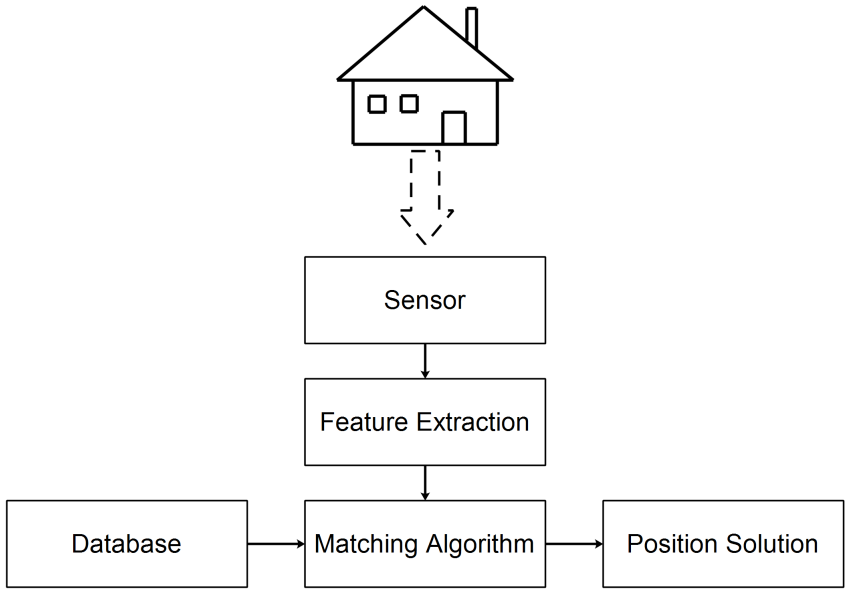


Figure 2.10: representation of the environmental feature mathing process [22].

2.4.1 Map Matching

Map matching technique aims to define a navigation solution by exploiting the map constrains. In outdoor navigation, the accuracy of the GNSS navigation systems can decrease due to a poor satellite visibility, in particular in urban context. In this case, vehicle travelling on road can exploit the lane direction to bound the position error. Moreover, when concerning indoor environment, pedestrian navigation can leverage a building map to constrain the navigation solution. Corridors, walls and doors can be exploited as constrains; for example, if both the navigation solution and database are indicating that the user is moving perpendicularly to through a wall, the position solution needs to be shifted to the closest doorway.

2.4.2 Terrain-referenced Navigation

Terrain-referenced navigation (TRN) compares measurements of the terrain heights with a database information. TRN is used in collision avoidance

to prevent unintentional contact between aircrafts and ground as well as in navigation. The aircraft subtracts the height above the terrain from the vehicle's height solution to obtain the terrain height, which is compared to the database information. The matching between the resolution of the terrain height measurements performed by the aircraft and the database resolution determines the best tradeoff in terms of database storage needed to cover a considered geogrphical area.

2.4.3 Image-based Navigation

Image-based Navigation (IBN) compares the sensor measurements with the image-based information database. An IBN system can use either passive sensors such as digital cameras or active sensors such as laser scanners. It has good performance in flat terrain, over which TRN lacks of feature information. An IBN system can estimate the orientation and the travelled distance of the user by evaluating the difference between the feature referred to images taken at successive time instants. Current fields of application refers to robot technology such as industrial robot arms and guidance of mobile robots.

Chapter 3

Global Positioning System

This chapter focuses on the global positioning system and its main characteristics. In particular, the system architecture and the signal used for ranging are described. Then, the coordinate frames involved in the navigation problem are characterized. Afterwards, the Global Positioning System receiver process and the errors sources which affect the user navigation solution are described. Finally, two augmenting systems which aims to enhance the accuracy and speed of the navigation solution are reported.

3.1 Introduction

The Global Positioning System (GPS), the abbreviated form of Navigation Satellite Timing and Ranging Global Positioning System (NAVSTAR GPS), is the global navigation satellites system developed and owned by the U.S. Department of Defense (DoD) [34]. At the moment of this writing, there are 31 satellites currently in orbit and healthy, which are moving around the Earth by following a medium Earth orbits (MEO) at the orbital height of approximately 20180 km. GPS exploits the Time of Arrival (TOA) ranging technique to compute the time of flight (TOF) of the signal transmitted from the satellites to the GPS receiver. GPS satellites are time synchronized to the GPS time base through atomic clocks and transmit ranging codes and navigation data by using the transmission technique called code division multiple access (CDMA). GPS provides different quality of services: standard positioning service (SPS) for civil use and precise positioning service (PPS)

for military purposes. There are four signals available for civil use: L1 C/A, L2C, L5, L1C. The L1 C/A, also named legacy signal, is the only one transmitted by all the satellites; the other signals belong to the modernization process and are transmitted by the newer satellite block generations. Considering the L1 C/A signal, all satellites transmit two identification ranging codes modulated over the same carrier frequency: the coarse-acquisition code (CA) and the precision code (P). The satellites also transmit the navigation data which enables the receiver to compute the position of satellites at the transmission time. The GPS receiver can determine the 3D position by performing TOA measurements from at least four satellites. This is because the receiver has to determine four unknown: its 3D coordinate (x, y, z) and the time synchronization error between its clock and the GPS base time.

3.2 GPS Modernization

In 1999, the United States government has announced the start of the GPS modernization process. The latter involves new civil and military signals. L2C, L5, L1C are the new civil signals in chronological order [21]. L2C is broadcast over the L2 carrier frequency at 1227.6 MHz and is available since 2005 with the IIR-M generation of satellites. When Combined with the originally existent L1 C/A signal, L2C enable dual-frequency receiver to compensate the error due to the ionospheric propagation of radio signals. Civil receivers in dual-frequency operation can achieve similar position accuracy with respect to military receivers. L5 signal has been designed for safety-of-life and high quality demanding applications and is available since 2010 with the IIF generation of satellites. It is broadcast over the L5 carrier frequency at 1176.45 MHz and is mostly used for aviation safety services. It features higher power, greater bandwidth, and an advanced signal design. Finally, L1C has been designed to be interoperable with the international satellite navigation system. It is broadcast over the L1 carrier frequency at 1575.42 MHz and relies on multiplexed binary Offset carrier (MBOC) modulation technique, which is also implemented by the Galileo satellites and other international satellite navigation systems. Noting that the L1 band includes the originally L1 C/A, also called legacy signal, which is broadcast by all GPS satellites. The new signals allows to improve the robustness against the interference: if a particular signals experiences an high interference, the receiver can move the processing to the other signals.

3.3 GPS Positioning Method

GPS system provides a self-positioning configuration in which a GPS receiver performs ranging measurements by radio signals transmitted from satellites [34]. The satellite-receiver distance is determined multiplying the speed of light in vacuum to the signal TOF. The latter is the time the signal takes to travel from the satellite to the receiver and is estimated through the TOA technique which is described in 2.2.3. The following expression represents the pseudorange for each satellite-receiver link:

$$\rho_c^{(k)} = r^{(k)} + c * \delta t_u + \epsilon_\rho^{(k)} = r^{(k)} + b + \epsilon_\rho^{(k)}, \tag{3.1}$$

where $r^{(k)}$ is the true range between the receiver and the *k-th* satellites, c is the speed of light in vacuum, δt_u is the time synchronization error between the clocks of the satellites and the one of the receiver, $b = c * \delta t_u$ is the receiver clock bias, and $\epsilon_\rho^{(k)}$ is the error source caused by factors like the satellite clock error and other error sources that are described in 3.8 The true satellite-receiver range is expressed as follows:

$$r^{(k)} = \sqrt{(x^{(k)} - x)^2 + (y^{(k)} - y)^2 + (z^{(k)} - z)^2} = \|x^{(k)} - x\|, \tag{3.2}$$

where $x^{(k)} = (x^{(k)}, y^{(k)}, z^{(k)})$ is the satellite position at the transmission time and $x = (x, y, z)$ is the receiver position at the measurement time. The 3.1 includes the four unknowns which define the positioning solution: the receiver 3D coordinates $x = (x, y, z)$ and clock time error δt_u. If the error term $\epsilon_\rho^{(k)}$ in 3.1 is neglected, then the unknowns can be precisely determined by solving for the system of equations composed by at least four equations, each representing a particular satellite-receiver pseudorange. Thus, at least four satellites must be "available"[1] to determine the receiver position. The Newton-Raphson method for non-linear least squares problems is commonly used to solve for the following non-linear system of equations which comprises the pseudorange measurements:

$$\begin{cases} \rho_c^{(1)} = r^{(1)} + c * \delta t_u \\ \rho_c^{(2)} = r^{(2)} + c * \delta t_u \\ \vdots \\ \rho_c^{(k)} = r^{(k)} + c * \delta t_u \end{cases} \tag{3.3}$$

[1] A satellite is "available" to the receiver whether the signal-to-noise ratio (SNR) value of the signal transmitted by the satellite is sufficiently high to enable the receiver to properly detect the signal.

Introducing an initial user position x_0 and bias b_0, the initial pseudorange relative to the *k-th* satellite is defined as

$$\rho_0^{(k)} = \|x^{(k)} - x_0\| + b_0, \tag{3.4}$$

which is subctracted from the actual *k-th* satellite pseudorange to obtain the following pseudorange difference expression:

$$\begin{aligned} \delta\rho^{(k)} &= \rho_c^{(k)} - \rho_0^{(k)} = \|x^{(k)} - x_0 - \delta x\| - \|x^{(k)} - x_0\| + (b - b_0) \\ &\approx \frac{(x^{(k)} - x_0)}{\|x^{(k)} - x_0\|}\delta x + \delta b + \epsilon_\rho^{(k)} = -1^{(k)}\delta x + \delta b, \end{aligned} \tag{3.5}$$

where $-1^{(k)}$ is the estimated line-of-sight unit vector directed from the initial estimate of the user position to the *k-th* satellite, $\delta x = (\delta x, \delta y, \delta z)$ and δb are respectively the user position and bias increments to generate the new estimates

$$\begin{aligned} x &= x_0 + \delta x, \\ b &= b_0 + \delta b. \end{aligned} \tag{3.6}$$

The Taylor series approximation of a vector norm allows the linearization of the pseudorange difference in (3.5), which introduces the line-of-sight term:

$$1^{(k)} = \frac{1}{\|x^{(k)} - x_0\|}(x^{(k)} - x_0, y^{(k)} - y_0, z^{(k)} - z_0)^T. \tag{3.7}$$

The non-linear system of equations in (3.3) is transformed in a linear system of equations in which the unknowns become the position and bias increments, respectively $(\delta x, \delta y, \delta z)$ and δb:

$$\delta\rho = \begin{bmatrix} \delta\rho^{(1)} \\ \delta\rho^{(2)} \\ \vdots \\ \delta\rho^{(k)} \end{bmatrix} = \begin{bmatrix} (-1^{(1)})^T & 1 \\ (-1^{(2)})^T & 1 \\ \vdots & \vdots \\ (-1^{(k)})^T & 1 \end{bmatrix} \begin{bmatrix} \delta x \\ \delta b \end{bmatrix}. \tag{3.8}$$

The expression in (3.8) is summarized as follows:

$$\delta\rho = G \begin{bmatrix} \delta x \\ \delta b \end{bmatrix}, \tag{3.9}$$

where G is the $k * 4$ geometry matrix:

$$G = \begin{bmatrix} (-1^{(1)})^T & 1 \\ (-1^{(2)})^T & 1 \\ \vdots & \vdots \\ (-1^{(k)})^T & 1 \end{bmatrix} = \begin{bmatrix} \frac{x_0 - x^{(1)}}{r_0^{(1)}} & \frac{y_0 - y^{(1)}}{r_0^{(1)}} & \frac{z_0 - z^{(1)}}{r_0^{(1)}} & 1 \\ \frac{x_0 - x^{(2)}}{r_0^{(2)}} & \frac{y_0 - y^{(2)}}{r_0^{(2)}} & \frac{z_0 - z^{(2)}}{r_0^{(2)}} & 1 \\ \vdots & \vdots & \vdots & \vdots \\ \frac{x_0 - x^{(k)}}{r_0^{(k)}} & \frac{y_0 - y^{(k)}}{r_0^{(k)}} & \frac{z_0 - z^{(k)}}{r_0^{(k)}} & 1 \end{bmatrix}. \tag{3.10}$$

The receiver position and bias increments are determined in the closed form by using the least-squares solution for linear system:

$$\begin{bmatrix} \delta\hat{x} \\ \delta\hat{b} \end{bmatrix} = (G^T G)^{-1} G^T \delta\rho \tag{3.11}$$

Finally, the new position and bias estimates are computed as follows:

$$\begin{aligned} \hat{x} &= x_0 + \delta\hat{x} \\ \hat{b} &= b_0 + \delta\hat{b} \end{aligned} \tag{3.12}$$

The new position and bias estimates can replace the initial estimates in 3.4, and the equations 3.4, 3.5, 3.9 3.11, 3.12 can be iterated until the position and bias increments turn into sufficiently small values, depending on the design specifications [34].

3.4 GPS Signals

The GPS signals consist of three components: carrier frequencies on L-band, pseudo-random Noise (PRN) codes and navigation data [34]. L1 and L2 were the first available signals on L-band before 2006 and their composition is illustrated in Fig.3.1. The navigation data is multiplied by the PRN code through the binary XOR operation and the result is translated over the currier frequency through binary phase-shift keying (BPSK) digital modulation. The power spectrum density function of the L1 signal is shown in Fig.3.2.

3.4.1 Carrier Frequencies on L-band

The GPS involves several carrier frequencies depending on the usage, as shown in Fig.3.3. Since a satellite travels approximately at 14000 Km/h,

the relative satellite-receiver velocity produces a frequency shifting in the received carrier frequency with respect to the original transmitted frequency: this effect is called Doppler shift. The Doppler shift measurements at the receiver can be used to improve the pseudorange determination based on code measurements [34]. GPS receiver can exploit different carrier frequencies in order to apply atmospheric correction to the pseudorange measurements. The ionosphere determines different signal delays depending on the frequency which is being considered. If a double pseudorange measurement is performed both on L1 (1.575,42 MHz) and L2 (1.227,6 MHz) frequencies, the ionospheric delay on the L1 pseudorange measurement can be computes as

$$I_{L1} = \rho_{IF} - \rho_{L1} = 2,546\rho_{L1} - 1,546\rho_{L2} - \rho_{L1} = 1,546(\rho_{L1} - \rho_{L2}), \tag{3.13}$$

where ρ_{IF} is the ionosphere-free pseudorange measurement, $(\rho_{L1} - \rho_{L2})$ is the measured difference in pseudorange between L1 and L2.

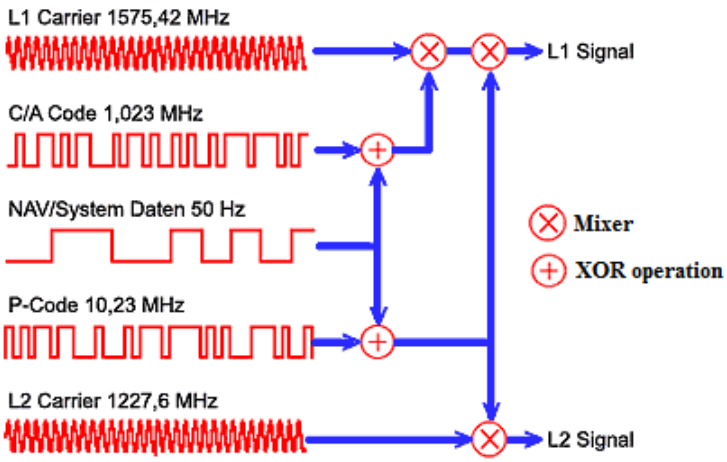


Figure 3.1: GPS signals.

3.4.2 PRN Codes

PRN codes are binary sequences which are different for each satellite. GPS receivers rely on code measurements to univocally identify the satellite and form the pseudorange estimates. Considering the L1 signal shown in Fig.3.1, two types of codes are involved: the civilian C/A and the military P(Y) codes. Moreover, these codes were the first available before the modernization introduced in 2006. The C/A is a Gold code with a period of 1023 chips and is transmitted periodically at 1.023 Mbit/s, implying a single period of 1 ms [34]. A chip is a term commonly used in direct-sequence spread spectrum (DSSS) and refers to a rectangular pulse of +1 or -1 amplitude. The P(Y) code is not available to civilian users and is primarily used by military: it is a binary sequence with a period of 10230 chips transmitted at 10.23 Mbit/s.

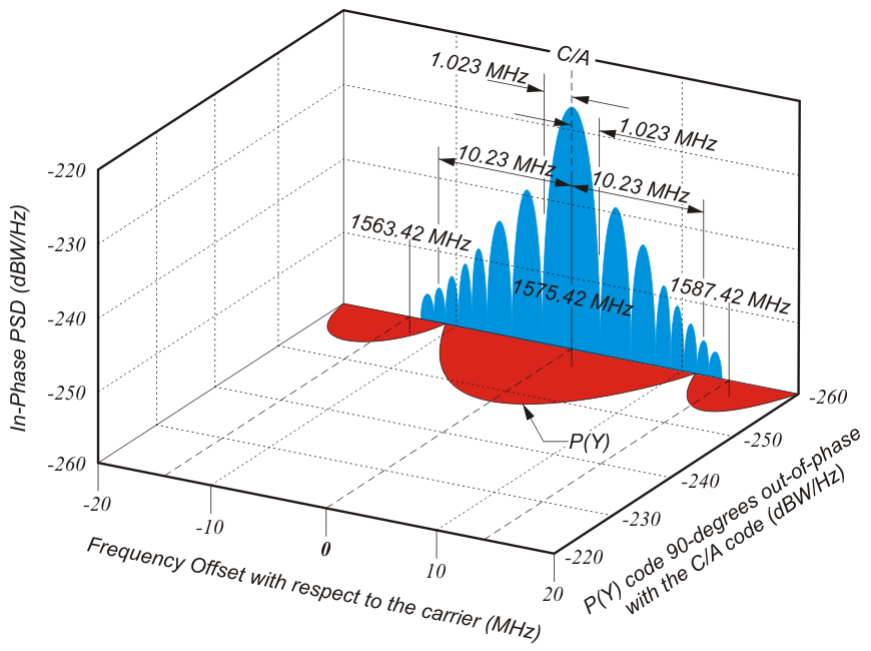


Figure 3.2: power spectrum density function of the L1 signal [67].

Band	Frequency (MHz)	Phase	Original usage	Modernized usage
L1	1575.42 (10.23×154)	In-phase (I)	Encrypted precision P(Y) code	
		Quadrature-phase (Q)	Coarse/acquisition (C/A) code	C/A, L1 Civilian (L1C), and Military (M) code
L2	1227.60 (10.23×120)	In-phase (I)	Encrypted precision P(Y) code	
		Quadrature-phase (Q)	Unmodulated carrier	L2 Civilian (L2C) code and Military (M) code
L3	1381.05 (10.23×135)		Used by Nuclear Detonation (NUDET) Detection System Payload (NDS); signals nuclear detonations/ high-energy infrared events. Used to enforce nuclear test ban treaties.	
L4	1379.913 (10.23×1214/9)		*(No transmission)*	Being studied for additional ionospheric correction
L5	1176.45 (10.23×115)	In-phase (I)	*(No transmission)*	Safety-of-Life (SoL) Data signal
		Quadrature-phase (Q)		Safety-of-Life (SoL) Pilot signal

Figure 3.3: GPS carrier frequencies usage [73].

3.4.3 Navigation Data

The navigation data is a binary stream transmitted at a data rate of 50 bit per second: it includes information about ephemeris (orbit information), satellite clock and health, almanac (constellation orbit information) and ionospheric correction parameters. The navigation message is repeated every 12,5 minutes and consists of 5 subframes, as shown in Fig.3.4. The first subframe includes the satellite clock corrections, health indicators and the age of data; the second and third subframes includes the satellite ephemeris parameters; the fourth subframe provides the ionosphere model parameters, the coordinated universal time (UTC) data, the almanac and health status data for satellites numbered 25 and higher; the fifth subframe includes the almanac and health status data for satellites numbered 1-24. The ephemeris provides a precise information about the satellite orbit, while the almanac is a coarse version of the ephemerides and refers to the orbits of the constellation as a whole [34].

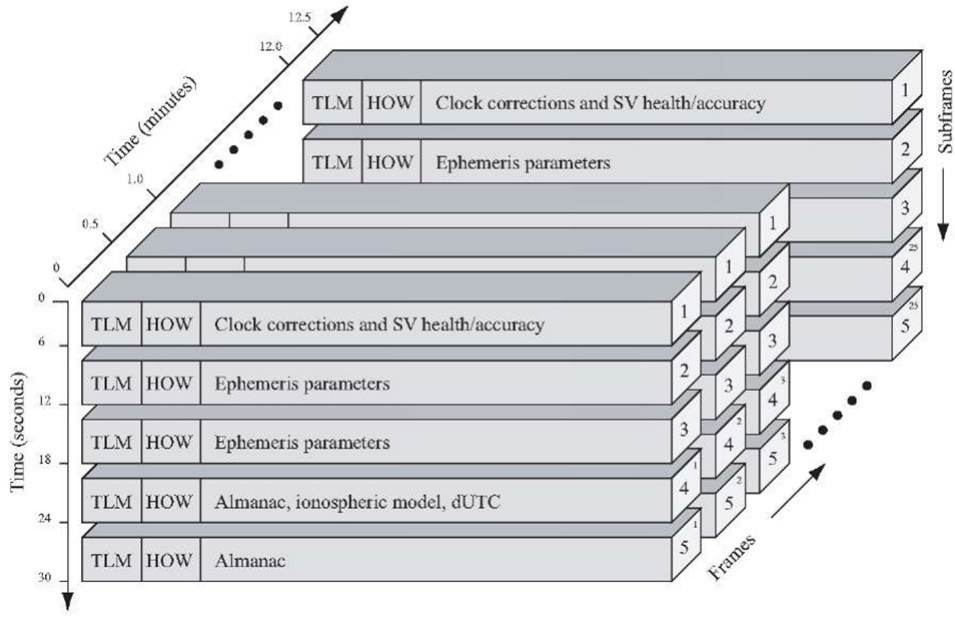


Figure 3.4: GPS navigation message [15].

3.5 Code Phase Measurements

The satellite-receiver distance is computed by measuring the propagation time required for a satellite-generated PRN code to transit from the satellite to the user receiver. Within the receiver, an identical coded ranging signal is generated, with respect to the receiver clock. This replica code is shifted in time until it achieves correlation with the received satellite-generated ranging code. If the satellite clock and the receiver clock were perfectly synchronized, the correlation process would yield the true propagation time. By multiplying this propagation time by the speed of light, the true satellite-to-user distance can be computed. However, the satellite and receiver clocks are generally not synchronized. The code phase measurement includes a bias due to the time synchronization error between the satellite and receiver clock. Thus, the range determined by the correlation process is denoted as the pseudorange. The measurement is called pseudorange because it is the

range determined by multiplying the signal propagation velocity, c, by the time difference between two non-synchronized clocks. The pseudorange measurement contains the geometric satellite-to-user range, an offset attributed to the difference between system time and the user clock, and an offset between system time and the satellite clock. Since the distance between a GPS receiver and the GPS satellites can vary between 20000 Km and 26000 Km, sensible values of pseudorange lie in the range of 67-90 ms. The GPS system deal with three time scales which refer to the satellite clock, the receiver clock and the reference GPS time (GPST). The pseudorange measurements is defined as follows:

$$\rho(t) = c * [t_u(t) - t^s(t - \tau)], \tag{3.14}$$

where t is the time expressed in GPST, while τ is the propagation time of the signal received at the time t. $t^s(t-\tau)$ is the transmission time stamped on the signal and $t_u(t)$ is the arrival time measured by the user's receiver clock. Since either t or τ are unknown at the receiver, the time references can be related to the GPST:

$$\begin{aligned} t_u(t) &= t + \Delta t_u(t), \\ t^s(t-\tau) &= (t-\tau) + \Delta t^s(t-\tau), \end{aligned} \tag{3.15}$$

where Δt_u is the receiver clock bias and Δs is the satellite clock bias. Both Δt_u and Δt_s are measured relative to the GPST. The pseudorange can be expressed as:

$$\begin{aligned} \rho(t) &= c * [t + \Delta t_u(t) - (t - \tau + \Delta t^s(t-\tau))] + \epsilon(t) \\ &= c * \tau + c[\Delta t_u(t) - \Delta t^s(t-\tau)] + \epsilon(t), \end{aligned} \tag{3.16}$$

where ϵ refers to the unmodeled effects, modeling errors and measurements errors. The product between the propagation time τ and the speed of light c is defined as:

$$c\tau = r(t, t-\tau) + I_\rho(t) + T_\rho(t), \tag{3.17}$$

where r is the true range, and I_ρ and T_ρ are respectively the ionospheric and the tropospheric time delay experienced by the signal. Finally, the pseudorange can be expressed as:

$$\rho = r + c[\Delta t_u - \Delta t^s] + I_\rho + T_\rho + \epsilon_\rho, \tag{3.18}$$

3.6 GPS Time

The GPS time is established by the control segment and is referenced to coordinated universal time (UTC). In contrast with the UTC, GPST is defined in real time and is continuous in time. Moreover, GPST differs from UTC by a certain number seconds plus a fraction of microsecond. In GPS, a time epoch is defined in term of week number and number of seconds of the week. The first GPS was started at midnight between the January 5 and 6 in 1980. Since GPST is continuous time, the GPS week change doesn't occur exactly at midnight.
The time difference between GPST and the GPS satellite clock is the satellite clock bias. The correction parameters of the satellite clock are transmitted in the navigation message and can be used by the GPS receiver to correct the satellite clock bias. The remaining range error due to the satellite clock bias after corrections is still about 1.5 m.
On the other hand, the time difference between the GPST and the receiver clock is the receiver bias. If the receiver is able to measure the pseudorange from at least four satellites, it can determine its clock bias and the 3D position coordinates [34].

3.7 Coordinate Frames

A coordinate frame is generally comprised of an origin and three mutually perpendicular axes. Any navigation problem involves at least two coordinate frame: the object (e.g. GPS receiver) frame, whose position and orientation are desired, and the reference frame describing a known body (e.g. the Earth) relative to which the object position and orientation are desired. The object frame defines the origin and the orientation of the object described by the navigation solution. In navigation, the main reference coordinate frames are the Earth-centered inertial (ECI) frame, the Earth-centered Earth-fixed (ECEF) frame, and the local navigation frame [22].

3.7.1 Earth-Centered Inertial Frame

Any coordinate frame that does not accelerate or rotate with respect to the rest of the Universe is an inertial frame. The ECI frame is oriented with respect to the Earth's spin axis and the stars, and its origin is at Earth's centre of mass. The x- and y- axes lie within the equatorial plane but do not rotate with Earth. The y-axis points 90° ahead of the x-axis in the direction of the Earth's rotation and the z-axis points from the origin to the true north pole. Actually, the ECI frame is not a strictly inertial frame: Earth experiences an acceleration in its orbit around the Sun, its spin axis slowly moves, and the galaxy rotates. However, these effects are smaller then the noise measurement of the inertial sensor, therefore they can be neglected for navigation purposes [22]. An ECI frame is convenient to express the motion of the objects which do not move with Earth, e.g. the satellites in a navigation system.

3.7.2 Earth-Centered Earth-Fixed Frame

In the ECEF frame, all axes remain fixed with respect to Earth. As for ECI frame, the ECEF frame is centered at the Earth's center of mass, the z-axis points from the centre to the true north pole, and the x- and y- axes lie with the equatorial plane. On the contrary, the x-axis points from the center to the intersection of the equatorial plane with the conventional zero meridian, which defines the 0° longitude. The y-axis completes the right-handed orthonormal set, and points from the origin to the 90° longitude [22]. The navigation solution of a GPS receiver are commonly computed in ECEF frame.

3.7.3 Local Navigation Frame

The local navigation frame defines the local position and orientation of an object. Its origin is the object itself described by the navigation solution. The axes are aligned with the topographic direction: north, east, and vertical. Conventionally, the down-axis is perpendicular to the Earth's surface and points towards the Earth's centre. The north-axis is the projection to the plane orthogonal to the down-axis of the line from the user to the north pole. The east-axis completes the orthonormal set and points to the east direction, as shown in Fig.3.5 [22].

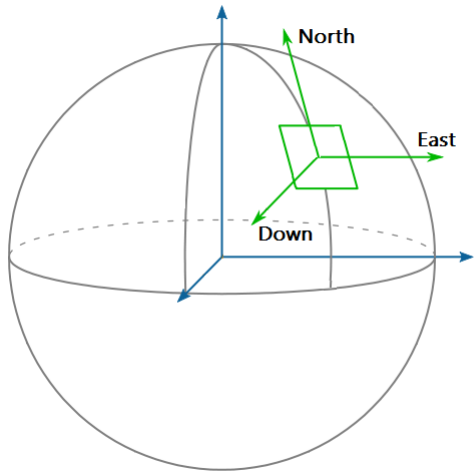


Figure 3.5: north east down (NED) local navigation frame.

3.7.4 World Geodetic System 1984

The word geodetic system (WGS) is the main standard physical model of Earth used for cartography, geodesy, and navigation including GPS. WGS is comprised of a consistent set of fundamental parameters, an ECEF coordinate frame, an ellipsoid of revolution as a geometrical Earth's model and a characterization of the Earth's gravity field and geoid.
Earth can be approximated as an ellipsoid of revolution with a semi-major axis a and a semi-minor axis b. The revolution is considered with respect to the semi-minor axis and the parameters of flattering and squared eccentricity are respectively defined as $f = \frac{a-b}{a}$ and $e^2 = 2f - f^2$. Considering this approximation, a point on Earth can be identified using the geodetic coordinates: longitude(γ), latitude(ϕ) and height (h), as shown in Fig.3.6. The lines which connect the points of the same latitude on the ellipsoid, generate a closed curve called parallel; while the lines joining points of the same latitude on the ellipsoid, generates a closed curve called meridian. The fundamental WGS parameters are:

- Ellipsoid parameters:
  -semi-major axis $a = 6378137\ m$
  -reciprocal of flattering $1/f = 298.257223563$

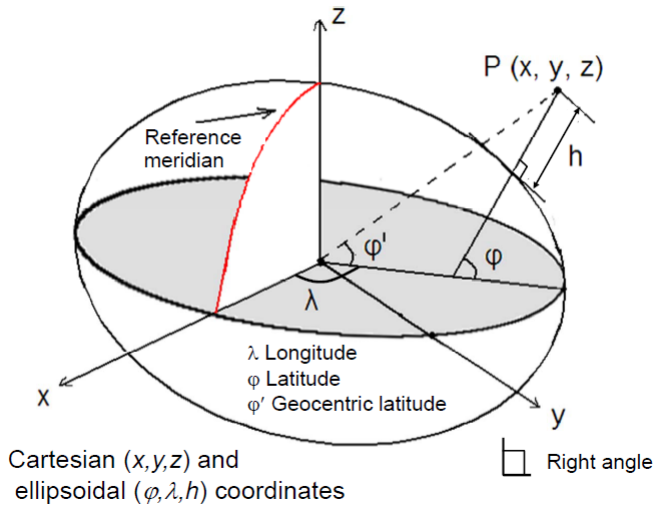


Figure 3.6: representation of the geodetic coordinates.

- Earth's angular speed $\omega_E = 7292115 * 10^{-11}\ rad/s$
- Earth's gravitational constant $GM = 3986004.418 * 10^8\ m^3/s^2$
- Speed of light in vacuum: $c = 299782458 * 10^8\ m/s$

The transformation between the geodetic and the cartesian coordinate can be performed as follows:

$$\begin{aligned} N &= \frac{a}{\sqrt{1 - e^2 sin^2\phi}} \\ x &= (N + h) cos\phi\ cos\gamma \\ y &= (N + h) cos\phi\ sin\gamma \\ z &= (N(1 - e^2) + h)\sin\phi. \end{aligned} \tag{3.19}$$

3.8 Error Sources and Models

In GPS, the error sources can be divided in three groups [48]:

- Errors in the clock and ephemeris parameters transmitted by satellites, for which the control segment is responsible. Considering an ephemeris update rate of one day, these errors causes an overall root-mean-squared error (RMSE) of about 3 meters on the satellite-receiver distance (range). A more frequently updating leads the error to decrease.

- Errors due to the propagation medium, which affects the propagation time of the signal transmitted from satellites to the receiver. The distance that the signal travels between satellites and the receiver varies between 20000 Km and 26000 Km, and they are affected by the ionosphere and the troposphere, which modidifiy both the speed and direction of signals.
  Errors due to the ionosphere depend on the solar activity and are highly variable from night to day and for different seasons. The modelling error can lead to range errors higher than 10 meters. The ionosphere is a dispersive medium for GPS frequency: for this reason the delay can be determined by dual-frequency receivers.
  On the other hand, the troposphere is not a dispersive medium for GPS signals. Errors due to the troposphere can significantly vary only under raining condition. The modelling error determine a range error about 5-10 cm.

- Errors due to the noise which affects the signal measurement and the interference caused by the multipath effect, i.e. the signal reflection in close vicinity of the receiver. The errors caused by the noise and multipath strictly depend on the elevation angle of the satellite [34]. Generally, if the satellite is low near the horizon, the received signal power of the satellite signal becomes lower and the multipath effect increases.

3.8.1 User Range Error and Dilution of Precision

Considering the three error sources mentioned in Section 3.8, their combined effect on the pseudorange measurements can be described by the user range

error (URE):

$$\sigma_{URE} = \sqrt{\sigma_{cs}^2 + \sigma_p^2 + \sigma_{rnm}^2} \tag{3.20}$$

where σ_{cs} is the RMSE due to the control segment errors, σ_p is the RMSE due to the atmospheric propagation, and σ_{rnm} is the RMSE due to the recevier noise and multipath.
Considering a zero-mean, uncorrelated and identically distributed vector ϵ_ρ, which includes the pseudorange errors in (3.1),

$$\begin{aligned} E(\epsilon_\rho) &= 0, \\ Cov(\epsilon_\rho) &= E(\epsilon_\rho \epsilon_\rho^T) = \sigma_{URE}^2 I, \end{aligned} \tag{3.21}$$

where I is the identity matrix.
Two factors affect the GPS positioning solution: the measurement errors due to the error sources described in this section, and the satellite geometry. Fig.3.7 depicts how the geometry of satellites affects the navigation solution accuracy. Considering the same variance for all pseudorange errors, the covariance of the position and bias errors can be expressed as [48]:

$$\begin{aligned} Cov\left(\begin{bmatrix} \Delta\hat{\boldsymbol{x}} \\ \Delta\hat{b} \end{bmatrix}\right) &= \sigma_{URE}^2 (G^T G)^{-1} = \sigma_{URE}^2 H, \\ H &= (G^T G)^{-1}, \end{aligned} \tag{3.22}$$

where G is the geometric matrix defined in (3.10). Considering each *i-th* term H_{ii} in the diagonal of the matrix H, the variances of the receiver 3D position components (x, y, z) and the bias-variance, can be expressed as follows:

$$\begin{aligned} &\sigma_x^2 = \sigma_{URE}^2 H_{11}, \quad \sigma_y^2 = \sigma_{URE}^2 H_{22}, \quad \sigma_z^2 = \sigma_{URE}^2 H_{33}, \\ &\sigma_b^2 = \sigma_{URE}^2 H_{44}. \end{aligned} \tag{3.23}$$

The RMSE of the receiver 3D position is [48]

$$RMSE_{pos} = \sqrt{\sigma_x^2 + \sigma_y^2 + \sigma_z^2} = \sigma_{URE}\sqrt{H_{11} + H_{22} + H_{33}} \tag{3.24}$$

In (3.24), the error of the estimated position and bias depend on both the variance of the URE and the geometry of the satellites. In order to char-



Figure 3.7: the influence of the geometry of satellites in the navigation solution accuracy.

acterize the influence of the satellite geometry on the receiver position and clock bias errors, the dilution of precision (DOP) parameters are defined:

$$\begin{aligned} GDOP &= Geometric\ Delution\ of\ Precision = \sqrt{H_{11} + H_{22} + H_{33} + H_{44}} \\ PDOP &= Position\ Delution\ of\ Precision = \sqrt{H_{11} + H_{22} + H_{33}} \\ TDOP &= Time\ Delution\ of\ Precision = \sqrt{H_{44}} \end{aligned} \tag{3.25}$$

The quality of the receiver position and clock bias estimates, which refer to a single measurements, can be described as:

$$\begin{aligned} RMSE_{pos} &= \sigma_{URE}\ PDOP \\ RMSE_{bias} &= \sigma_{URE}\ TDOP \\ RMSE_{pos+bias} &= \sigma_{URE}\ GDOP \end{aligned} \tag{3.26}$$

where the $RMSE_{pos}$ is the RMSE of the receiver 3D position, the $RMSE_{bias}$ is the RMSE of the receiver clock bias, and the $RMSE_{pos+bias}$ is the joined RSME value of the receiver 3D position and clock bias.

3.9 GPS Receiver

The signals transmitted by the GPS satellites are intercepted by the GPS receiver antenna and provided as input to the front-end block, as shown in Fig.3.8. The front-end performs the filtering, amplification and down-conversion operations. Filtering and amplification are necessary to ensure

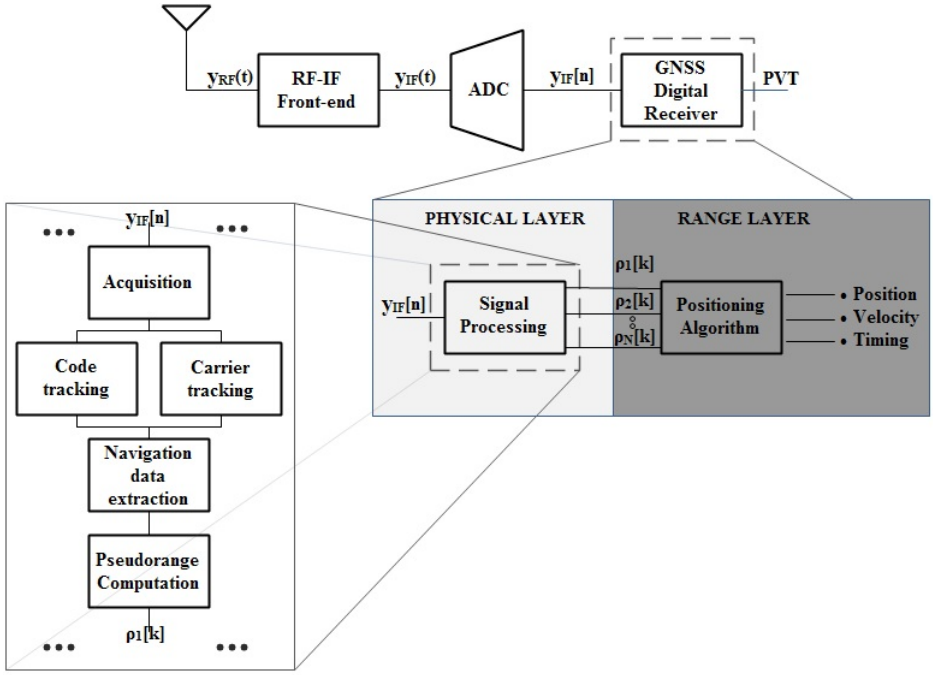


Figure 3.8: GPS receiver process.

low noise and out-of-band rejection in the received signals, as well as amplification stages to compensate for transmission losses. The down-conversion converts the radio frequency (RF) spectrum directly to an intermediate frequency (IF), with the appropriate band filtering, ultimately converting the IF signals to baseband [48]. The output signal from the front-end is digitized through analog to digital converter (ADC), and finally provided as input to the GNSS digital receiver. The latter can be divided into the signal processing block and the position, velocity, and time (PVT) computation block, as shown in Fig. 3.8. The signal processing routine elaborates the signals transmitted by each satellite and determines the pseudoranges for each satellite-receiver link. It consists of four phases: acquisition, code and phase tracking, navigation data extraction and pseudorange calculation. The purpose of acquisition is to identify and determine the code phase and carrier frequency of the satellites visible to the receiver.

The frequency of the received signal can vary from its nominal value due to the relative satellite-receiver velocity. The latter introduces a Doppler frequency shift which can approach value as high as 10 kHz when the maximum satellite velocity and an high receiver velocity are combined.
On the other hand, the code phase for a particular satellite denotes the point in the current data block where the PRN code begins.
In order to determine both the code phase and carrier frequency, the receiver performs a scanning operation in the time-frequency domain. After defining an appropriate time-domain search space, the incoming signal from the satellite is correlated with a local generated replica shifted both in time and frequency. The maximum correlation peak between the received signal and the shifted replica defines the code phase and carrier frequency values [48].
The tracking operation aims to refine the coarse values of the code phase and the carrier frequency and to keep track of these as the signal properties change over time. The accuracy of the final value of the code phase is connected with the accuracy of the pseudorange computed later on. The code tracking is most often implemented as a delay lock loop (DLL) where three local code replicas typically separated by a half-chip length are correlated with the incoming signal. The tracking is running continuously to follow the changes in frequency as function of time [34, 48]. When the signals are properly tracked, both code and carrier can be removed from the signal, and the navigation data for each satellite can be extracted. The navigation data includes the time at which the data has been transmitted by the satellite and the ephemeris, which are used to determine the satellite position at the transmission time. In order to determined the pseudoranges, the speed of light in vacuum is multiplied by the difference between the time of transmission and the time of arrival of the signal at the receiver. The PVT computation routine processes the pseudoranges and the position of satellites in order to compute the receiver position, velocity and clock time.
The GNSS receiver implementation can be either hardware-based or software-based : the first one doesn't allow the user to modify the fundamental parts of the receiver. Alternatively, these limitations can be overcome by considering a software-defined implementation, which is a flexible architecture in which the user can modify via software most of the receiver procedures [10].

3.10 Differential and Assisted GPS

Several solutions can be adopted to enhance the GPS performance. This section gives a brief description of differential GPS (DGPS) and assisted-GPS (A-GPS), while the Chapter 4 defines a cooperative GPS positioning technique.

3.10.1 Differential GPS

In GPS navigation, the receiver experiences position errors which are correlated both in space and time. The signals received in the same time and area exhibit similar errors due to the atmospheric propagation, control segment and multipath. The Differential GPS (DGPS) is a GPS augmentation system which aims to decrease the errors in the receiver measurements. Reference stations equipped by a GPS receiver, whose position is known, estimate the combined errors for each satellite and transmits the error estimates (DGPS corrections) to the GPS receivers in the vicinity. The measurements errors refer to the satellite clock, ephemeris computation and atmospheric propagation. The shorter is the distance between the reference station and the receiver, the better the improvement in the measurement errors [34, 48].

3.10.2 Assisted GPS

The A-GPS system aims to improve the startup phase of a GPS receiver by providing information, through an alternative communication channel, that the GPS receiver would ordinarily have received from the satellites themselves. The signal transmitted by satellites results with frequency shift at the GPS receiver, due to the Doppler effect. As shown in Fig.3.9, A-GPS aims to provide several information to the GPS receiver: the Doppler shifts, the position of satellites, the time, an approximate position of the receiver and other aiding data like [15]. In particular, either a coarse or a fine time information can affect the performance of the satellite acquisition and positioning procedures carried out by the assisted terminal. A fine time assistance allows the aided receiver to speed up the satellite acquisition process by reducing the code delay search space and to improve the accuracy of the positioning solution. The impact of the fine and coarse time assistance is detailed in Chapter 4.
A-GPS is extensively used with GPS-capable cellular base station, which

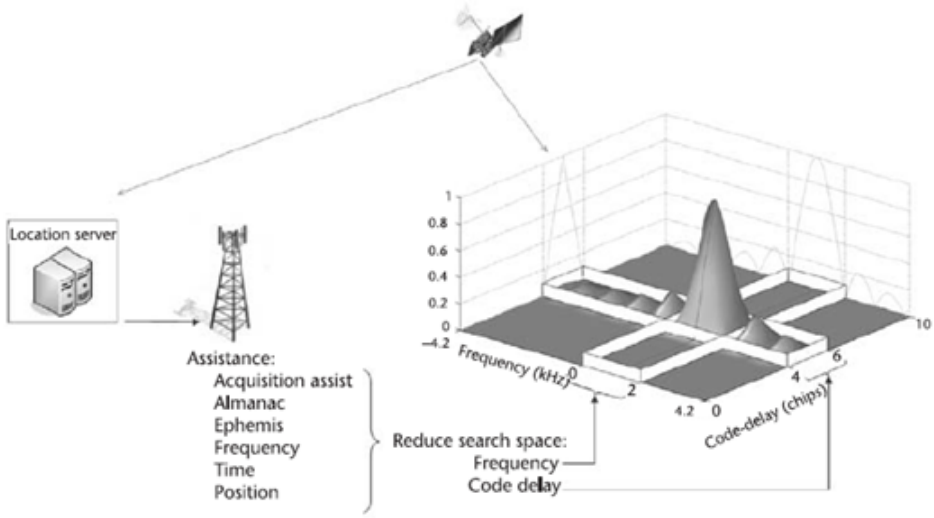


Figure 3.9: aiding information provided by the A-GPS system [15].

are exploited to transmit the aiding information to the GPS receiver in the coverage area.

Chapter 4

Peer-to-Peer Cooperation for GPS Positioning

This Chapter presents a peer-to-peer cooperative GPS positioning technique together with its performance assessment. The cooperation between the two GPS receivers is realized by means of a Wireless LAN connection and is significantly influenced by the accuracy of the synchronization between the two terminals. Both the Outdoor-to-Indoor and Outdoor-to-Outdoor scenarios are considered. For each scenario we assess the satellite signal acquisition and its computational load and the performance in terms of position accuracy and Time-to-First-Fix of the positioning procedure.

4.1 Introduction

Nowadays the wider and wider spread of smart phones and mobile devices permits an impressive growth of Location Based Services with potential application in several areas [7, 36, 62], making positioning and navigation techniques one of the most popular research and development topics. Global Navigation Satellite System (GNSS) is the leader technology in outdoor positioning: it is characterized by global coverage that significantly increases the availability of the localization and enables an increasing adoption of related services. This trend will be even enforced by the upcoming multi-constellation system that involves several GNSS systems such as GPS, GLONASS, QZSS, Beidou and Galileo. Unfortunately, even in outdoor sce-

narios, the pursue of an accurate position fix may become a complex issue in the presence of harsh environments such as dense urban canyons, light shadowing, or more generally when GNSS signals cannot be received with a sufficiently high signal-to-noise ratio (SNR). On the other hand, as for the indoor environments, many technologies may be adopted for localization purposes [36], but most of them requires a dedicated infrastructure and their cost-effectiveness, reliability and standardization have still to be completely analyzed and assessed; moreover, an effective and seamless position service between outdoor and indoor positioning is still an open research issue at the moment. The Cooperative Positioning (CP) [7, 19, 49, 62, 71] system which is represented in Fig. 4.1, might be a solution to meet the positioning requirements such as accuracy and service availability through the cooperation between peers, especially in harsh environments where a stand-alone receiver cannot achieve the position fix.

In this Chapter we present an overview about the state of the art of the CP, focusing on the open points and the design and implementation challenges. Then, we describe the proposed Peer-to-Peer Cooperative technique that has been proposed in [62]. Afterwards, we focus on the sensitivity-complexity trade-off in the acquisition procedure, by comparing the effects of the Local Oscillator stability, the Doppler shift and the correlation operation in both the stand-alone and cooperative cases. Then we take into account the synchronization issue which may affect both the acquisition and the positioning routines. Particularly, in the considered system the cooperation is carried out between two GPS software defined receivers that are both implemented in the MATLAB simulation environment, namely the aiding and aided receivers: the former is a stand-alone GPS software receiver [17] which performs the procedures which are illustrated in Fig. 3.8 and relies on the separation between physical and range layers, as for the general GNSS receiver; the latter is a GPS software defined receiver which has been also implemented in MATLAB and performs the assisted acquisition and positioning algorithms with fine or coarse time assistance as defined by the synchronization level between the receivers. In the fine time case the common view [78] of at least one satellite is assumed for the aiding and aided terminals while a coarse time assistance may be carried out by means of NTP protocol [42], that is to say by a software application, running on both the receivers. With respect to [10] and [14] the present work provides a new and wider set of results in addition to a general assessment of all the cooperative positioning features, which are

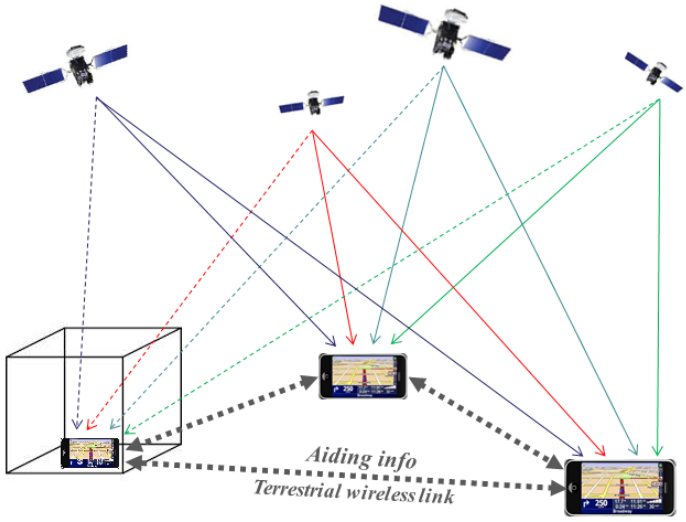


Figure 4.1: cooperative Positioning scenarios.

evaluated in terms of satellite signal acquisition, computational load in the acquisition procedure and performance concerning receiver position accuracy and Time-to-First-Fix (TTFF). The tests involve two scenarios: Outdoor-to-Indoor (O2I) and Outdoor-to-Outdoor (O2O). The former is relative to a case in which the aiding and the aided receivers are located outdoor and indoor, respectively, whereas in the latter case both the receivers are located outdoor. The results highlight the cooperation benefits either in the O2I case where the localization accuracy improvements enable the aided receiver to get a position fix or in the O2O scenario in which the aided receiver reduces the TTFF with respect to the stand-alone case.

4.2 Cooperative positioning: state of the art

As anticipated in the Introduction, Location Based Services are becoming very popular in the people's daily life and most of the mobile applications rely on the device location information in order to access the context-aware services. At the same time, the positioning requirements in terms of service availability and accuracy are becoming more and more demanding. There-

fore, in order to overcome the limitations of the stand-alone GNSS receiver and get a reliable position fix, innovative techniques have to be adopted: the Cooperative Positioning (CP) paradigm might be a solution in some particular scenarios such as outdoor or dense urban areas as well as light indoor environments. In the CP context, two or more peers work together to improve their position information; in particular, the cooperation may exploit concepts such as proximity positioning [53], Assisted/cooperative GNSS positioning [62], [10], [50], [51], [33] and opportunistic navigation [15]. Proximity positioning considers the user location as the position of the closest devices while the assisted GNSS positioning exploits the cellular network to provide data information to speed up the Time-To-First-Fix. On the other hand, Cooperative GNSS positioning exploits peers that are close to each other, by resorting to the exchange of information and allowing the aided users which are not in non-line of sight to determine their positions: with respect to the assisted GNSS, this technique better exploits the environment information and permits the aided device to improve the location accuracy. The concept of opportunistic navigation refers to the localization techniques which exploit the signals of opportunity such as cellular, DVB, FM, AM, or Wi-Fi signals to obtain landmarks that are often registered through the Received Signal Strength. In the cooperation context, it is possible to take advantage of the location map information when available and perform map matching algorithms to speed up the positioning procedure.

In the considered framework an issue which is still to be effectively addressed is how to combine the previously cited concepts to improve the GNSS receiver performance in harsh environments where CP technology is not able to improve on the user positioning. This kind of integration might be limited by the traditional hardware-based devices, whereas a Software-defined Radio (SDR) approach can be an elegant solution to obtain a flexible architecture receiver and to allow a dynamic selection of parameters for the individual modules. Moreover, the SDR implementation allows to effectively tackle the complexity of some specific tasks such as the satellite signal acquisition since this approach permits to easily replace the burdensome parallel correlation with a simple frequency domain multiplication [50]; particularly, the following relation holds:

$$(f(t) \star g(t)) = (f^*(-t) \otimes g(t)), \tag{4.1}$$

where the $\star$ and $\otimes$ symbols refer to the correlation and convolution operators,

respectively. Hence, the correlation of the received signal with the PRN code can be substituted by a multiplication in the frequency domain, while the convolution result in the time domain can be obtained by an inverse Fourier transform (IFT), as depicted in Fig.4.2. The convolution procedure in the frequency domain can be described by the following expression:

$$\begin{aligned} z(t) &= IFT(X(jw) * Y(jw)) \\ &= IFT(FT(x(t) \otimes y(t))). \end{aligned} \tag{4.2}$$

Another crucial CP issue is related to the fine time synchronization between peers that are close to each other and connected by wireless networks. To this aim, even if the IEEE 802.11v which has been ratified as a formal amendment to the 802.11 standard in 2011 defines the basis for a fine time synchronization in a Wi-Fi network, its use is still limited and not widespread.

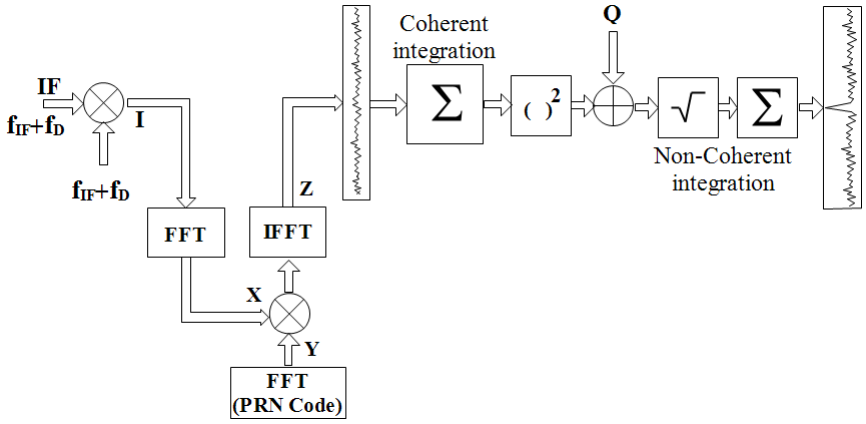


Figure 4.2: acquisition scheme for software defined GNSS receiver using FFT implementation [15].

4.3 P2P GPS Cooperative Positioning Algorithm

The CP technique which is proposed herein involves two GPS receivers whose cooperation is tested in the two scenarios which are illustrated in Fig.4.1, namely the O2I and the O2O. The satellite signal acquisition and positioning

algorithms that are running on the aided receiver and are implemented in the physical and range layers, respectively, will be affected by the accuracy of the time synchronization with the aiding terminal, leading to a fine or coarse time acquisition and positioning. The aiding information includes a combination of approximated user position, ephemerides, almanac, time and frequency assistance.
Concerning the signal acquisition procedure, the fine-time assistance is possible when the synchronization error between the aiding and the aided terminals is <1 ms [50]. The GPS C/A PRN codes are Gold sequences [34] with a period of 1023 chips trasmitted at 1023 Mbit/s, implying a period of 1 ms. A synchronization error more than 1 ms would not enable the aided receiver to identify an effective estimate of the code phase within the considered code period. A fine-time acquisition procedure permits the aided receiver either to speed the acquisition up by allowing the use of narrow search windows in the time domain, or to increase its sensitivity by extending the coherent integration time during the process.
In contrast with the signal acquisition process, the time assistance in the positioning procedure is defined as fine when the time synchronization error is <10 ms [50]. A GNSS receiver in LOS condition with the satellites decodes the navigation message which include the time-of-week (TOW) information. The latter refers to the transmission time from the satellite and permits to form the complete pseudorange measurements. Conversely, if the received signal power is weak, as in the NLOS case (e.g. the receiver in light-indoor scenario), a GNSS terminal could not be able to correctly decode the TOW due to the high Bit Error Rate and has to rely on external assistance to compute a reliable position fix. Furthermore, if the aided terminal undergoes to a coarse time assistance with the aiding one, the data which is transmitted by the aiding receiver cannot be directly used by the aided one. Since the satellites move at high velocity, the TOW value that is received by an aided terminal which does not compensate the time error leads to a wrong computation of the position of the satellites [1]. Therefore, when only coarse time assistance is available, the aided receiver has to estimate the synchronization error as an addition unknown in the navigation solution, i.e. in addition to

[1]Since the maximum pseudorange rate of a GPS satellite is about 800 m/s, it can be noted that the satellite position computation that is based on a TOW estimate whise tolerance is less than ±1 second would lead to a maximum geometric range error of 800 meters. User positions that are derived using such measurements can be mistaken by several kilometers [58]

the usual four unknowns: user spatial coordinates and clock bias.
While the knowledge of the satellite velocity for each satellite can be obtained by the ephemeris information provided as external aiding information, the pseudorange rates for all satellites can be obtained from the relative velocities and included in the set of navigation equations together with the unknown position, the unknown receiver common bias, and the unknown coarse-time error. In order to understand this approach, it is worth considering how the residuals δz of the of the a-priori pseudorange measurement is formed by the aided receiver [50]:

$$\delta z^{(k)} = z^{(k)} - \hat{z}^{(k)}, \tag{4.3}$$

$$\hat{z}^{(k)} = |x^{(k)}(\hat{t}_{tx}) - x_{xyz0}| - \delta t^{(k)}(\hat{t}_{tx}) + b_0, \tag{4.4}$$

where

- $z^{(k)}$ is the measured pseudorange relative to the k-th satellite;
- $\hat{z}^{(k)}$ is the estimated pseudorange relative to the k-th satellite;
- $\hat{t}_{tx}$ is the estimated time at which the satellite trasmits the signal;
- $x^{(k)}(\hat{t}_{tx})$ is the satellite position at time $\hat{t}_{tx}$;
- x_{xyz0} is the receiver a-priori position;
- $\delta t^{(k)}(\hat{t}_{tx})$ is the satellite clock error at time $\hat{t}_{tx}$;
- b_0 is the a-priori estimate of the common bias.

If an uncompensated TOW by the aided receiver causes an error in the $\hat{t}_{tx}$ computation, then $x^{(k)}$, $\delta t^{(k)}$ and $\hat{z}^{(k)}$ in (4.4) will be wrong [15]. By computing the relative satellite-receiver velocities and the clock rate for all the satellites through the ephemeris information trasmitted by an aiding terminal, we are able to compute the pseudorange rate which can be exploited to determine the error in the $\hat{z}^{(k)}$ term caused by the time synchronization error in the provided a-priori time:

$$\begin{aligned} \hat{z}^{(k)}(\hat{t}_{tx}) - \hat{z}^{(k)}(t_{tx}) &= \hat{z}^{(k)}(\hat{t}_{tx}) - \hat{z}^{(k)}(\hat{t}_{tx} + \delta_{tc}) \\ &= -p^{(k)} * \delta_{tc}, \end{aligned} \tag{4.5}$$

where

- δ_{tc} is the update to the coarse-time state;
- t_{tx} is the "true" time at which the satellite transmits the signal;
- $p^{(k)} = (e^{(k)} * v^{(k)} - \delta^{'(k)})$ is the psudorange rate relative to the k-th satellite;
- $v^{(k)}$ is the satellite velocity vector;
- e^{k} is the unit vector from the receiver to the satellite k;

By considering the relation between z and $\delta_t c$ in (4.6), we can express (4.3) as follows:

$$\delta z^{(k)} = z^{(k)} - \hat{z}^{(k)} = -e^{(k)} * \delta x_{xyz} + \delta b + p^{(k)} * \delta_{tc} + \epsilon^{(k)}, \tag{4.6}$$

where

- $\delta x_{xyz} = (\delta_x, \delta_y, \delta_z)$ is the update to the a-priori position;
- δ_b is the update to the a-priori receiver clock bias.

Thus, when dealing with coarse-time assistance, the geometry matrix is defined as:

$$H = \begin{pmatrix} e^{(1)} & 1 & p^{(1)} \\ \vdots & \vdots & \vdots \\ e^{(k)} & 1 & p^{(k)} \end{pmatrix}$$

If we assume at least five independent rows in H, we can achieve $\delta\hat{x}$ (vector of updates to the a-priori aided receiver position) by using, for example, the standard least-squares solution:

$$\delta\hat{x} = (H^T * H)^{-1} * \delta z = [\delta_x, \delta_y, \delta_z, \delta_b, \delta_{tc}]^T. \tag{4.7}$$

Hence, a close-form five-state solution to the position problem with no precise time is derived [50]. To to this aim, the following set of a-priori information is required:

- A valid set of ephemeris;
- An approximation of the user position within a few kilometers;

- An approximation of the TOW within a few seconds.

In the P2P-CP case, the a-priori information which is required for coarse-time positioning can be obtained by the aiding receiver. The types of information provided to the aided receiver by the aiding information are summarized in Table 4.1. The sub-millisecond pseudorange can be computed by the aided receiver exploiting the aiding information that is provided at the physical layer. The integer-millisecond pseudorange has to be added to the submillisecond one to obtain an unambiguous pseudorange measurement. This operation has to be handled properly in order to avoid position errors resulting from a combination of sub-ms clock bias, measurement noise and sub-ms pseudoranges. These combined values might exceed the one millisecond boundary, thus leading to rollovers. In [12, 50] an algorithm is described which determines millisecond ambiguity. The TOW estimation in the coarse-time navigation algorithms allows the following benefits:

- a faster TTFF;
- the achievement of a position fix under signal power conditions near or below data decoding threshold;

4.4 Acquisition procedure: Sensitivity vs Complexity trade-off

In this paragraph, the sensitivity and the complexity which characterize the acquisition procedures are described and put in relation with a particular

Table 4.1: Types of information provided by each component of the aiding information

Aiding information	**Type of information provided**
A valid set of ephemeris	Satellite position and velocity
Aiding user position	• Initial aided user position • Integer-millisecond pseudorange
Time of week (TOW)	Initial estimate of the satellite transmission time

attention to the trade-off between these requirements. Both the stand-alone and the cooperative contexts are considered.

4.4.1 Stand-alone Positioning

The signal acquisition that is performed by the GNSS receiver aims to determine a PRN code, a code delay τ and the Doppler offset f_D of the signal which has been transmitted by the satellites [63]. The correlation values that are determined by the IFFT block are commonly referred as Cross Ambiguity Function (CAF) between the incoming and the local generated signals [16, 56]. The CAF value is calculated for the time and the frequency bins in the discretized signal acquisition search space as depicted in Fig.4.3. Note that the $\Delta\tau$ and the Δf_D bin widths determine the cell size in the time

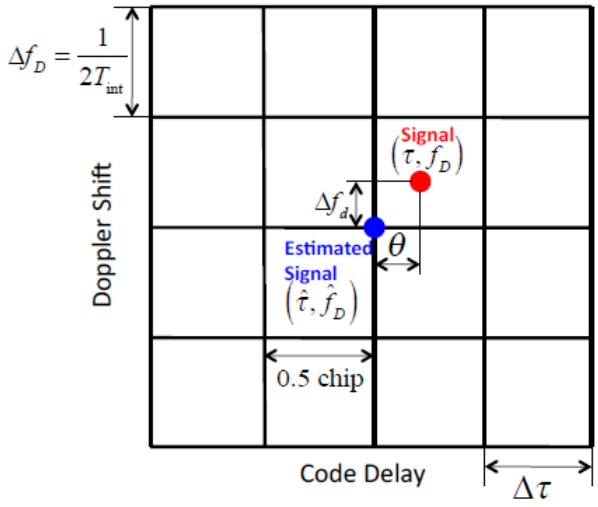


Figure 4.3: acquisition code delay-frequency search-space [31].

and frequency domains and therefore have to be chosen carefully in order to limit the cross-correlation loss. In particular, we focus on the frequency search space since the code delay may be sought by performing the correlation operation in the frequency domain as depicted in Fig.4.2 in order to reduce the complexity of the acquisition procedure in the time search space. Since the frequency bin width Δf_D is inversely proportional to the acqui-

sition procedure complexity, it has to be carefully defined: particularly, it has be chosen together with the coherent integration time, which in turn is directly proportional to the sensitivity feature. Therefore, as described the following function:

$$sinc(\Delta\bar{f}_{d_m} * T_{int}) = \frac{sin(\Delta\bar{f}_{d_m} * T_{int})}{\Delta\bar{f}_{d_m} * T_{int}} \tag{4.8}$$

is responsible of post-correlation SNR losses which affect the acquisition statistics where $\Delta\bar{f}_{d_m} = f_D - \hat{f}_{D_m}$ is the difference between Doppler shifts during the interval m and T_{int} is the coherent integration time; for clarity's sake, the function is depicted in Fig.4.4. Note that the $(\Delta\bar{f}_{d_m} * T_{int})$ product brings out a complexity-sensitivity trade off: when the T_{int} is increased, a post-correlation SNR raise (sensitivity augmentation) is observed which leads to a frequency bin width reduction (complexity augmentation). Note that the theoretical assessment of the acquisition performance is not always possible, since it requires also the knowledge of the pdf of the decision variables [56]; therefore Monte-Carlo simulations are often employed to assess the acquisition schemes in different conditions; nonetheless, if the sensitivity of a single acquisition scheme in different conditions has to be evaluated, an easy-to-compute parameter such as the peak-to-floor ratio α_{max} [56] can be used:

$$\alpha_{max} = \frac{|S_{peak}|^2}{max|S_{floor}|^2}, \tag{4.9}$$

where S_{peak} and S_{floor} are the maximum and the floor of the CAF magnitude, respectively. This metric highlights the overall trend of the post-correlation SNR.

4.4.2 Peer-to-Peer Cooperative Positioning

As for the acquisition, in the scenario which is depicted in Fig.4.1, an aided receiver may increase its sensitivity or reduce the computational load depending on its position: if the receiver is located in a light-indoor situation, then an increase of the sensitivity will be pursued that will afford a correlation peak in the time-frequency search space with a sufficiently high value of α_{max} (4.9); on the other hand, if the aided receiver is placed outdoor, a computational load reduction will be obtained by reducing the satellite signal acquisition time. A different sensitivity-complexity trade-off will be defined in the two situations by exploiting the information that is transmitted by an

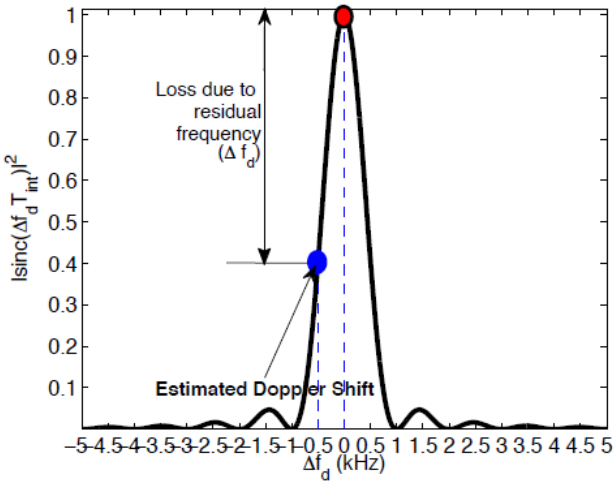


Figure 4.4: sinc function describing the post-correlation SNR losses after the square function [31].

aiding receiver. In the case of sensitivity augmentation, the aided receiver generally increases the coherent integration time and performs non-coherent sums, as represented in the scheme in Fig.4.2. In this case, a reduction of the post-correlation SNR loss due to the $sinc(\Delta \bar{f}_{d_m} T_{int})$ term [56] will be achieved by lowering the frequency bin width Δf_D in the frequency search space, as depicted in Fig.4.3. Unfortunately, the reduction may bring to a large number of frequency bins to be scanned, but, on the other hand, thanks to the Doppler information by the aiding receiver, the aided one can shrink the frequency search space and limit the number of bins. Conversely, in the case of computation load reduction, the aided receiver can leave unaltered the coherent integration time and the frequency bin width with respect to the aiding receiver and exploit the Doppler information aid to directly reduce the number of frequency bins in the acquisition search space. The example of Fig.4.5 shows the acquisition parameters [50] and illustrates how the Frequency Search Space (FSS) can be reduced thanks to the Doppler information aid. As illustrated in Fig.4.5, the aiding receiver FSS_1 is composed by the summation of the satellite Doppler ($f_{D_{sat}} = \pm 4.2$ kHz), the term concerning the Local Oscillator frequency offset from its nominal value

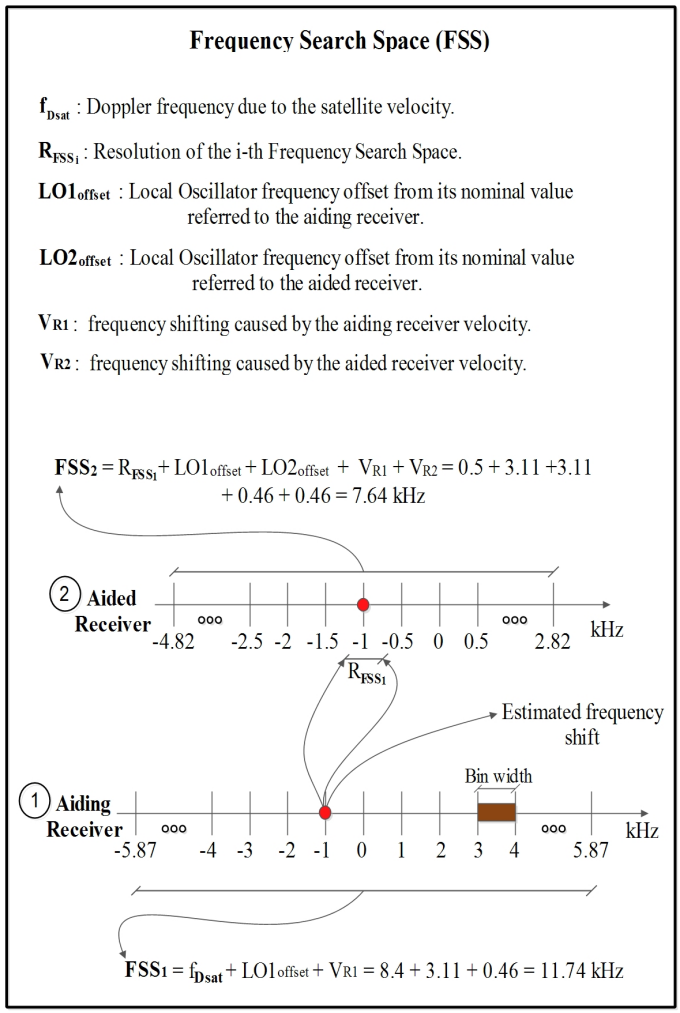


Figure 4.5: frequency search space reduction for the aided receiver acquisition thanks to the Doppler information aid.

($LO1_{offset} = \pm 1.555$ kHz) and the frequency shift which is caused by the receiver velocity ($V_{R1} = \pm 0.23$ kHz). The resulting FFS_1 is equal to 11.74 kHz. In this case the acquisition correlation peak of the aiding receiver is assumed to be experienced at -1 kHz. This value is transmitted to the aided

receiver which can reduce its FFS_2 which turns out to be the summation of the resolution of the $FFS_1 = \pm 0.5$ kHz, the terms concerning the Local Oscillator frequency offset from its nominal value referring to both the receivers ($LO1_{offset} + LO2_{offset} = \pm 1.555 \pm 1.555$ kHz) and the frequency shift that is originated by the velocities of both the receivers ($V_{R1} + V_{R2} = \pm 0.23 \pm 0.23$ kHz). As a result the FSS_2 becomes equal to 7.64 kHz($FSS_2 = 0.65 * FSS_1$). In conclusion, we can assert that the P2P-CP is advantageous in the acquisition process for several reasons: the information that is provided by the aiding receiver allows the aided receiver to perform the acquisition process for a limited number of satellites, i.e., the ones that are indicated by the aiding receiver, and reduce the FSS with a time save in the acquisition procedure. Note that in order to limit the losses in the post-correlation SNR, a longer coherent integration time has to be balanced by a narrower frequency bin width, as described by [56] and depicted in Fig.4.4.

4.5 Time Synchronization

Since Cooperative Positioning is based on the exchange of time-sensitive information between peers, the time synchronization ends up being a fundamental issue to be dealt with. As described in the previous paragraph, the positioning algorithms which are considered in this work and developed for the assisted GPS receiver can resort to a fine or a coarse time synchronization. As far as this issue is concerned, the time synchronization requirements between the cooperative receivers are different depending on the considered operations, namely the Acquisition and the Positioning Algorithms [50], as represented in the scheme of Fig.3.8.
The acquisition procedure is considered to operate under fine-time synchronization if the time error between the clocks of the aiding and the aided receivers is less than 1ms: this choice allows to reduce the time search space in the aided receiver acquisition procedure. Since the considered acquisition algorithms rely on the use of the outputs of the FFT and the IFFT blocks, as shown in Fig.4.2, the time correlation synchronization is only performed in the fine case for the identification of the bit transition in the navigation message: as a matter of facts, this operation permits to enhance the receiver sensitivity by increasing the coherent integration time. Moreover, the navigation message detection allows to compute the position of the satellites at the transmission time. Since the satellite-receiver range changes at a rate

Table 4.2: Acquisition and positioning synchronization constraints

	fine-time	**coarse-time**
Acquisition	$err_{sync} < 1ms$	$err_{sync} \geq 1ms$
Positioning	$err_{sync} < 10ms$	$err_{sync} \geq 10ms$

of up to ±800 m/s, a time synchronization error of 10 ms may affect the satellite position with an error whose value could be up to 8 m. As a first fix is preferably within the range of acceptable accuracy, the 10 ms value is considered as a nominal cut-off point for precise time algorithm adoption in navigation [4, 12]. The Table 4.2 summarizes the time synchronization requirements for the aided receiver.
At the time being, the fine-time positioning synchronization is not possible through Wi-Fi protocol, until the new 802.11 chips implementing the amendment (v) will become available so permitting accurately synchronized clocks. On the other hand a software-based synchronization does not guarantee an accurate timing. In the present work, a fine-time synchronization is implemented assuming an initial common view [78] of at least one satellite. For what concerns coarse-time synchronization, Network Time Protocol (NTP) may be a possible solution. NTP is one of the most popular protocols for internet time synchronization: it is used to synchronize the computer clocks within a network to a common reference: therefore, it allows to achieve synchronization between a trusted time-server and its clients [42]. On a local area network, NTP can achieve a precision of tens of milliseconds. The synchronization architecture uses a stratum concept [42], where each server on one level (stratum) is a time reference to lower levels. Primary servers are set at the root of the tree as stratum 1 and they are synchronized to external precise clock reference. Note that in Wireless LAN, multipath effects may contribute to the physical level jitter; therefore, when dealing with WLAN, the synchronization protocols may show worse performance than in wired LAN.

4.6 Experimental Setup

As anticipated in the previous paragraphs, the peer-to-peer cooperative algorithm with coarse/fine time acquisition and positioning is implemented on GPS software-defined receivers. The cooperation is carried out between two close GPS software receivers, namely the aiding and the aided receivers. The aiding receiver is a stand-alone GPS software receiver which is implemented in MATLAB [17]: it is able to perform acquisition (through a fast parallel acquisition technique, in which the correlation function is evaluated by means of FFT operations), code and carrier tracking, navigation bit extraction, navigation data decoding, pseudorange estimations, and position computations. Also the aided GPS receiver is implemented in MATLAB and performs assisted acquisition and positioning algorithms with fine/coarse time assistance. In this experiment, both the software receivers run over common laptops and process data which are sampled at 16.368 MHz. The sampled data are achieved from a front-end module, i.e., Sige GN3S v3 [31], which is connected via USB to the laptops. The front-end processes the



(a) (b)

Figure 4.6: a) Outdoor-to-Indoor scenario. The green and red stars represent the aiding GPS receiver located outdoor and the indoor aided one, respectively. b) Outdoor-to-Outdoor scenario. Both the aiding (green star) and the aided (yellow star) receivers are located outdoor.

satellite signals (L1 GPS signal at 1575.42 MHz) that is received by a GPS patch antenna: a sampled output is provided after filter, amplifier, mixer and ADC operations. The receivers are connected through an ad-hoc Wireless LAN that allows to exchange assistance and synchronization data. In

the coarse time context, both the receivers run a background application implementing an NTP protocol which is used for coarse synchronization. The aiding receiver is a time server while the aided one is considered to be the client. The scenarios which are considered in this work are illustrated in Fig.4.6. Particularly, Fig.4.6(a) represents the O2I case: the aiding receiver is located outdoor (above the roof top), about 8 meters far from the aided receiver, which is located indoor (below the roof top). On the other hand, the Fig.4.6(b) illustrates the O2O scenario, where both the aiding and the aided receivers are located outdoor in LOS condition, at a mutual distance of about 30 meters. Four tests will be performed for each O2I/O2O scenario; moreover, two synchronization time levels will be considered for each test: the former refers to an off-line ideal synchronization between the aiding and the aided receivers in the context of fine-time assistance, while the latter considers the coarse-time assistance, i.e., the receivers are synchronized by means of the NTP protocol.

4.7 Experimental Result

The results of the performed acquisition and positioning tests are described in Tables 4.3, 4.4, 4.5, 4.6. Each table refers to a particular satellite configuration and to specific O2I/O2O scenarios and illustrates the Pseudo-random Noise (PRN) sequences and the SNR levels that are relative to the four satellite geometries which are acquired by the aided receiver. The statistical descriptions of the positioning errors in the east and north directions are also shown: it is worth highlighting that 100 trials have been performed for each configuration and that the average of the obtained results are presented. For sake of space, the following subsections only refer to the first tests of Table 4.3 and are used to assess the satellite signal acquisition, the computational load in the acquisition procedure and the performance concerning the receiver position accuracy and Time-to-First-Fix.

4.7.1 Satellite signal acquisition assessment

Outdoor-to-Indoor (O2I) aiding scenario: the aiding receiver performs acquisition and tracking in the stand-alone mode: the acquisition results are shown in Fig.4.7(a). The receiver acquires the 2, 4, 5, 7, 8, 10, 13, 16 and 23 satellites by means of an 1 ms coherent integration and

Table 4.3: Aided receiver acquisition and positioning results - test n.1.

N.Test	**Outdoor-to-Indoor (fine-time)**						
1	**PRN**	2	7	8	10	13	23
	SNR	2.3	6	17.9	9.2	14.9	7.8
	STATs	$E[e_{East}] = 5.6$ m , $\sigma_{e_{East}} = 3.4$ m					
		$E[e_{North}] = 6.2$ m , $\sigma_{e_{North}} = 3.1$ m					
	Outdoor-to-Indoor (coarse-time)						
	PRN	2	7	8	10	13	23
	SNR	2.2	5.1	11.1	5.8	10.2	5.9
	STATs	$E[e_{East}] = 6.7$ m , $\sigma_{e_{East}} = 4.1$ m					
		$E[e_{North}] = 7.2$ m , $\sigma_{e_{North}} = 4.7$ m					
	Outdoor-to-Outdoor (fine-time)						
	PRN	2	4	5	7	8	10
	SNR	2.5	2.9	3.3	6.7	6.1	5
	STATs	$E[e_{East}] = 3.3$ m , $\sigma_{e_{East}} = 2.4$ m					
		$E[e_{North}] = 2.6$ m , $\sigma_{e_{North}} = 2.8$ m					
	Outdoor-to-Outdoor (coarse-time)						
	PRN	2	4	5	7	8	10
	SNR	2.7	3.1	3.5	6.5	5.9	5.1
	STATs	$E[e_{East}] = 4.4$ m , $\sigma_{e_{East}} = 3.6$ m					
		$E[e_{North}] = 3.1$ m , $\sigma_{e_{North}} = 4.3$ m					

Table 4.4: Aided receiver acquisition and positioning results - test n.2.

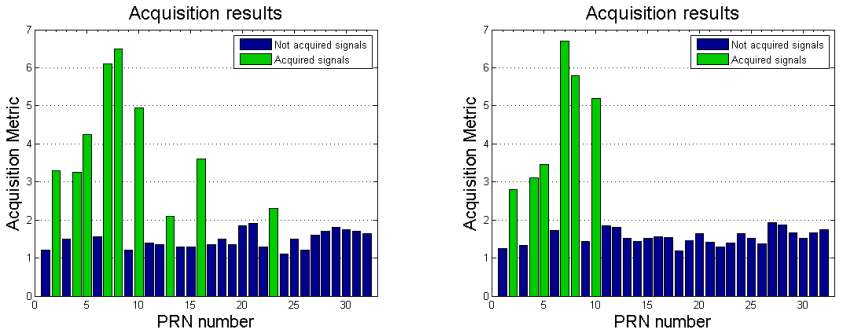
N.Test	Outdoor-to-Indoor (fine-time)					
2	**PRN**	2	12	24	25	29
	SNR	5.5	15.5	2.4	16.2	6.7
	STATs	$E[e_{East}] = 6.1$ m , $\sigma_{e_{East}} = 3.2$ m				
		$E[e_{North}] = 7.1$ m , $\sigma_{e_{North}} = 3.8$ m				
	Outdoor-to-Indoor (coarse-time)					
	PRN	2	12	24	25	29
	SNR	4.1	11.2	2.1	12.9	5.6
	STATs	$E[e_{East}] = 7.7$ m , $\sigma_{e_{East}} = 4.9$ m				
		$E[e_{North}] = 8.1$ m , $\sigma_{e_{North}} = 5.2$ m				
	Outdoor-to-Outdoor (fine-time)					
	PRN	12	13	15	17	24
	SNR	4.8	3.9	4.2	3.1	7.3
	STATs	$E[e_{East}] = 3.9$ m , $\sigma_{e_{East}} = 2.8$ m				
		$E[e_{North}] = 3.3$ m , $\sigma_{e_{North}} = 2.9$ m				
	Outdoor-to-Outdoor (coarse-time)					
	PRN	12	13	15	17	24
	SNR	4.3	4.2	5.3	3.9	7.6
	STATs	$E[e_{East}] = 4.7$ m , $\sigma_{e_{East}} = 4.1$ m				
		$E[e_{North}] = 4.5$ m , $\sigma_{e_{North}} = 4.4$ m				

Table 4.5: Aided receiver acquisition and positioning results - test n.3.

N.Test	**Outdoor-to-Indoor (fine-time)**						
3	**PRN**	14	18	19	21	22	27
	SNR	2.3	9.5	7.5	2.4	12.5	15.9
	STATs	$E[e_{East}] = 4.9$ m , $\sigma_{e_{East}} = 2.8$ m					
		$E[e_{North}] = 5.5$ m , $\sigma_{e_{North}} = 3.5$ m					
	Outdoor-to-Indoor (coarse-time)						
	PRN	14	18	19	21	22	27
	SNR	2.1	7.5	4.2	2	8.3	11.1
	STATs	$E[e_{East}] = 6.2$ m , $\sigma_{e_{East}} = 3.6$ m					
		$E[e_{North}] = 7.2$ m , $\sigma_{e_{North}} = 3.9$ m					
	Outdoor-to-Outdoor (fine-time)						
	PRN	4	11	19	22	27	32
	SNR	3.5	2.8	7.4	4.1	4.9	5.3
	STATs	$E[e_{East}] = 1.9$ m , $\sigma_{e_{East}} = 3.1$ m					
		$E[e_{North}] = 2.6$ m , $\sigma_{e_{North}} = 2.5$ m					
	Outdoor-to-Outdoor (coarse-time)						
	PRN	4	11	19	22	27	32
	SNR	3.9	3.5	7.9	2.9	5.6	4.5
	STATs	$E[e_{East}] = 3.5$ m , $\sigma_{e_{East}} = 2.9$ m					
		$E[e_{North}] = 3.8$ m , $\sigma_{e_{North}} = 3.1$ m					

Table 4.6: Aided receiver acquisition and positioning results - test n.4.

N.Test	Outdoor-to-Indoor (fine-time)					
4	**PRN**	16	18	20	21	22
	SNR	15.7	12.9	4.1	8.5	3.2
	STATs	$E[e_{East}] = 7.2$ m , $\sigma_{e_{East}} = 4.4$ m				
		$E[e_{North}] = 6.5$ m , $\sigma_{e_{North}} = 4.1$ m				
	Outdoor-to-Indoor (coarse-time)					
	PRN	16	18	20	21	22
	SNR	10.1	6.9	3.2	4.5	2.2
	STATs	$E[e_{East}] = 8.3$ m , $\sigma_{e_{East}} = 4.5$ m				
		$E[e_{North}] = 8.5$ m , $\sigma_{e_{North}} = 4.7$ m				
	Outdoor-to-Outdoor (fine-time)					
	PRN	18	21	25	29	31
	SNR	2.2	8.3	3.1	5.3	6.2
	STATs	$E[e_{East}] = 2.9$ m , $\sigma_{e_{East}} = 2.2$ m				
		$E[e_{North}] = 3.3$ m , $\sigma_{e_{North}} = 3.4$ m				
	Outdoor-to-Outdoor (coarse-time)					
	PRN	18	21	25	29	31
	SNR	2.4	7.6	3.4	5.2	5.9
	STATs	$E[e_{East}] = 5.1$ m , $\sigma_{e_{East}} = 2.4$ m				
		$E[e_{North}] = 4.6$ m , $\sigma_{e_{North}} = 3.4$ m				



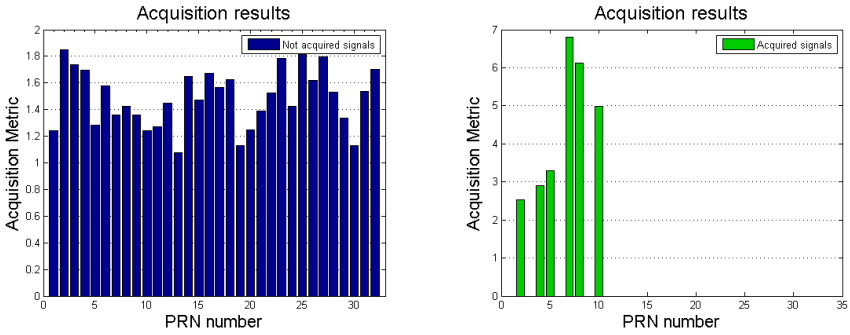
(a) (b)

Figure 4.7: a) Aiding receiver acquisition results, one ms coherent integration, one non-coherent integration, O2I scenario. b) Aiding receiver acquisition results, 1 ms coherent integration, one non-coherent integration, O2O scenario.

of an 1ms non-coherent integration. The green bars in Fig.4.7(a) refer to the acquired satellites. Each single peak represents the ratio between the highest and second highest peak in the correlation performed over the code delay-frequency search space for each satellite.
Assuming fine-time assistance condition, the aided receiver performs an assisted acquisition thanks to the following information which is broadcasted by the aiding receiver:

- Satellite IDs for the visible satellites;
- Doppler frequency relative to each satellite (to reduce the frequency search space in the acquisition process);
- Time stamp of the first sub-frame of the navigation message (to identify the bit transition time).

The aided receiver will try to acquire only the satellites which are indicated by the aiding receiver. As shown in Fig.4.8(a), it is not able to acquire satellites with a 1 ms coherent integration and one non coherent integration since the received signal is weak because of the indoor location: particularly, the post-correlation procedure that is illustrated in Fig.4.2 produces a value of n α_{max} (4.9) that is lower than the threshold $\alpha_{Tsh} = 2$ which has been chosen

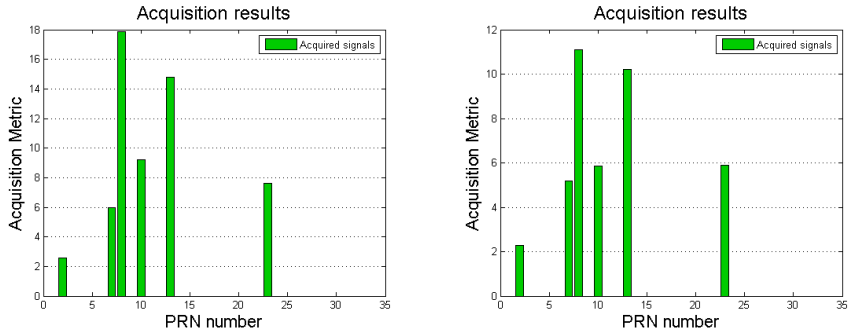


(a) (b)

Figure 4.8: a) Aided receiver acquisition results, 1 ms coherent integration, one non-coherent integration, O2I scenario. b) Aided receiver acquisition results, 1 ms coherent integration, one non-coherent integration, O2O scenario.

as a design parameter and used for all the considered satellites. Therefore, the receiver sensitivity has to be improved. [36] In the fine-time acquisition case, the aided receiver gets to know precisely when the bit transitions of the navigation message occur. Thus, it can wipe off the signal from the navigation message end extend the coherent integration period to increase the receiver sensitivity. Hence, by considering 100 ms as the overall integration time[2], the coherent integration time is set equal to 20 ms while 5 non-coherent integrations are performed: as a result, the $\alpha_{max} > 2$ constraint is respected for all the six satellites that are identified in Fig.4.9(a). In this study the $sinc(\Delta \bar{f}_{d_m} T_{int})$ term has been defined by assuming that $\Delta f_D = \frac{1}{2T_{int}}$: hence, the loss factor is less than or equal to $|sinc(0.5)|^2 = 0.4$. The acquisition results with the new integration parameters are shown in Fig.4.9(a). When a fine-time synchronization cannot be realized, the acquisition procedure has to resort to a coarse-time approach. In this case, the aiding receiver performs the same tasks as in the fine-time assistance case; the main difference concerns the aiding information: in this case the time stamp of the first sub-frame of the navigation message is not broadcasted. Therefore, the coherent integration time of the aided receiver has to be ex-

[2] A 100 ms integration time is chosen since during this long interval the satellite-receiver dynamic changes are not considerably affecting the signal acquisition.



(a) (b)

Figure 4.9: a) Aided receiver acquisition results, 20 ms coherent integration, 5 non-coherent integrations, fine time assistance, O2I scenario. b) Aided receiver acquisition results, 11 ms of coherent integration, 9 non-coherent integrations, coarse time assistance, O2I scenario.

tended to a shorter interval than in the fine-time assistance because of the uncertainty about the bit transitions in the navigation message. In the signal acquisition routine, the coherent integration time has been set equal to 11 ms while 9 non-coherent sums are considered to keep a total integration time of about 100 ms. Once again, the coherent integration procedure leads to a post-correlation loss factor equal to 0.4 since the $(\Delta \bar{f}_{d_m} T_{int})$ product is unchanged with respect to the fine-time case. The acquisition results are shown in Fig.4.9(b).

Outdoor-to-Outdoor (O2O) aiding scenario: the aided receiver acquisition procedure does not need to take advantage of fine-time assistance to increase its sensitivity; this is not surprising since, thanks to the LOS condition of the satellites, the aided receiver does not need an extension of the coherent integration time. As described in the example depicted in Fig.4.5, the aided receiver can directly exploit the Doppler information to reduce the number of bins and, consequently, the complexity of the receiver acquisition. It is important to note that the Doppler information that is provided by the aiding receiver is related to the resolution of the frequency search space that is determined by the acquisition and illustrated in Fig.4.5. In all

the considered tests, the resolution of the aiding receiver frequency search space is equal to 500 Hz which becomes the initial space in the aided receiver frequency search space. In both fine and coarse time assistance cases, the aiding receiver performs acquisition and tracking in stand-alone mode with the results that are depicted in Fig.4.7(b): by means of 1 ms coherent and 1 non-coherent integrations, the receiver acquires the 2, 4, 5, 7, 8 and 10 satellites. The aided receiver performs the assisted acquisition thanks to the received information which is the same of the O2I scenario. The integration parameters are equal to 1 ms for both the coherent and the non-coherent parts. The acquisition results are shown in Fig.4.8(b).

4.7.2 Computational load assessment in the signal acquisition procedure

Outdoor-to-Indoor (O2I) aiding scenario: in order to compare the computational load of the acquisition of both the aided and the aiding receivers, we consider the number of bins in the frequency search space. The overall frequency search space in the aided acquisition is defined by the following parameters:

- assistance reference-frequency uncertainty which is given by the sum of the frequency search space resolution ($R_{FSS-aiding}$) and the local oscillator frequency offset ($LO_{offset-aiding}$), both referred to the aiding receiver case;
- local oscillator frequency offset of the aided receiver ($LO_{offset-aided}$);
- time assistance;
- a-priori position (aiding receiver position);
- Doppler frequency due to the satellite-aiding/aided receiver relative velocity.

We can ignore the last three uncertainties by assuming that the receivers are not moving and their distance is less than 1 km [50]. Considering the tolerance of the front-end TCXO (Temperature Compensated Crystal Oscillator)

equal to ±1 ppm either for the aided or aiding receiver, the aided receiver frequency search space (FSS_{aided}) is given by:

$$\begin{aligned} FSS_{aided} &= R_{FSS-aiding} + LO_{offset-aiding} \\ &+ LO_{offset-aided} = 0.5 + 3.11 + 3.11 \\ &= 6.72 * 10^3 kHz. \end{aligned} \tag{4.10}$$

Hence, in the fine time synchronization case, the frequency bin width in the acquisition frequency search space of the aided receiver can be determined as:

$$FW = \frac{\frac{1000}{CIT}}{2} = \frac{\frac{1000}{20}}{2} = 25\ Hz, \tag{4.11}$$

where CIT is the coherent integration time and FW is the frequency width. Therefore, the number of frequency bins for the aided receiver acquisition is:

$$\begin{aligned} &N_{\text{BIN}}(AidedReceiver)_{\text{Fine-time}} = \frac{FSS_{aided}}{FW} = \\ &= \frac{6.72 * 10^3}{25} = 268\ bins. \end{aligned} \tag{4.12}$$

On the other hand, the number of frequency bins for the aiding receiver acquisition is equal to:

$$\begin{aligned} &N_{\text{BIN}}(AidingReceiver)_{\text{Fine-time}} = \frac{FSS_{aiding}}{FW} = \\ &= \frac{8.4 * 10^3 + 3.1 * 10^3}{500} = 23\ bins, \end{aligned} \tag{4.13}$$

where $8.4 * 10^3$ Hz is the frequency range due to the Doppler effect of satellite motion and 500 Hz is the frequency bin width resulting from 1 ms coherent integration. For what concerns the computation load, by taking into account the number of bins to be scanned during the acquisition procedure, we can conclude that the aided receiver acquisition is about 11 times more complex than the aiding one. In the case of coarse time synchronization, the number of frequency bins in the search space of the aiding receiver acquisition is equal to 23, as in the fine-time assistance test. Conversely, the number of frequency bins for the aided receiver is:

$$\begin{aligned} &N_{\text{BIN}}(AidedReceiver)_{\text{Coarse-time}} = \frac{FSS_{aided}}{FW} = \\ &= \frac{6.72 * 10^3}{45} = 150\ bins, \end{aligned} \tag{4.14}$$

where 45 Hz is the frequency bin width which is defined by the choice of the coherent integration equal to 11 ms. By considering the number of bins to be scanned during the acquisition process, we can conclude that the aided receiver acquisition lasts about 6 times more than in the aiding one.

Outdoor-to-Outdoor (O2O) aiding scenario: if a 1ms coherent-time integration and 1 non-coherent integration are considered, the number of frequency bins for the aided receiver acquisition, either in the fine or in the coarse-time assistance case, is computed as follows:

$$N_{\text{BIN}}(AidedReceiver)_{\text{Fine/Coarse-time}} = \frac{FSS_{aided}}{FW} = \\ = \frac{6.72 * 10^3}{500} = 13\ bins, \tag{4.15}$$

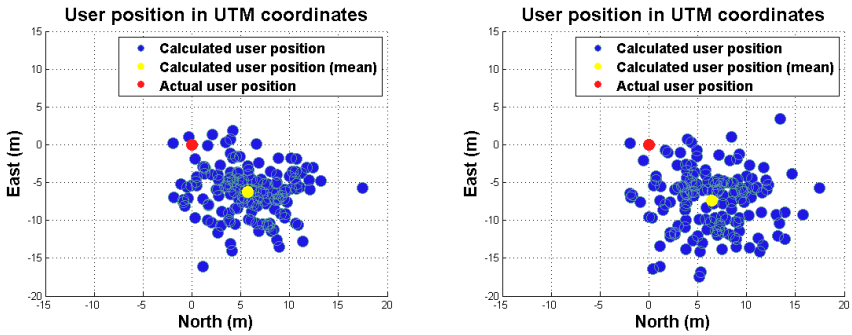
where 500 Hz is the frequency bin width resulting from the 1 ms coherent integration time. The number of bins in the aiding receiver acquisition can be considered the same as in (4.12). In conclusion, in the O2O aiding scenario, the aided receiver acquisition time is about 2 times smaller than the aiding receiver acquisition one.

4.7.3 Performance assessment: position accuracy and Time-to-First Fix

Outdoor-to-Indoor (O2I) aiding scenario: while the aiding receiver performs the usual stand-alone positioning procedure, the aided one takes benefit from the following information that is broadcasted by the aiding terminal:

- position of the aiding receiver;
- navigation message (Ephemeris and almanac in order to compute the satellite position at the transmission time, ionospheric model and satellite clock corrections).

Once the aided receiver has accomplished the acquisition, the sub-ms pseudoranges are available. After the integer millisecond ambiguity is eliminated, the complete pseudoranges for the aided receiver are determined together



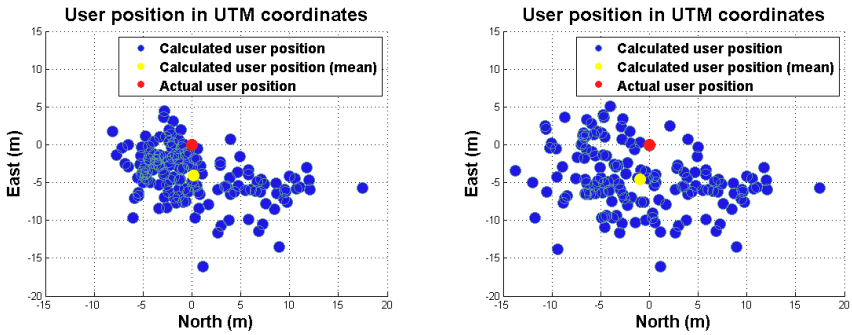
(a) (b)

Figure 4.10: a) Aided receiver position with fine-time assistance in O2I scenario. b) Aided receiver position with coarse-time assistance in O2I scenario.

with the satellite position at the transmission time thanks to the ephemeris knowledge. If fine time assistance is guaranteed, the position of the aided receiver is determined by means of Extended Kalman Filter (EKF) method (using the position of the aiding terminal as a-priori position [28]). The positioning procedure results are shown in Fig.4.10(a), while the statistical description (STATs) that are represented in Table 4.3 reports the mean error and the standard deviation which are relative to East and North axes.

On the other hand, when the coarse time synchronization takes place, the aiding receiver performs the positioning procedure in a stand-alone mode and broadcasts the same aiding quantities to the aided receiver as in the fine-time assistance case. After the aiding information has been received, the aided receiver computes the complete pseudoranges; then, since coarse time assistance is supposed, the time error has to be compensated to avoid satellite position errors. The compensation is performed by computing the pseudorange rates (for each satellite-receiver link) and including them in the geometry matrix [50]; afterwards, the five-state updates are computed using the EKF method. The position results are shown in Fig.4.10(b), while Table 4.3 reports the performance which is relative to East and North axes in terms of mean error and standard deviation. The position error is larger than in the fine-time assistance case mostly because of two reasons:

- in the coarse-time tests the SNRs that are relative to the acquired satellites (depicted in Fig.4.9(b)) are lower than in the fine-time assistance



(a) (b)

Figure 4.11: a) Aided receiver position with fine-time assistance in O2O scenario. b) Aided receiver position with coarse-time assistance in O2O scenario.

case (depicted in Fig.4.9(a)),

- in the coarse-time tests the pseudorange rates are included in the geometry matrix, leading to an Horizontal Dilution of Precision degradation [50].

For what concerns the computational load of the positioning procedure, it is important to note that the provision of the navigation message leads to a drastic reduction of the TTFF for the aided receiver in both coarse and fine time assistance.

Outdoor-to-Outdoor (O2O) aiding scenario: the position results for both fine and coarse time assistance tests, are shown in Fig.4.11, while Table 4.3 reports the performance which is relative to the East and North axes in terms of mean error and the standard deviation. Also in the O2O scenario, the fine-time positioning is more accurate than the coarse-time one while the computational loads of the positioning procedure, either in presence of fine or coarse time assistances, are comparable with the ones of the O2I case. As in the O2I scenario, the provided information allows the aided receiver to take advantage of the TTFF reduction.

4.8 Conclusion

In this Chapter we evaluated the benefits and the disadvantages of the cooperation between peers in the positioning algorithms, by focusing on the effects of the time synchronization on the acquisition and positioning procedures. In particular, we considered two GPS software receivers which have been implemented in MATLAB and cooperate in both the O2I and the O2O scenarios. For each of them we assessed the satellite signal acquisition effectiveness, the computational load in the signal acquisition procedure and the performance in terms of position accuracy and Time-to-First Fix in the positioning routine.
In the O2I aiding scenario, the indoor aided receiver has to improve its sensitivity, causing a computational load increase in the acquisition process, either in presence of fine or coarse time assistance. The positioning results confirm that the aided receiver position with fine-time is more accurate than the coarse-time.
In O2O aiding scenario, the outdoor aided receiver does not need to strongly increase its sensitivity. Therefore, it can directly exploit the aiding information to reduce the TTFF, even in the acquisition process, either in presence of fine or coarse time assistance. The fine-time positioning is more accurate than coarse-time positioning (as in the O2I scenario) and the computational loads of the positioning procedures are comparable to the O2I scenario ones.

Chapter 5

Dead Reckoning

This chapter gives an overview of dead reckoning navigation. The problem of determining the orientation and distance traveled by the navigation vehicle is considered. Finally, techniques for height and depth measurements are described.

5.1 Introduction

In navigation, a dead reckoning (DR) system either measures the change in position or measures the velocity and integrates it. This information is added to the previous position to obtain the current position [22]. A DR system can determine the changing in position or the velocity by processing data collected by sensors, which are usually in a strapdown configuration, i.e. rigidly attached to the navigation vehicle. A DR system is self-contained aboard the navigation vehicle without relying on external infrastructure. This characteristic makes DR navigation very attractive for those applications like military and emergency rescue operations, in which external infrastructures cannot be deployed. The DR approach assumes that the actual position is dependent on the previous one, therefore the position errors tend to grow epoch by epoch, as shown in Fig.5.1. However, either environmental features or signal-based positioning system can be used to calibrate the navigation solution. Inertial sensors, as well as magnetometer and barometric pressure sensors, can be used in dead reckoning application to determine the traveled distance, the heading and the variation in height performed by the navigation vehicle.

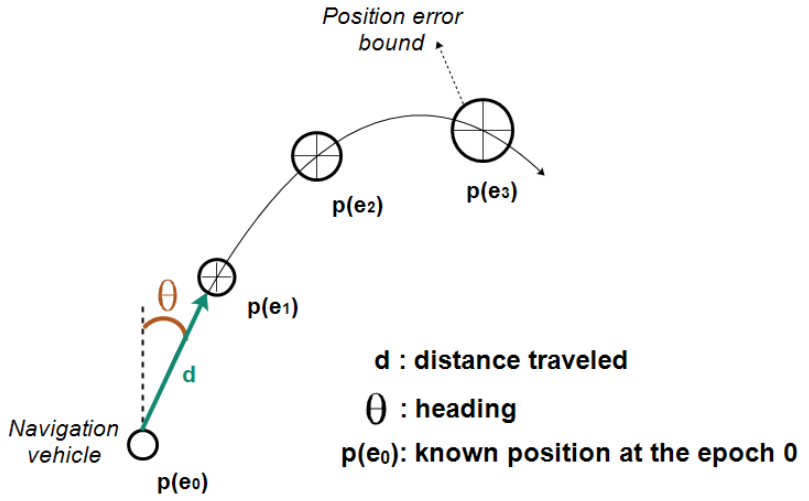


Figure 5.1: dead reckoning positioning.

5.2 Distance measurement

An inertial navigation system (INS) is a complete three-dimensional DR navigation system: it comprises an inertial measurement unit (IMU), which includes a tri-axial accelerometer and gyroscope, and a navigation processor, as shown in Fig.5.2. An INS-based DR system measures the traveled distance by integrating the velocity, which in turn, is determined by integrating of the acceleration [22]. In the navigation processing, the integration of the accelerometer and gyroscope biases produces errors that grow with time. In addition, the attitude errors contribute to the velocity and position errors [22]. Moreover, INS error propagation is affected also by the host vehicle trajectory. For this reasons, a double-integration provided by the INS systems generally requires additional sources to calibrate the navigation solution. In newer application, such as light aircraft, unmanned air vehicles, mobile mapping, and pedestrians, low-cost on low cost micro-electro mechanical system (MEMS) sensors [74] are typically used and the INS is part of INS/GNSS integrated navigation systems [22].
In the case of particular applications, such as pedestrian navigation, inertial sensors are used for detecting steps and estimating the step length. A pedestrian dead reckoning system comprises three phases: step detection,

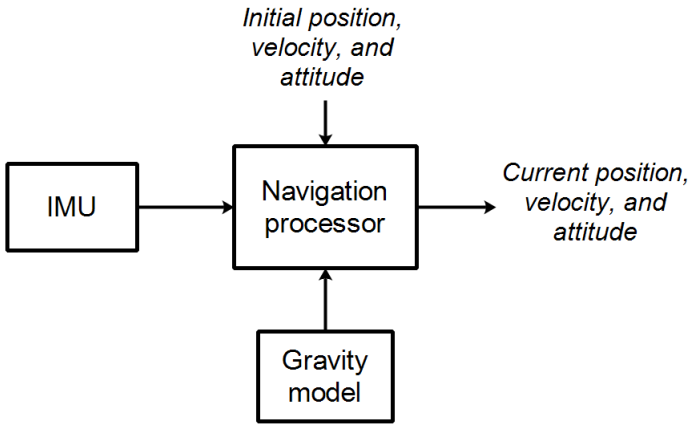


Figure 5.2: inertial navigation system [22].

step length estimation and position update, as shown in Fig.5.3. During a pedestrian motion activity like walking, a body-worn accelerometer generates a periodic signal pattern, as shown in Fig.5.4. The step detection routine aims to detect when steps occur typically using peak detection algorithms [61, 75]. The step length estimation algorithms generally exploit empirical relations to relate the data information collected by sensors to the

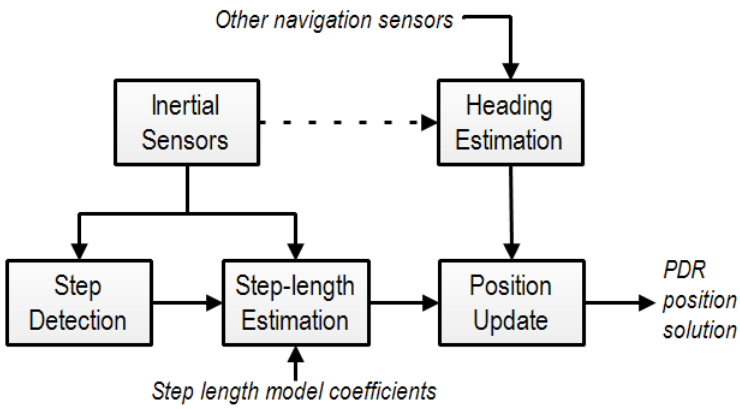


Figure 5.3: dead reckoning process [22].

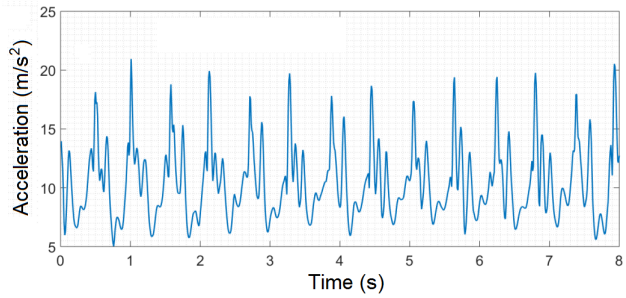


Figure 5.4: acceleration pattern generated by a body-worn accelerometer during a walking activity.

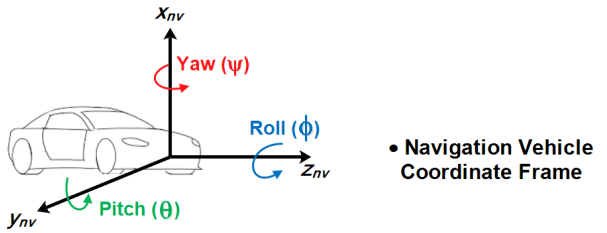
step length [29, 40, 55, 66].

5.3 Attitude measurement

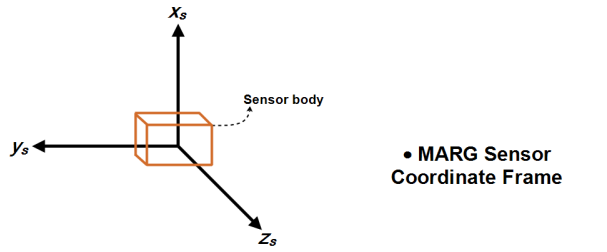
The attitude measurement provides information about the object's orientation. It defines three angles: yaw (ψ), pitch (θ) and roll (ϕ), which represent the orientation of the vehicle coordinate frame with respect to a reference coordinate frame. Fig.5.5 illustrates an example of car navigation scenario using a magnetic, angular rate and gravity (MARG) sensor in a strapdown configuration: the sensor coordinate frame (x_s, y_s, z_s) is aligned with the vehicle coordinate frame (x_{nv}, y_{nv}, z_{nv}). A MARG sensor comprises an IMU together with a magnetic compass. The east north up (ENU) coordinate system is considered as the reference frame: it is a geographical coordinate system which is useful to describe local movement along the Earth's surface. The ENU frame defines a 3-axes orthogonal system: the east axis points to the east direction, the north axis points to the geodetic north and the up axis points to the direction perpendicular to the Earth's surface, as illustrated in Fig.5.5. In a car navigation scenario, a magnetic compass sensor can be used to determine the heading of the car with respect to the magnetic north, as shown in Fig.5.6. The yaw angle (Ψ) is computed as follows:

$$\Psi = arctan_2\begin{pmatrix} -m_y cos\Phi + m_z sin\Phi, \\ m_x cos\Theta + m_y sin\Theta sin\Phi + m_z cos\Phi sin\vartheta \end{pmatrix}, \tag{5.1}$$

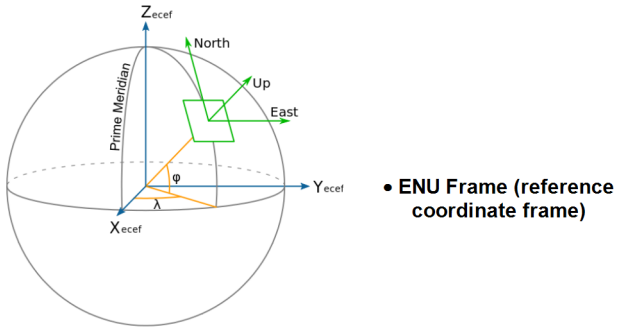
!



(a)



(b)



(c)

Figure 5.5: a) Body coordinate frame. b) Sensor coordinate frame. c) Reference coordinate frame.

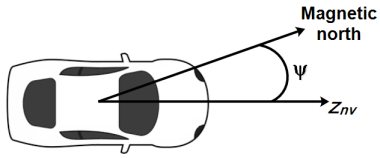


Figure 5.6: the specific directions of the gravity g and the specific force f.

where (m_x, m_y, m_z) is the total magnetic flux density along the sensor coordinate frame. Θ and Φ are the pitch and roll angles which refer respectively to the rotations about the y_{nv} and z_{nv} directions of the navigation vehicle coordinate fame:

$$\Theta = arctan\left(\frac{f_x}{\sqrt{f_y^2 + f_z^2}}\right), \tag{5.2}$$

$$\Phi = arctan_2(-f_y, -f_z), \tag{5.3}$$

where the (f_x, f_y, f_z) vector represents the specific force measured by the accelerometer in the body coordinate frame. Specific force is a non-gravitational force, sensed with respect to an inertial system. It is what the people and instruments sense: under zero acceleration the reaction to the gravity is sensed, and the specific force is equal and opposite the acceleration due to gravitation [22], as shown in Fig.5.7. The specific force is used to estimate

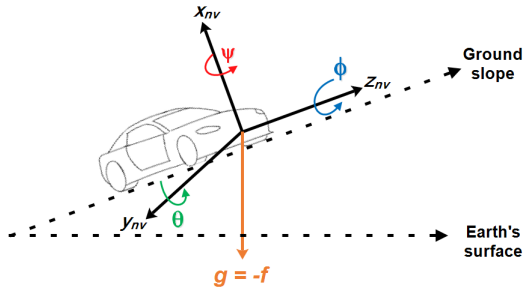


Figure 5.7: the specific force f is equal and opposite to the acceleration due to gravity g.

the pitch and roll angles as described in 5.2 and 5.3.

The gyroscope sensor is used to determine the angle rotation rate about the sensor body axes. In the car navigation scenario, since the y_{nv}-z_{nv} plane is approximately parallel to the road surface, a strapdown yaw-axis gyroscope can be used to detect the yaw rotation about the x_{nv}-axis.
MARG sensors are commonly used for attitude and heading reference system (AHRS) which provides 3-axes inertial attitude solution and it is generally used for low-cost aviation applications [22].

5.4 Height and Depth Measurements

The height measurements are crucial for aviation application as well as the depth measurements are fundamental for maritime scenarios.
The height determination is also important in pedestrian applications in order to determine at which floor the user is moving on. Barometric altimeter uses a barometer sensor to measure the air pressure and to calculate the height from the Earth's surface:

$$h_b = \frac{T_s}{k_T}\left[\left(\frac{p_b}{p_s}\right)^{-\frac{R*k_T}{g_0}} - 1\right] + h_s, \tag{5.4}$$

where p_s and T_s are respectively the surface pressure and the temperature which are measured at a reference geodetic height h_s, $R = 287.1$ J $\text{Kg}^{-1}\text{K}^{-1}$ is the gas constant, $k_T = 6.5 * 10^{-3}$ K m^{-1} is the atmospheric temperature gradient, and $g_0 = 9.80665$ m s^{-2} is the average surface acceleration due to gravity. For standard barometer, the reference geodetic height is the sea mean level [22].
On the other hand, the depth pressure sensor measures the water pressure p_b to determine the depth d_b at which the navigation vehicle is located:

$$d_b = h_b - h_s \approx \frac{p_b - p_s}{\rho * g}, \tag{5.5}$$

where h_s and h_b are respectively the geodetic heights of the water surface and pressure sensor, p_s is the atmospheric pressure at the water surface, ρ is the water density, and g is the acceleration due to the gravity. The water density is approximately 10^3 Kg m^{-3} and can vary as function of temperature and salinity [22].

Chapter 6

Probabilistic Context-aware Step Length Estimation for Pedestrian Dead Reckoning

This chapter proposes a weighted context-based step length estimation algorithm for pedestrian dead reckoning. Instead of computing the step length based on a single context, the step lengths computed for different step modes as a linear combination between a constant, the step frequency and the specific force variance, are weighted by the pedestrian context probabilities. This provides a more robust performance when the context is uncertain. A step detection algorithm detects the step time boundaries using continuous wavelet transform analysis. The context classification algorithm determines the pedestrian context probabilities using a relevance vector machine. Six step modes are considered: stationary, walking, walking sideways, climbing and descending stairs, and running. A dataset of pedestrian activities and actions has been collected. Fifteen subjects, which have been equipped with a waist-belt smartphone, traveled along a predefined path incorporating a range of different activities. Acceleration, angular rate and magnetic field data were recorded. The results show that the computed distance traveled is more accurate using weighed-context step lengths compared to using step lengths based on the highest context.

6.1 Introduction

The rapid growth of location-based services (LBS) over the past few years [1], led positioning and navigation to assume a significant role in people's daily lives. LBS mainly involve sectors like military, emergency services, and commercial [38]: they imply the use of smartphones and other mobile computing devices, which are commonly carried or worn by people. The pedestrian navigation techniques are used to determine the user position and allow the exploitation of LBS by mobile devices. Pedestrian navigation is one of the most challenging applications of navigation technology. It must work in environments where coverage of GNSS and most other radio signals used for navigation is poor. Inertial sensors can be used to measure pedestrian motion by dead reckoning, and micro electro-mechanical systems (MEMS) sensors are particularly suited for pedestrian navigation purposes: they are small, light and low cost [22]. Moreover, MEMS sensors are built-in to smartphones, which can be exploited for pedestrian navigation. However, MEMS sensors provide poor inertial navigation performance stand alone, while the combination of low dynamics and high vibration limits the calibration obtainable from global navigation satellite systems (GNSS) or other positioning systems [22].
Pedestrian dead reckoning (PDR) is a promising solution for pedestrian navigation by using inertial sensor [32, 35, 47]. A PDR system comprises three phases: step detection, step length estimation (SLE) and position-solution update, as shown in Fig.5.3. The step detection algorithm aims to identify when steps occur, while SLE determines the length of each detected step using sensor data. SLE works relatively well when walking in a straight line; however, real paths include turns, sidesteps, stairs, variations in speed, and various actions performed by the subject. These all affect the step length and must be considered to provide an accurate estimate of the distance traveled during daily activities as well as laboratory tests.
This work proposes a weighted context-based SLE algorithm in which the step lengths computed for different step modes are weighted by the pedestrian context probabilities. The proposed SLE algorithm is compared with other two SLE approaches: the highest context-based method, which considers the step lengths computed for the step mode corresponding to the context with the highest probability, and the single event-based method, which does not take the context probabilities into consideration, and determines the length of each step depending on the step mode classification

result. In order to determined the single step length, all considered SLE methods exploit the relation in which the step length can be expressed as a linear combination of a constant, step frequency and specific force variance [32, 39]. The SLE procedures are part of a PDR system which includes the step detection, the step mode classification, and the context classification algorithms, as illustrated in Fig.6.2. The step detection algorithm is based on the acceleration pattern analysis through the continuous wavelet transform (CWT) [44], which allows the detection and characterization of the signal singularieties originated by the step. The step mode classification algorithm aims to determined the step mode for each detected step and compares three methods: decision tree (DT) [68], support vector machine (SVM) [45, 75] and k-nearest neighbour (KNN) [37]. The context classification routine exploits the relevance vector machine (RVM) [9] to determine the pedestrian context probabilities over the context time window [18, 23], which may include several steps and different step modes.
A dataset of pedestrian activities and actions were collected. Fifteen subjects, which have been equipped with a waist-belt smartphone, traveled along a predefined path, shown in Fig.6.3. Acceleration, angular rate and magnetic field data were recorded at a 100 Hz sample rate by the relevant 3-axis MEMS sensors, which are integrated into the smartphone. Six step modes and pedestrian contexts are considered: stationary, walking, walking sideways, climbing and descending stairs, and running, as shown in Fig.6.1.
Section 6.2 reports the background and related work, while Section 6.3 describes the proposed approach and the dataset collection in detail. Sections 6.4 and 6.5 respectively characterize the step detection algorithm and the step mode and context classification techniques. Section 6.6 defines the SLE algorithms. Section 6.7 reports and discusses the results obtained for the step detection, the step mode classification, and the context classification techniques, and compares the total distance traveled by the subjects for each SLE algorithms. Finally, Section 6.8 presents the conclusions.

6.2 Backgound and Related Work

In PDR, the step detection procedure is commonly based on specific force data processing [43, 61], while angular rate information is less frequently used [69]; moreover, since the pedestrian motion is usually not aligned with the sensor coordinate frame, the signal magnitude is provided by the sensor

is considered. When focusing on step detection through the specific force signal analysis, the steps are revealed through detection techniques which depend on the on-body sensor location. In the case of foot-mounted sensors, step detection can easily be performed by identifying the stance and swing phases of the foot corresponding to zero velocity periods (ZVPs) [54,75].The latter approach cannot be applied when dealing with handheld, wrist- or waist-mounted sensors [2,61,75], since these configurations do not lead to a zero velocity period occurrence. In these cases zero-crossing (ZDT) or peak detection (PDT) can be adopted for the step detection routine. However, both PDT and ZDT may lead to revealing multiple steps when actually only one step occurs [75], leading to detection errors which can affect the resulting PDR navigation solution.

Step mode classification aims to recognize the type of motion activity the subject is performing, e.g walking or running. The classification routine extracts features [5,24] from the signals provided by body-worn sensors, e.g. accelerometer, gyroscope, barometer and magnetic field. Step mode classification is also dependent on the sensor location: the same movement may generate different signals for different on-body sensor locations. This is the reason that step mode and sensor location classification are frequently tied together [75] [69]. When dealing with PDR on the smartphone, the sensor location may also be related to the device pose which relates to particular actions the subject can perform: texting, calling, swinging or simply to keep the device in a pocket.

In order to reveal a particular activity in a certain time interval, the algorithms based on pedestrian activity classification use sensor data from multiple epoch over a sliding time window which is typically a few seconds long [68]. The classified activity can be exploited to get landmarks on building maps in order to calibrate the PDR routines particularly in locations such as stairs or elevator [57]. The signal information included in the time window, most likely does not refer to an individual step movement, but rather to a group of movements which may also involve different activities. The length of the time window affect the time response of the PDR system. The supervised learning field provides a number of classification algorithms adopted for step mode and sensor location classification: decision tree (DT), supervised vector machine (SVM), k-nearest Neighbour (KNN) [76] [24]; each of which presents different characteristics in terms of memory usage, fitting speed, prediction speed, and predictive accuracy [45]. Furthermore, the relevance

vector machine (RVM) is used for pedestrian context classification, in order to provide the context probabilities for each considered context class. [18,23].
Step length estimation has a significant impact on the performances of PDR systems and can be implemented through several approaches: regression-based [41, 65] , biomechanical model [29, 55] and empirical relationships [27,29]. Regression-based methods aims to model the step length as a linear combination of a constant, the step frequency, and the specific force variance during the step interval.
A Biomechanical model estimator relates the step length to the specific force measurement at the center of mass (COM) of the user. The vertical displacement of the COM during one step is calculated via double integration of the vertical acceleration while the COM is ascending.
Empirical relationships determine the step length estimates through mathematical expressions, which generally relate the step length to particular specific force parameters, which commonly correspond to the maximum and minimum, acceleration values measured within the step interval.

6.3 Proposed method and Dataset

The present work proposes a weighted context-based SLE algorithm in which the step lengths computed for different step modes are weighted by the pedestrian context probabilities; in particular, the single step lengths determined as a linear combination of a constant, the step frequency and the specific force variance, are weighted by the pedestrian context probabilities.
In this work, both the step mode and pedestrian context terms refer to pedestrian cyclic movements, e.g. walking and running; however, they assume different concepts: the step mode refers to an individual step, whereas the context refers to a wider time interval which may include several steps and different step modes. In particular, six step mode and pedestrian contexts are considered: stationary, walking, walking sideways, climbing and descending stairs, and running, as illustrated in Fig.6.1.
The proposed weighted context-based SLE is compared with other two SLE approaches: the highest context-based method, which considers the step lengths computed for the step mode corresponding to the context with the highest probability; and the single event-based, which does not take the context probabilities into consideration, and determines the length of each step

Context	C_1	C_2	C_3	C_4	C_5	C_6
Step Mode	m_1	m_2	m_3	m_4	m_5	m_6
Type	stationary	walking	walking upstairs	walking dowstairs	walking sideways	running

Figure 6.1: pedestrian contexts and step modes.

depending on the step classification result.
The SLE algorithms are part of a PDR framework which defines the procedures of step detection, step mode classification, and context classification, as shown in Fig.6.2 The step detection algorithm aims to identify the step time boundaries by performing the continuous wavelet transform (CWT) analysis of the specific force signal [**?**,46]. Both the step and the context classification algorithms rely on supervised learning techniques. The step classification algorithm compares the DT, SVM and KNN methods, and uses the one with best predictive accuracy, in order to classify the single detected step into several possible step modes. On the other hand, the context classification algorithm exploits the probabilistic RVM method and aims to classify a fix portion of data, which generally may include several steps, into several contexts, each with an associated probability. The considered step modes and contexts are illustrated in Fig.6.1.
In order to assess the performance of the proposed PDR system in a real scenario, a dataset of pedestrian activities were collected. Fifteen subjects in the 20-50 age range traveled along a predefined path, shown in Fig.6.3. The subjects have been equipped with a waist-belt smartphone Samsung Galaxy S4, as shown in Fig.6.4. Acceleration, angular rate and magnetic field data were recorded at a 100 Hz sample rate by the relevant 3-axis sensors, which are integrated into the smartphone. Six pedestrian activities, which correspond to the contexts and step modes shown in Fig.6.1, were performed. Moreover, the subjects were asked to perform specific actions during the test, in order to yield a realistic daily life scenarios. As shown in Fig.6.3, the actions are numbered from 1 to 5 and comprise:

1. Watching a notice board (Fig.6.5).
2. Entering an office and sitting down for a while (Fig.6.5).
3. Opening a door (Fig.6.5).

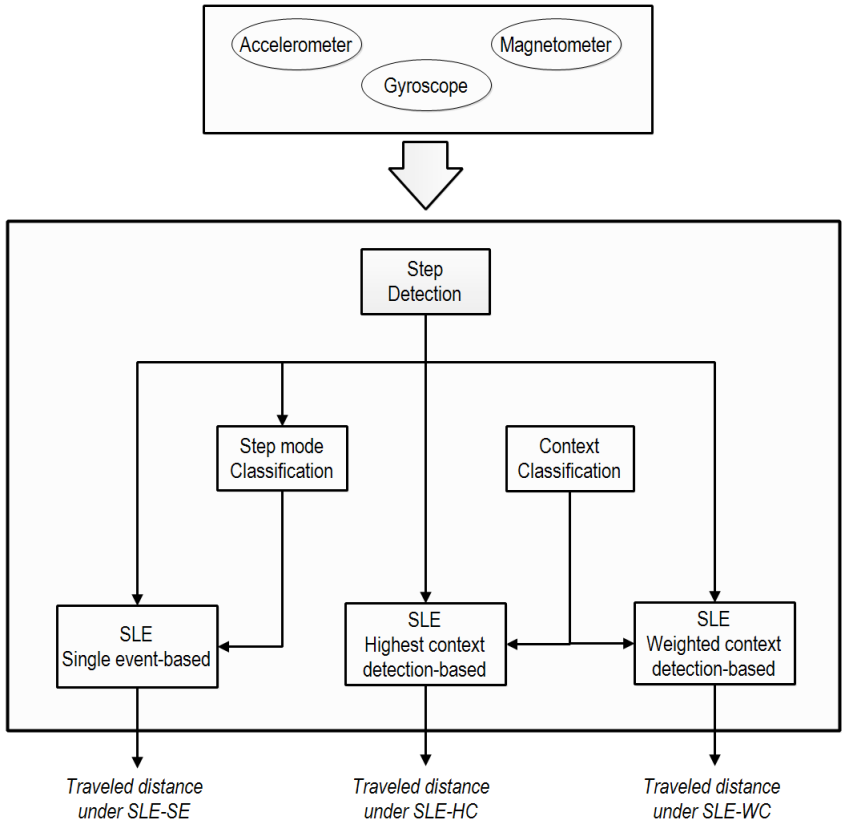


Figure 6.2: representation of the proposed PDR system.

4. Lacing up shoes (Fig.6.5).
5. Taking a bottle of water from an automatic vending machine (Fig.6.5).

The dataset has been collected at the School of Engineering of the University of Florence.

6.4 Step Detection

In PDR navigation, the accelerometer signal pattern is generally exploited to determine the presence of steps over time [32, 75]. The specific force signal provided by body-worn sensors during pedestrian activities like walking,

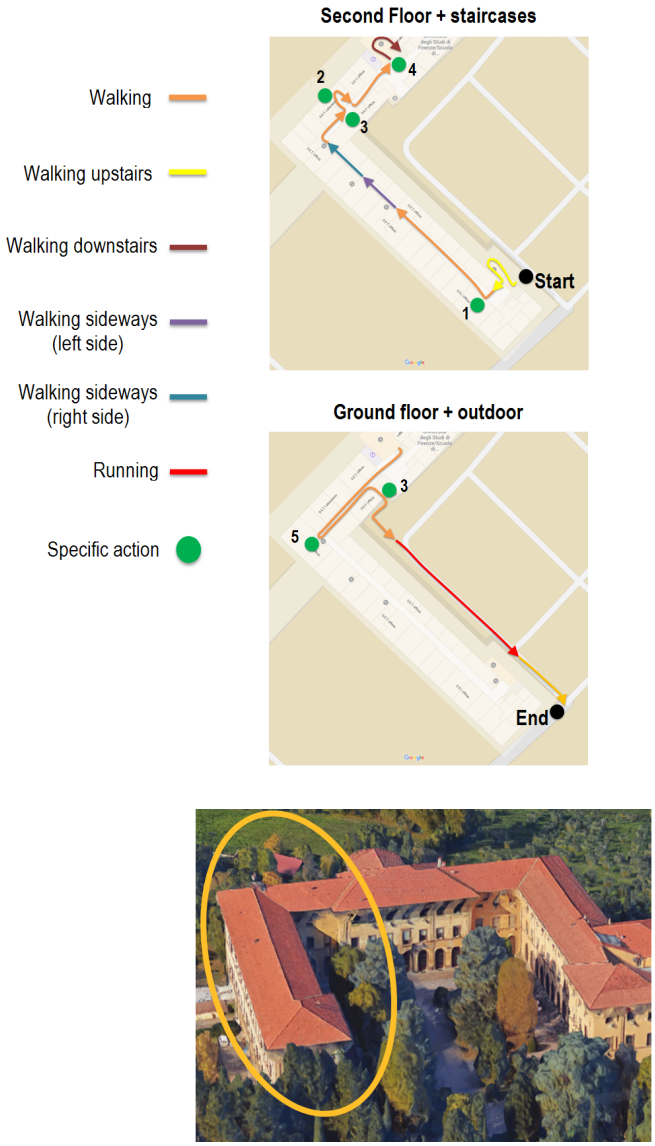


Figure 6.3: path and pedestrian activity description.

shows a periodic pattern which depends on the principal frequency of the movement, as illustrated in Fig.6.6. The purpose of the step detection routine is to reveal the step time indexes which correspond to the step boundaries, in order to separate consecutive steps [61], [43]. Since the step detection is the primary stage in a PDR process, either false or missed step detections can strongly affect the estimation of the traveled distance.
In this work, the step detection algorithm exploits the continuous wavelet transform (CWT) analysis [46] and follows the block diagram illustrated in Fig.6.7. The specific force is used from multiple epoch over a 50% overlapped sliding time window of 1-second duration. In order to perform a detection independently of the sensor orientation, the magnitude of the specific force is computed:

$$||f|| = \sqrt{f_x^2 + f_y^2 + f_z^2} \tag{6.1}$$

where f_x, f_y, and f_z are the specific force components in the expressed in the body coordinate frame. Then, a band-pass filtering operation is performed, in order to filter the signal noise at the higher frequencies and to obtain a zero-mean specific force magnitude to provide as input to the CWT block. The latter aims to identify the local maxima which correspond to the step boundaries, while discarding the local maxima and minima due to the signal irregularities, as illustrated in Fig.6.8. The CWT processing brings out specific time events in the signal by decomposing the signal over dilated and translated wavelets [44]. A wavelet is a short waveform generally named

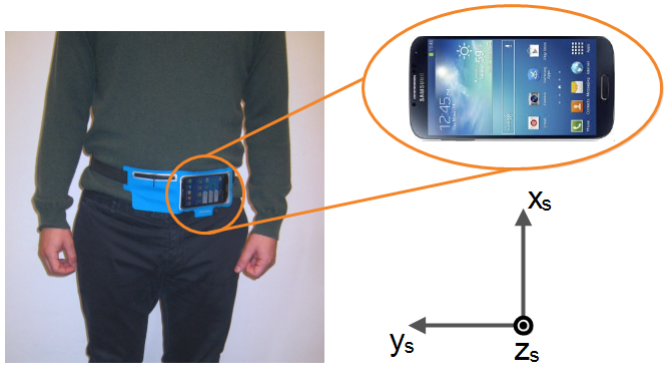
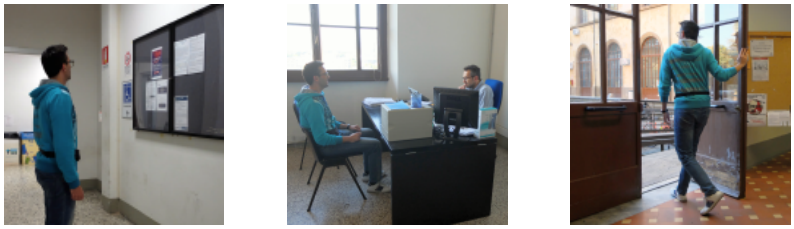
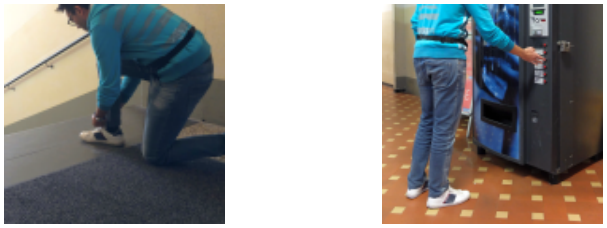


Figure 6.4: on-body smartphone location and sensor body frame.



(1) (2) (3)



(4) (5)

Figure 6.5: illustration of the pedestrian actions: (1) watching a notice board, (2) entering an office and sitting down for a while, (3) opening a door, (4) lacing up shoes, and (5) taking a bottle of water from an automatic vending machine.

$\psi \in L^2(\Re)$: $|\psi| = 1$ and centered in the neighbour of $t = 0$ such that:

$$\int_{-\infty}^{+\infty} \psi(t)dt = 0 \tag{6.2}$$

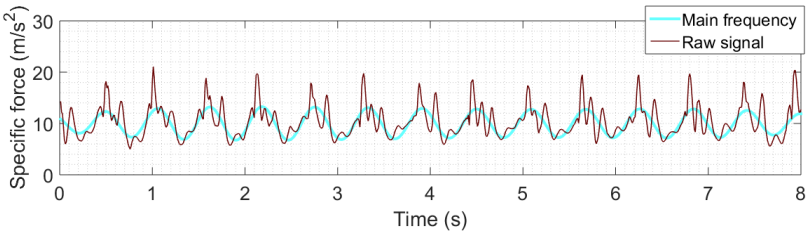


Figure 6.6: pattern of the specific force magnitude provided by the waist-worn specific force during the walking activity.

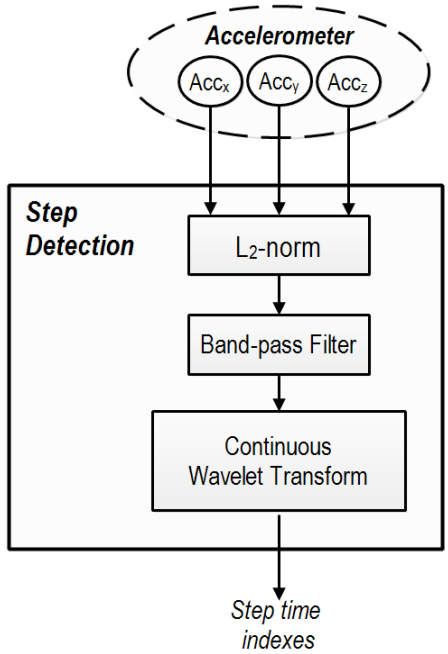


Figure 6.7: step detection block diagram.

Suppose that the ψ is a real wavelet, the corresponding real wavelet transform of the function f is given as:

$$W\left[f(u,s)\right] = \int_{-\infty}^{+\infty} f(t)\frac{1}{\sqrt{s}}\psi^*\left(\frac{t-u}{s}\right)dt \tag{6.3}$$

where $*$ indicates conjugate complex operator. The CWT measures the variation of the function f in a neighbour of u proportional to s. In our case, the variable u represents the time translation variable which enables the wavelet to scan the entire time window. On the other hand, the variable s represents the scale which permits to dilate the wavelet in order to bring out particular events coming up in a certain time within the analysed signal waveform. The expression in (6.3) represents the inner product between the considered wavelet and the given function f which in our case represents the band-pass filtered specific force magnitude. The higher the correlation between the function and the appropriately dilated wavelet, the higher the

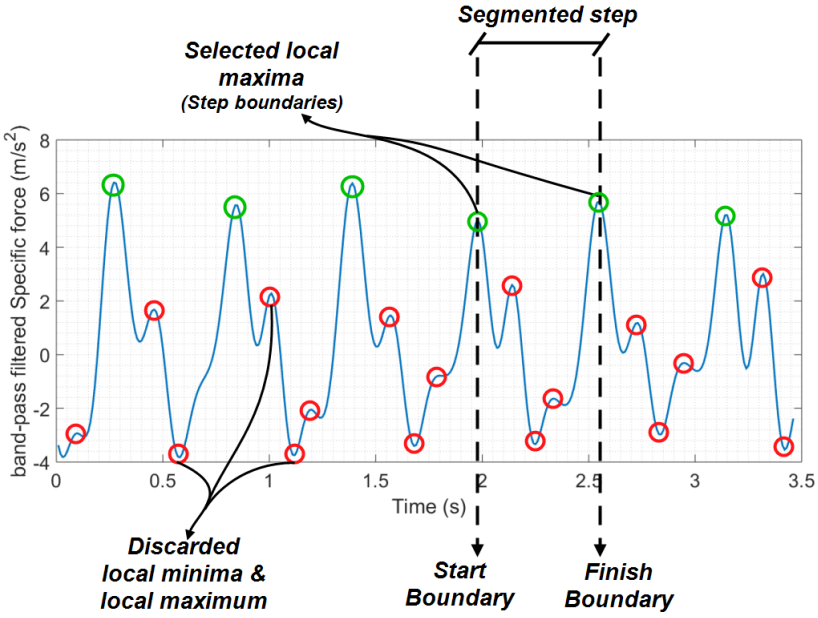


Figure 6.8: the purpose of the step detection algorithm.

resulting inner product value. High values of the correlation between the band-pass filtered specific force magnitude and the fine scales of the wavelet are expected at the local maxima which refer to the step boundaries, as shown in Fig.6.7. By knowing that the Local Lipschiz regularity [44] of a function f at a particular time v depends on the decay at fine scale of $|W[f(u,s)]|$ in the neighbour of v, the local maxima in the pass-band filtered specific force magnitude can be detected from the local maxima values of $|Wf[(u,s)]|$ [46] [44]. In this work, the wavelet scale value equal to 16 and the time window overlapping factor equal to 50% have been chosen in order to provide the best trade-off between the step detection accuracy and computational load [46].

6.5 Step mode and Context Classification

The proposed step mode and context classification algorithms are based on supervised learning techniques and use the same set of features. However, they operate under different time frameworks. The step mode classification algorithm processes the sensor data within the single-step start and finish time boundaries indicated by the step detection routine, whereas the context classification works over a fixed-length sliding window, which may contain several steps. Supervised learning methods are used to model the relationships between the target vectors and the corresponding input vectors of the classification algorithm using training samples. Then, the model is used to predict target values for the test data [9]. The step mode and context classification techniques are illustrated in Fig. 6.9.

6.5.1 Feature Extraction

Feature extraction is a crucial operation in classification problems. A good set of feature can often provide accurate and comprehensive descriptions of patterns from which the differences between context categories are easily discerned. In this work, both time-domain and frequency-domain features are considered, in order to capture either temporal variations or periodic characteristics of motion [18]. Range, standard deviation, skewness, kurtosis, energy and zero-crossing rate are extracted over time-domain, while the maximum peak and the relative frequency index are extracted over frequency-domain, as summarized in Table 6.1 and Table 6.2[1]. The aforesaid features

[1]In Table 6.1 and Table 6.2, "a" refers to the specific force signal, "g" refers to the gyroscope signal, "m" refers to the magnetometer signal, LPF refers to the low-pass

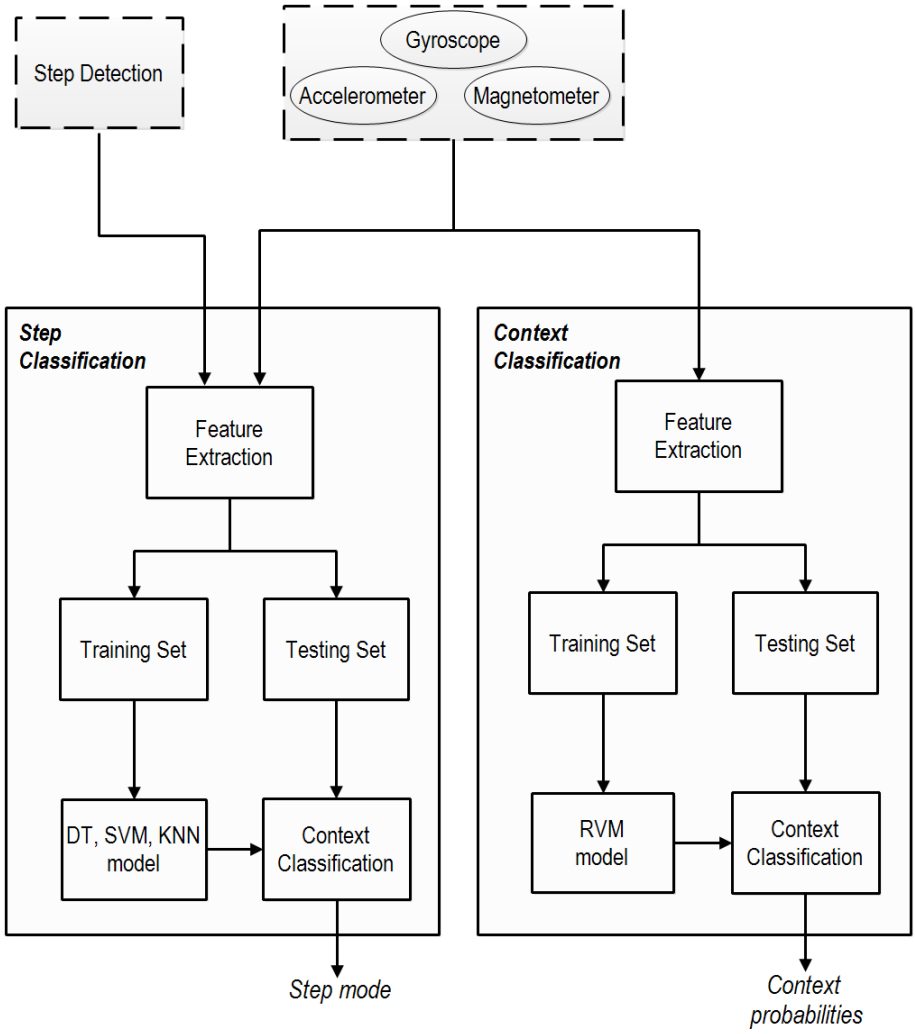


Figure 6.9: representation of the step mode and context classification block diagrams.

filtering operation, DFT refers to the discrete Fourier transform operation, ZCR is the zero-crossing rate, N is the length of the sample window, and $I(.)$ is the indicator function which is 1 if its argument is true and 0 otherwise.

Table 6.1: FEATURE DESCRIPTION - Part I

F1	$range_{acc} = max(\|a\{t\}\|) - min(\|a\{t\}\|)$
F2	$range_{acc_f} = max(LPF(\|m\{t\}\|)) - min(LPF(\|m\{t\}\|))$
F3	$range_{gyro} = max(\|g\{t\}\|) - min(\|g\{t\}\|)$
F4	$range_{magn} = max(\|m\{t\}\|) - min(\|m\{t\}\|)$
F5	$\sigma_{acc} = \sqrt{\frac{1}{N}\sum_{t=1}^{N}(\|a_t\| - \overline{\|a\|})^2}$
F6	$\sigma_{acc_f} = \sqrt{\frac{1}{N}\sum_{t=1}^{N}(LPF(\|a_t\|) - \overline{\|a\|})^2}$
F7	$\sigma_{gyro} = \sqrt{\frac{1}{N}\sum_{t=1}^{N}(\|g_t\| - \overline{\|g\|})^2}$
F8	$\sigma_{magn} = \sqrt{\frac{1}{N}\sum_{t=1}^{N}(\|m_t\| - \overline{\|m\|})^2}$
F9	$skewness_{acc} = \frac{1}{N\sigma^3}\sqrt{\frac{1}{N}\sum_{t=1}^{N}(\|a_t\| - \overline{\|a\|})^3}$
F10	$skewness_{acc_f} = \frac{1}{N\sigma^3}\sqrt{\frac{1}{N}\sum_{t=1}^{N}(LPF(\|a_t\|) - \overline{\|a\|})^3}$
F11	$skewness_{gyro} = \frac{1}{N\sigma^3}\sqrt{\frac{1}{N}\sum_{t=1}^{N}(\|g_t\| - \overline{\|g\|})^3}$
F12	$skewness_{magn} = \frac{1}{N\sigma^3}\sqrt{\frac{1}{N}\sum_{t=1}^{N}(\|m_t\| - \overline{\|m\|})^3}$
F13	$kurtosis_{acc} = \frac{1}{N\sigma^4}\sqrt{\frac{1}{N}\sum_{t=1}^{N}(\|a_t\| - \overline{\|a\|})^4}$
F14	$kurtosis_{acc_f} = \frac{1}{N\sigma^4}\sqrt{\frac{1}{N}\sum_{t=1}^{N}(LPF(\|a_t\|) - \overline{\|a\|})^4}$

are extracted from the magnitude signal of all available sensors: accelerometer, gyroscope and magnetometer. The effectiveness of features similar to these for pedestrian activity classification have been shown in different studies [5], [24], [64], [26].

Table 6.2: FEATURE DESCRIPTION - Part II

F15	$kurtosis_{gyro} = \frac{1}{N\sigma^4}\sqrt{\frac{1}{N}\sum_{t=1}^{N}(\|g_t\| - \overline{\|g\|})^4}$
F16	$kurtosis_{magn} = \frac{1}{N\sigma^4}\sqrt{\frac{1}{N}\sum_{t=1}^{N}(\|m_t\| - \overline{\|m\|})^4}$
F17	$Energy_{acc} = \sum_{t=1}^{N}\|a_t\|^2$
F18	$Energy_{acc_f} = \sum_{t=1}^{N} LPF(\|a_t\|^2)$
F19	$Energy_{gyro} = \sum_{t=1}^{N}\|g_t\|^2$
F20	$Energy_{magn} = \sum_{t=1}^{N}\|m_t\|^2$
F21	$max\|DFT(\|a_t\|)\|$
F22	$max\|DFT(LPF\|a_t\|)\|$
F23	$max\|DFT(\|g_t\|)\|$
F24	$frequency\ index\ of\ F21$
F25	$frequency\ index\ of\ F22$
F26	$frequency\ index\ of\ F23$
F27	$ZCR_{acc} = \frac{1}{N-1}\sum_{n=1}^{N-1} I\{\|a_t\|\ \|a_{t+1}\| < 0\}$
F28	$ZCR_{acc_f} = \frac{1}{N-1}\sum_{n=1}^{N-1} I\{LPF(\|a_t\|)\ LPF(\|a_{t+1}\|) < 0\}$

6.5.2 Step mode Classification

The step mode classification algorithm aims to build up a mathematical model able to effectively map the extracted features from the single detected steps, into the step modes illustrated in Fig.6.1. The proposed approach compares the performance of three families of classification algorithms: decision tree (DT), support vector machine (SVM) and k-nearest neighbour

(NN) [76], [24].
The DT method recursively partitions the feature space to reach a decision. The leaves of the tree represent all the possible classes that can be assigned to the input vectors. Each internal node specifies a test related to one or more features and splits the data into two or more segments according to the decision criteria. In this way, the full classification problem is divided in smaller, less complex classification tests. Given training samples and the corresponding label values, the dataset is split into branches such that samples with the same labels are grouped together. The samples are classified while navigating from the root down to the leaves. A simple DT for samples with only three features is illustrated in Fig.6.10. [68]. The DT method allows a fast prediction, low memory usage, and medium predictive accuracy.

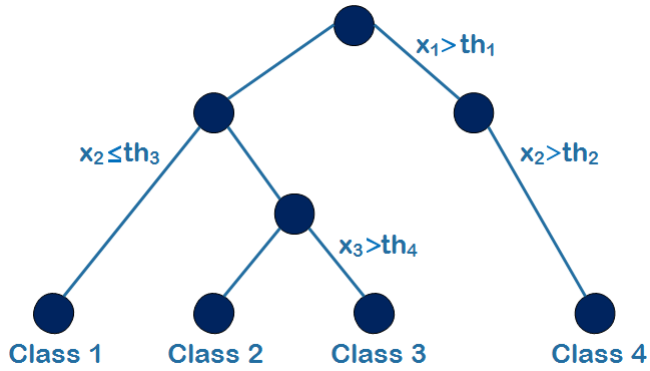


Figure 6.10: example of a decision tree model which considers four classes, three features (x_1, x_2, x_3) and four thresholds (th_1, th_2, th_3, th_4).

The SVM is a classification model which aims to find the optimum hyperplane in the feature space in order to maximise the margin between the classes, as shown in Fig.6.11. First, training samples with distinct labels are separated on each side of the hyperplane. Second, the distances of the hyperplane to the nearest training data points of any classes is maximised. This distance is called the optimal margin and those samples on the margin are called as support vectors [45, 60, 75]. The SVM algorithm has a very good predictive accuracy but low memory usage and fast predictive speed only for a few support vectors.
The KNN algorithm tries categorizing new data based on their distance from

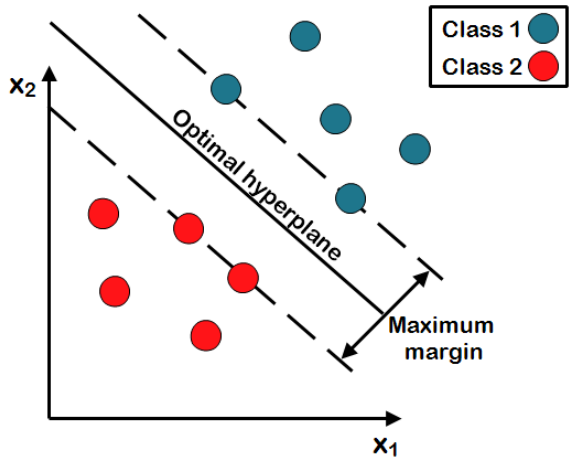


Figure 6.11: example of an SVM model which considers two classes and two features (x_1, x_2).

neighbours in the training set [37], as shown in Fig.6.12. KNN is a simple algorithm that stores all available samples and classifies new samples based on a similarity measure, e.g the Euclidean distance. A sample is classified by a majority vote of its neighbours, with the sample being assigned to the class most common amongst its k nearest neighbours measured by a distance function. If $k = 1$ then the sample is simply assigned to the class of its nearest neighbour, as illustrated in the example in Fig.6.12. Choosing the optimal value for k is best done by first inspecting the data. In general, a large k value is more precise as it reduces the overall noise. It envisages high memory usage and provides a very good predictive accuracy and a fast prediction speed only with low feature space dimension.
Either when the classification model selects too many features with respect to a relative low number of examples, or when the model has low capability to generalize the relation between the input and output vectors, the classification performance may decrease due to overfitting. In order to avoid overfitting and properly evaluating the predictive accuracy of the fitted models, the 10-fold cross-validation method is used [45]. In particular, the data are partitioned into 10 separate sets: each single model is trained for each set using all data outside the set. Then, the performance of each model is tested using the data inside the considered set; finally the average test error

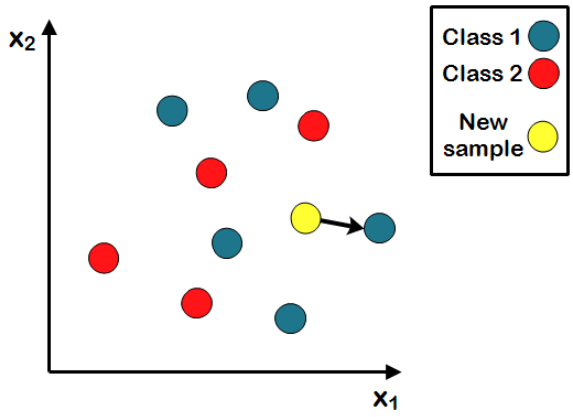


Figure 6.12: example of a KNN model which considers two classes and two features (x_1, x_2).

over all sets is calculated.

6.5.3 Context Classification

The purpose of the context classification subsystem is to arrange the extracted features from the context window, into one of six context categories, shown in Fig.6.1. To this aim, the RVM algorithm is exploited: several studies have effectively applied the RVM method to context classification for pedestrian activities [18] [70]. RVM is a Bayesian sparse kernel technique [9] for regression or classification, sharing many of the main characteristics of SVM. The advantage of RVM beyond Boolean classifiers, like the ones used for step mode classification (DT, SVM and KNN), is that it can provide probabilistic classification results for each category. Thus the subsequent mechanism can adapt different strategies based on the uncertainty of the classification decisions. Note that in the algorithms described in this section, we assume that there are $L = 6$ possible pedestrian contexts $\boldsymbol{C} = \{C_k | k = 1, 2, \ldots, L\}$, as illustrated in Fig.6.1. Given a training dataset $\boldsymbol{X} = \{X_{i,j} | i = 1, 2, \ldots, N; j = 1, 2, \ldots, M\}$, each sample $\boldsymbol{X_i} = \{X_{i,1}, X_{i,2}, \ldots, X_{i,M}\}$ is assigned to a target value $y_i \in \boldsymbol{C}$. M is the number of features and N is the number of the samples in the dataset. Fundamentally, RVM is a binary classifier ($y \in \{0, 1\}$) under a Bayesian

probabilistic framework [9]. The relationship of the input vector and their real-valued predictions $t(\boldsymbol{X}_i)$ are modelled by a linearly weighted function

$$t(\boldsymbol{X_i}; \boldsymbol{w}) = \sum_{i=1}^{N} w_i \phi(\boldsymbol{X_i}) = \boldsymbol{w}^T \boldsymbol{\phi}(\boldsymbol{X_i}), \tag{6.4}$$

where $\boldsymbol{w}$ denotes the weights of samples and $\phi(\boldsymbol{X}_i)$ is a nonlinear basis function. The input data samples $\boldsymbol{X}_i$ are classified according to the sign of $t(\boldsymbol{X}_i)$. To infer the function $t(\boldsymbol{X}_i)$, we need to define the basis function and to estimate the weights as well. In here, the radial basis kernel function is used, so that:

$$\boldsymbol{\Phi_{ij}} = \boldsymbol{\phi}^T(\boldsymbol{X_i})\boldsymbol{\phi}(\boldsymbol{X_j}) = exp\left(- \frac{\|\boldsymbol{X_i} - \boldsymbol{X_j}\|^2}{2\sigma^2} \right). \tag{6.5}$$

A Bayesian probabilistic framework infers a distribution over the weights. According to Bayes rule, the posterior probability of $\boldsymbol{w}$ is

$$p(\boldsymbol{w}|\boldsymbol{y}, \boldsymbol{\alpha}) = \frac{p(\boldsymbol{y}|\boldsymbol{w}, \boldsymbol{\alpha})p(\boldsymbol{w}|\boldsymbol{\alpha})}{p(\boldsymbol{y}|\boldsymbol{\alpha})}, \tag{6.6}$$

where $\boldsymbol{y} = (y_1, ..., y_N)^T$, α_i represents the precision of the corresponding parameter w_i, and $\boldsymbol{\alpha} = (\alpha_1, ..., \alpha_N)^T$. $p(\boldsymbol{y}|\boldsymbol{w}, \boldsymbol{\alpha})$ is the likelihood of the target values given the training dataset. The conditional prior probability distribution $p(\boldsymbol{w}|\boldsymbol{\alpha})$ in Equation (6.6) is modelled by a Gaussian function where the parameters w_i are weighted by parameters α_i.

$$p(\boldsymbol{w}|\boldsymbol{\alpha}) = \prod_{i=1}^{N} \frac{\sqrt{\alpha}}{\sqrt{2\pi}} exp\left(- \frac{\alpha_i w_i^2}{2} \right). \tag{6.7}$$

Because $y \in \{0, 1\}$ is a binary variable, the likelihood function can be described by a Bernoulli distribution:

$$p(\boldsymbol{y}|\boldsymbol{w}, \boldsymbol{\alpha}) = \prod_{i=1}^{N} [\sigma(t(\boldsymbol{X_i}; \boldsymbol{w}))]^{y_i} [1 - \sigma(t(\boldsymbol{X_i}; \boldsymbol{w}))]^{1-y_i}], \tag{6.8}$$

where $\sigma(y) = 1/(1 + e^{-y})$ is the logistic sigmoid link function. Equation (6.6) with the probability densities given by (6.7) and (6.6) cannot be solved analytically. Therefore, a numerical method, the Laplacian approximation,

is proposed to find the maximum a posterior (MAP) weights $\boldsymbol{w}^*$ based on the training dataset,

$$\begin{aligned} &ln\{p(\boldsymbol{y}|\boldsymbol{w})p(\boldsymbol{w}\boldsymbol{\alpha})\} \\ &= \sum_{i=1}^{N}[y_i lnt_i + (1-y_i)ln(1) - t_i] - \frac{1}{2}\boldsymbol{w}^T\boldsymbol{A}\boldsymbol{w}, \end{aligned} \tag{6.9}$$

where $\boldsymbol{A} = diag(\boldsymbol{\alpha})$. By computing the maximum value of (6.9) with respect to $\boldsymbol{\alpha}$ and $\boldsymbol{y}$, the mean $\boldsymbol{w}^*$ and covariance $\boldsymbol{\Delta}$ of the Laplacian approximation are obtained:

$$\begin{aligned} \boldsymbol{w}^* &= \boldsymbol{B}\boldsymbol{\Delta}\boldsymbol{\Phi}^T\boldsymbol{y} \\ \boldsymbol{\Delta} &= (\boldsymbol{\Phi}^T\boldsymbol{B}\boldsymbol{\Phi} + \boldsymbol{A})^{-1}, \end{aligned} \tag{6.10}$$

where $\boldsymbol{B} = diag(\beta_1, \beta_2, \ldots, \beta_N)$ is a diagonal matrix with $\beta_i = \sigma(y_i)[1 - \sigma(y_i)]$. After obtaining $\boldsymbol{w}^*$, the parameters α are iteratively updated using

$$\alpha_i^{new} = \frac{1 - \alpha_i^{old}\Delta_{ii}}{\mu_i^2}, \tag{6.11}$$

where μ_i is the *i-th* posterior mean weight w_i^* and Δ_{ii} is the *i-th* diagonal element of the covariance. The procedure is repeated until it converges to a fixed value or the maximum number of iterations is reached. In order to tackle multiclass situations using the RVM method, two possible strategies could be used [9]. The first one is the "one-against-all" strategy. L binary classifiers will be created for an L-class classification and each classifier is trained to separate one class from the others. The second strategy is "one-versus-one". There are $L(L-1)/2$ binary classifiers created to separate every two classes. In this work, the first method is adopted as it is more computational efficient. The context classification uses the accelerometer, gyroscope and magnetometer data, from multiple epochs over a 50% overlapped sliding time window of 2-second duration.

6.6 Step Length Estimation

6.6.1 Step Length k-parameters Calibration

According to the state of the art [65], [66], the step length can be expressed as a linear combination of a constant, the step frequency f_s, and the specific

force variance σ_f^2:

$$SL = k_0 + k_1 f_s + k_2 \sigma_f^2, \tag{6.12}$$

where k_1 and k_2 are respectively the coefficients of the step frequency and the specific force variance, and k_0 is the constant term which refers to the individual subject.
In this work, the k_0,k_1 and k_2 parameters are determined for several step modes: walking, walking sideways, climbing stairs, descending stairs and running. Considering the path illustrated in Fig. 6.3, the segments which correspond to walking, walking sideways and running, have been fitted out with benchmarks arranged every 10 meters: the subject has been followed with a video camera along the path and the video recordings have enabled the sensor data collected within the physical benchmarks to be time tagged. The collected dataset have been divided into two groups, as shown in Fig.6.13: *Group A* includes walking, walking sideways and running, and consists of

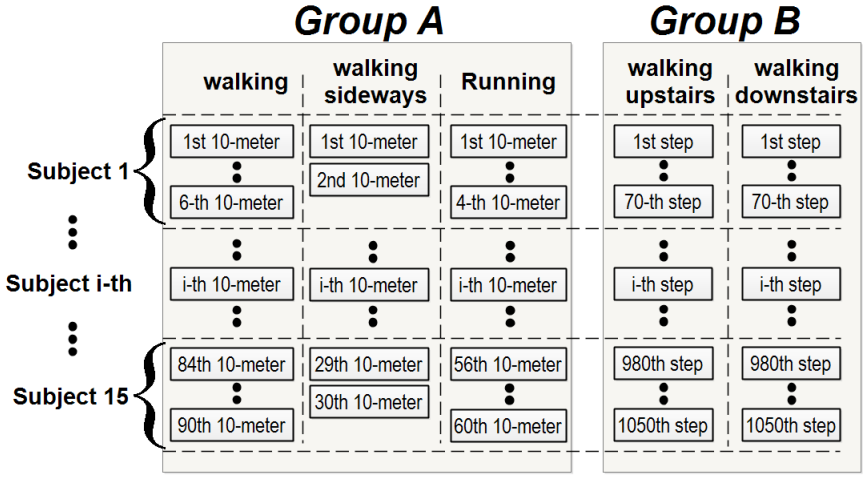


Figure 6.13: data separation for step length k-parameters estimation.

subgroups of 10-meter segments for each subject, accordingly with the segmentation by benchmarks; while *Group B* includes the walking upstairs and downstairs, and consists of subgroups of single step segments for each subject.
The k_0, k_1 and k_2 coefficients are determined for each step mode by solving

for the linear system of equations

$$\boldsymbol{H}\boldsymbol{k}_{0,1,2} = \boldsymbol{d}, \tag{6.13}$$

where,

$$H = \begin{bmatrix} n_{1,1} & 0 & \dots & 0 & F_{1,1} & \Sigma^2_{1,1} \\ 0 & n_{1,2} & \ddots & \vdots & F_{1,2} & \Sigma^2_{1,2} \\ \vdots & \ddots & \ddots & 0 & \vdots & \vdots \\ 0 & \dots & 0 & n_{1,15} & F_{1,15} & \Sigma^2_{1,15} \\ n_{2,1} & 0 & \dots & 0 & F_{2,1} & \Sigma^2_{2,1} \\ 0 & n_{2,2} & \ddots & \vdots & F_{2,2} & \Sigma^2_{2,2} \\ \vdots & \ddots & \ddots & 0 & \vdots & \vdots \\ 0 & \dots & 0 & n_{2,15} & F_{2,15} & \Sigma^2_{2,15} \\ & & & \vdots & & \\ & & & \vdots & & \\ n_{s,1} & 0 & \dots & 0 & F_{s,1} & \Sigma^2_{s,1} \\ 0 & n_{s,2} & \ddots & \vdots & F_{s,2} & \Sigma^2_{s,2} \\ \vdots & \ddots & \ddots & 0 & \vdots & \vdots \\ 0 & \dots & 0 & n_{s,15} & F_{s,15} & \Sigma^2_{s,15} \end{bmatrix}, \tag{6.14}$$

$$\begin{aligned} \boldsymbol{k}_{0,1,2} &= \begin{bmatrix} k_{0,1},\ k_{0,2},\ \dots,\ k_{0,15},\ k_1,\ k_2 \end{bmatrix}^T, \\ \boldsymbol{d} &= \begin{bmatrix} d_{1,1},\ d_{1,2},\ \dots,\ d_{s,15} \end{bmatrix}^T, \\ F_{i,j} &= \sum_{p=1}^{N} f_{s,p}, \quad \Sigma^2_{i,j} = \sum_{p=1}^{N} \sigma^2_{f,p}. \end{aligned} \tag{6.15}$$

In the case of *Group A*, $n_{i,j}$ is the total number of steps detected in the *i-th* data segment which refers to the *j-th* subject; $\boldsymbol{d}$ is the vector which comprises the lengths corresponding to the data segments, i.e. 10 meters; $F_{i,j}$ and $\Sigma^2_{i,j}$ are respectively the summations of the step frequencies and specific force variances of the N steps detected in the *i-th* data segment which refers to the *j-th* subject; the s index refers to the last data segment for each subject. In the case of *Group B*, $n_{i,j}$ refers to a single step and is equal to 1; $\boldsymbol{d}$ comprises the stair length values, which are equal to 0.29 m in the case of climbing stairs or 0.43 m in the case of descending stairs. The

least squares solution for the (6.13) is

$$\boldsymbol{k}_{0,1,2} = (\boldsymbol{H}^T\boldsymbol{H})^{-1}\boldsymbol{H}^T\boldsymbol{d}. \tag{6.16}$$

6.6.2 Step Length Estimation Methods

This Section describes the considered SLE algorithms: single event-based, weighted context-based and highest context-based. All these methods follow the time diagram illustrated in Fig. 6.14: the traveled distance is updated at each k-th epoch, which corresponds to the end boundary of each (k-1)th context time window. The latter is 50% overlapped and its duration is 2 seconds.

Single Event-based SLE: the results of the step detection and classification routines are provided as input to the single event-based method, as shown in Fig.6.2. In particular, the step detection algorithm provides the time indexes of the single steps, while the step classification algorithm associates a particular step mode to each detected step. This approach doesn't consider the pedestrian context probabilities and determines the lengths of the steps performed between the (k-1)th and the k-th epoch by using the relation in (6.12). Assuming the k-epoch as the current one, the single event-based distance d_k^{SE}, which refers to the distance traveled between the epochs (k-1) and k is determined as

$$d_k^{SE} = \sum_{p=1}^{M} k_0^{m_{p,n}} + k_1^{m_{p,n}} f_{s,p} + k_2^{m_{p,n}} \sigma_{f,p}^2, \tag{6.17}$$

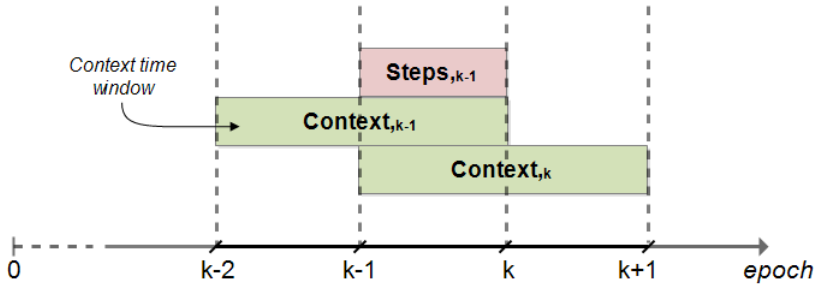


Figure 6.14: time framework of the PDR system.

where the k_0, k_1 and k_2 refer to the step length parameters determined in (6.16); in particular, $k_0^{m_{p,n}}$ is the constant term which refers to the *p-th* step mode m_n which has been detected and classified; $k_1^{m_{p,n}}$ and $k_2^{m_{p,n}}$ are the linear coefficients which refer to the *p-th* step mode m_n; f_s and σ_f are respectively the step frequency and the specific force variance of the *p-th* detected step; M is the total number of steps detected within the epochs (k-1) and k. Then, the total distance D_k^{SE}, which refers to the distance traveled between the 0-epoch and the epoch k, is determined by adding up d_k^{SE} to the total distance computed at the epoch (k-1):

$$D_k^{SE} = D_{k-1}^{SE} + d_k^{SE} \tag{6.18}$$

Weighted Context Detection-based SLE: as shown in Fig.6.2, the results of the step detection and the context classification routines are provided as input to the weighted context-based SLE algorithm. The latter, weigths the step lengths determined for different step modes by the pedestrian context probabilities. Referring to the time diagram in Fig.6.14, let us assume the k-epoch as the current one, and define

$$Stationary_{,k-1} = Pr\{C_{k-1,1}\}, \tag{6.19}$$

$$\boldsymbol{Context}_{,k-1} = \begin{bmatrix} Pr\{C_{k-1,2}\} \\ Pr\{C_{k-1,3}\} \\ \vdots \\ Pr\{C_{k-1,6}\} \end{bmatrix}^T, \quad \boldsymbol{d}_{k,m^*}^{SE} = \begin{bmatrix} d_{k,m_2}^{SE} \\ d_{k,m_3}^{SE} \\ \vdots \\ d_{k,m_6}^{SE} \end{bmatrix}, \tag{6.20}$$

where $Stationary_{,k-1}$ is the stationary context probability and the $\boldsymbol{Context}_{,k-1}$ row vector comprises the context probabilities for each context C_n, with $n = 2, .., 6$ (see Fig.6.1). The context information included in both $Stationary_{,k-1}$ and $\boldsymbol{Context}_{,k-1}$ refers to the context window (k-1) and is determined at the epoch k. d_{k,m^*}^{SE} is the single event-based distance vector in which each term corresponds to the single event-based distance computed in (6.17) for the step mode m_n with $n = 2, .., 6$ (see Fig.6.1). In this case, the single steps between the epochs (k-1) and k are not classified by the step mode classification routine as in the single event-based SLE algorithm. Each term defined in d_{k,m^*}^{SE} considers the same step mode m_n for all M detected steps within the epochs (k-1) and k. The algorithm 1 below describes how the

weighted context-based SLE routine determines the distances pd_k^{WC}, d_{k-1}^{WC}, D_{k-1}^{WC}, PD_k^{WC} based on the information (6.19) and (6.20), which is determined at the epoch k. Even if these distances may refer to distances traveled within different time interval, they are all computed at the epoch k.

Algorithm 1 Weighted Context-based SLE method

if $Stationary_{,k-1} <= max(\boldsymbol{Context}_{,k-1})$ **then**

$\boldsymbol{Context}_{,k-1} = \boldsymbol{Context}_{,k-1} \frac{1}{||\boldsymbol{Context}_{,k-1}||_1}$

$pd_k^{WC} = \boldsymbol{Context}_{,k-1}\ \boldsymbol{d}_{k,m^*}^{SE}$

$d_{k-1}^{WC} = \boldsymbol{Context}_{,k-1}\ \boldsymbol{d}_{k-1,m^*}^{SE}$

$D_{k-1}^{WC} = D_{k-2}^{WC} + \frac{1}{2}(d_{k-1}^{WC} + pd_{k-1}^{WC})$

$PD_k^{WC} = PD_{k-1}^{WC} + \frac{1}{2}(d_{k-1}^{WC} - pd_{k-1}^{WC}) + pd_k^{WC}$

else

$pd_k^{WC} = d_{k-1}^{WC} = 0$

$D_{k-1}^{WC} = D_{k-2}^{WC} + \frac{1}{2} pd_{k-1}^{WC}$

$PD_k^{WC} = PD_{k-1}^{WC} - \frac{1}{2} pd_{k-1}^{WC}$

end if

If the probability of the stationary context is lower then the probabilities of the other contexts determined at the epoch k, then the subject is assumed to be moving. Afterwards, the context row vector $\boldsymbol{Context}_{,k-1}$ is scaled by its L_1-$norm$, in order to obtain the sum of its context probabilities equal to 1.
The provisional distance pd_k^{WC} traveled between the epochs (k-1) and k is computed by weighting the context probabilities determined at the epoch k and the single event-based distances traveled between the epochs (k-1) and k.

The final distance d_{k-1}^{WC} traveled between the epochs (k-2) and (k-1) is computed by weighting the context probabilities determined at the epoch k and the single event-based distances traveled between the epochs (k-2) and (k-1). Then, the total final distance D_{k-1}^{WC} traveled between the epochs 0 and (k-1) is computed by adding up the total final distance traveled between the epochs 0 and (k-2) and the arithmetic mean between the final and the provisional distances traveled between the epochs (k-2) and (k-1).
Finally, the total provisional distance PD_{k}^{WC} traveled between the epochs 0 and k is computed by adding up the total provisional distance traveled between the epochs 0 and (k-1), the half of the difference between the final and the provisional distances traveled between the epochs (k-2) and (k-1), and the provisional distance traveled between the epochs (k-1) and k.
Alternatively, if the probability of the stationary context is the highest, the subject is assumed to keep still. Thus, either the provisional distance traveled between the epochs (k-1) and k, or the final distance traveled between the epochs (k-2) and (k-1) are set equal to zero. As a result, the total final distance traveled between the epochs 0 and (k-1) is determined as the sum of the total final distance traveled between the epochs 0 and (k-2) and the half provisional distance traveled between the epochs (k-1) and (k-2). Finally, the total provisional distance traveled between the epochs 0 and k is determined as the difference between the total provisional distance traveled between the epochs 0 and (k-1) and the half provisional distance traveled between the epochs (k-2) and (k-1).

Highest Context Detection-based: the highest context-based SLE algorithm considers the step lengths computed for the step mode corresponding to the pedestrian context with the highest probability. Referring to the time diagram in Fig.6.14, let us assume the k-epoch as the current one, and define

$$\boldsymbol{Context}_{,k-1} = \begin{bmatrix} Pr\{C_{k-1,1}\} \\ Pr\{C_{k-1,2}\} \\ \vdots \\ Pr\{C_{k-1,6}\} \end{bmatrix}^{T}, \; \boldsymbol{d}_{k,m^*}^{SE} = \begin{bmatrix} d_{k,m_1}^{SE} \\ d_{k,m_2}^{SE} \\ \vdots \\ d_{k,m_6}^{SE} \end{bmatrix}, \tag{6.21}$$

$$j = \underset{i}{\text{argmax}}\left\{ Pr\{C_{k-1,i}\} \in \boldsymbol{Context}_{,k-1} \right\}$$
$$\boldsymbol{Selection}_{,k-1} = \left[\delta_{j,1},\ \delta_{j,2},\ \ldots,\ \delta_{j,6}\right], \tag{6.22}$$

where $\boldsymbol{Context}_{,k-1}$ is determined at the epoch k and comprises the context probabilities for each context C_n, with $n = 1, .., 6$ (see Fig.6.1); $\boldsymbol{d}^{SE}_{k,m^*}$ is the single-event distance vector which includes the distances traveled between the epochs (k-1) and k for the step mode m_n, with $n = 1, .., 6$ (see Fig.6.1); $\boldsymbol{Selection}_{,k-1}$ is a row vector which is determined at the epoch k and comprises Dirac delta functions. All terms in $\boldsymbol{Selection}_{,k-1}$ are equal to zero except the one which corresponds to the context with the highest probability defined $\boldsymbol{Context}_{,k-1}$. The algorithm 2 below describes how the highest context-based SLE routine determines the distances pd^{HC}_k, d^{HC}_{k-1}, D^{HC}_{k-1}, PD^{HC}_k based on the information (6.21) and (6.22), which is determined at the epoch k. Even if these distances may refer to distances traveled within different time interval, they are all computed at the epoch k.

Algorithm 2 Highest Context-based SLE method

$pd^{HC}_k = \boldsymbol{Selection}_{,k-1}\ \boldsymbol{d}^{SE}_{k,m^*}$

$d^{HC}_{k-1} = \boldsymbol{Selection}_{,k-1}\ \boldsymbol{d}^{SE}_{k-1,m^*}$

$D^{HC}_{k-1} = D^{HC}_{k-2} + \frac{1}{2}(d^{HC}_{k-1} + pd^{HC}_{k-1})$

$PD^{HC}_k = PD^{HC}_{k-1} + \frac{1}{2}(d^{HC}_{k-1} - pd^{HC}_{k-1}) + pd^{HC}_k$

The provisional distance pd^{HC}_k traveled between the epochs (k-1) and k is computed by selecting the single event-based distance traveled between the epochs (k-1) and k, which corresponds to the context in $\boldsymbol{Context}_{,k-1}$ with the highest probability. The final distance d^{HC}_k traveled between the epochs (k-2) and (k-1) is computed by selecting the single event-based distance traveled between the epochs (k-2) and (k-1), which corresponds to the context in $\boldsymbol{Context}_{,k-1}$ with the highest probability.
Then, the total final distance D^{HC}_{k-1} traveled between the epochs 0 and (k-1) is computed by adding up the total final distance D^{HC}_{k-2} traveled between the epochs 0 and (k-2) and the arithmetic mean between the final and the

provisional distances traveled between the epochs (k-2) and (k-1).
Finally, the total provisional distance PD_k^{HC} traveled between the epochs 0 and k is computed by adding up the total provisional distance traveled between the epochs 0 and (k-1), the half of the difference between the final and the provisional distances traveled between the epochs (k-2) and (k-1), and the provisional distance traveled between the epochs (k-1) and k.

6.7 Results and Discussion

6.7.1 Step Detection

The overlapping factor of the acquisition window and the wavelet scale of the CWT analysis are empirically determined. The accuracy performance of the step detection algorithm tested during the walking activity, is illustrated in Fig.6.15. The step detection error percentage is computed as follows:

$$DE = \frac{\#DS - \#S}{\#S} * 100, \tag{6.23}$$

where $\#DS$ is the number of the detected steps by the algorithm and $\#S$ is the actual number of steps performed by the subject.
The change in wavelet scale influences the sensitivity on detecting the acceleration variations due to steps. This is the motivation because a too small wavelet scale leads to overestimate the number of steps, while a too high value causes an underestimation, as shown in Fig.6.15.
The step detection errors decreases when an overlapping factor in the acquisition time window is introduced: the performance improvement is negligible for an overlapping factor over 50%. Higher values of wavelet scales and overlapping factor implies an higher computation load. In this work, the wavelet scale value equal to 16 and the time window overlapping factor equal to 50% have been chosen in order to provide the best trade-off between the step detection accuracy and computational load [46]. The proposed approach is robust against the acceleration signal irregularities caused by the pedestrian motion vibrations and the sensor noise, as shown in Fig.6.16.

6.7.2 Step Mode and Context Classification

This Section reports the results of the step mode and the context classification algorithms described in Section V. The classification models are trained

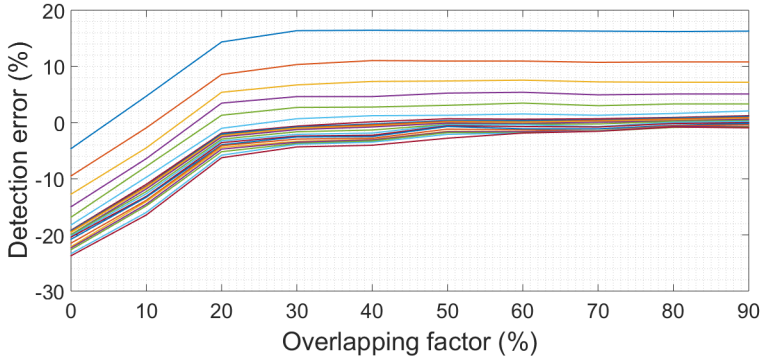


Figure 6.15: the step detection error percentage against the window overlapping factor, considering different wavelet scale values. This plot refers to the walking step mode and each line corresponds to a particular wavelet scale value: the ordered group of lines from the top to the bottom of the figure, corresponds to the ordered wavelet scale range from 5 to 25. The highest line corresponds to the scale 5, while the lowest line corresponds to the scale 25.

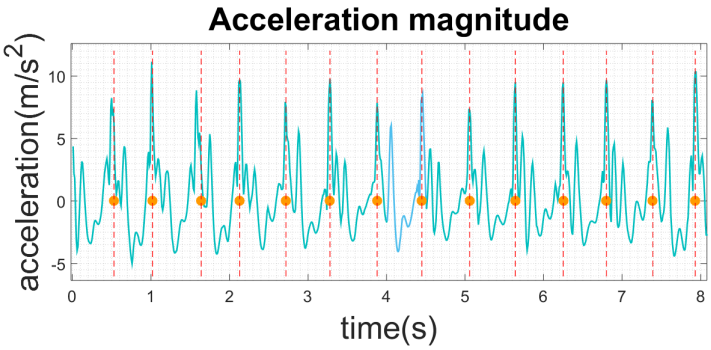


Figure 6.16: result of the proposed step detection algorithm on a raw acceleration signal during walking activity. The orange dots represents the detected step time indices.

with sensor data from fifteen subjects and a 10-fold model validation is used. The predictive accuracy results of the step mode and the context classifi-

cation algorithms are shown in Table 6.3. The SVM method exhibits an accuracy of 90.2 % which is the best performance among the considered step mode classification algorithms. The confusion matrix of the SVM algorithm is shown in Fig.6.17: walking and climbing stairs produce the predominant contribution to the overall misclassification error and are more frequently mixed up. The RVM method used for context classification achieves a predictive accuracy of 92.5 % and its confusion matrix is illustrated in Fig.6.18. As for the SVM, walking and climbing stairs are the most confused movements up and produce the main contribution to the overall misclassification rate.
The SVM and RVM algorithms respectively considered for the step mode classification and the context classification routines, show similar accuracy results. The reason is because both algorithms share many characteristics and they process the same sensor data. In particular, the RVM context classification algorithm exhibits a slightly better predictive accuracy then the SVM step mode classification algorithm because the RVM processes the sensor data within the context time window, which is usually longer than the time interval between two time step indexes used by SVM.

Table 6.3: Predictive accuracy of the step mode and the context classification methods

Step mode classification			**Context classification**
DT	SVM	KNN	RVM
85.3%	90.2%	80.5%	92.5%

6.7.3 Step Length Estimation

This Section describes the results of the SLE algorithms described in Section 6.6.2.
The results are divided into three parts. In each part, all subjects are split up into two subgroups: the first one includes 10 subjects whose data are used to train the step mode SVM and the context RVM classification models, while the second subgroup includes 5 subjects whose data are used to test the SLE algorithms. The total final distances D^{SE}, D^{HC}, D^{WC} which respectively refer to each SLE algorithms defined in Section 6.6.2, are deter-

TRUE CLASS \ PREDICTED CLASS	stationary	walking	walking sideways	climbing stairs	descending stairs	running
stationary	94.6 %	0 %	5.4 %	0 %	0 %	0 %
walking	0 %	85.2 %	5.1 %	9 %	0.7 %	0 %
walking sideways	2.7 %	6.4 %	85.9 %	2.5 %	2.5 %	0 %
climbing stairs	0 %	9.4 %	4.3 %	83.5 %	2.7 %	0 %
descending stairs	0 %	1.6 %	0.9 %	4.1 %	93.4 %	0 %
running	0 %	0 %	0 %	0 %	1.8 %	98.2 %

Figure 6.17: confusion matrix related to the SVM model, which is exploited for step mode classification.

mined at the end of the path illustrated in Fig.6.3. The traveled distance result for each subject and for each SLE method is shown in Fig.6.19. The root-mean-square percentage error (%RMSE) is computed by comparing the actual path distance with the total final distances determined by the SLE algorithms. Table 6.4 shows the %RMSE obtained for each subgroup of testing subjects and across all subjects. The weighted context-based SLE algorithm exhibits the best %RMSE performance for the subgroup of subjects 11-15. The highest context-based SLE algorithm reveals the best %RMSE performance for the subgroup of subjects 1-5, while the single event-based SLE algorithm exhibits the best %RMSE performance for the subgroup of subject 6-10. However, the weighted context-based SLE algorithm reveals the best %RMSE performance across all subjects.

6.8 Conclusion

In this work, a weighted context-based SLE algorithm has been demonstrated: the single step lengths determined as a linear combination of a

TRUE CLASS \ PREDICTED CLASS	stationary	walking	walking sideways	climbing stairs	descending stairs	running
stationary	95.5 %	0 %	4.5 %	0 %	0 %	0 %
walking	0 %	86.5 %	4.5 %	8.5 %	0.5 %	0 %
walking sideways	0 %	5 %	92 %	2.2 %	0.8 %	0 %
climbing stairs	0 %	9 %	3 %	84.3 %	3.7 %	0 %
descending stairs	0 %	1 %	0.3 %	2 %	96.7 %	0 %
running	0 %	0 %	0 %	0 %	0 %	100 %

Figure 6.18: confusion matrix related to the RVM model, which is exploited for context classification.

constant, the step frequency and the specific force variance, are weighted by the pedestrian context probabilities. The proposed SLE algorithm is compared with other two SLE approaches: the highest context-based method, which considers the step lengths computed for the step mode corresponding to the highest probability context, and the single event-based method, which does not take the context probabilities into consideration, and determines the length of each step depending on the detected step mode. The SLE algorithms are part of a PDR system which defines the step detection, the step mode classification and the context classification routines. The step detection aims to detect the step time boundaries and is based on continuous wavelet transform (CWT) analysis. The step mode classification algorithm aims to determine the step mode and compares three methods: DT, SVM, KNN. The context classification routine exploits the RVM method to determine the pedestrian context probabilities over the context time window. Moreover, a dataset of pedestrian activities and actions were collected. Fifteen subjects, which have been equipped with a waist-belt smartphone, traveled along a predefined path, shown in Fig.6.3. Six step modes and pedestrian contexts have been considered: stationary, walking, walking side-

ways, climbing and descending stairs, and running.
The SVM method has exhibited a predictive accuracy of 90.5 % which results the best accuracy performance among the compared step mode classification methods. The RVM method used for context classification has achieved a predictive accuracy of 92.5 %. For both the SVM and the RVM algorithms, walking and climbing stairs are the most confused movements and produce the main contribution to the overall misclassification rate. The total distance traveled by the subjects has been determined for each SLE methods. The %RMSE has been computed by comparing the actual path distance with the total distances determined by the SLE algorithms. The weighted context-based SLE algorithm has exhibited a %RMSE of 5.7% across all subjects providing the best performance among the assessed SLE methods.

Table 6.4: %RMSE on distance traveled by each subgroup of testing subjects and across all subjects.

	Subgroup of subject 1-5		
SLE method	Single event-based	Highest context-based	Weighted context-based
%RMSE	7.1%	4.5%	6.6%

	Subgroup of subject 6-10		
SLE method	Single event -based	Highest context-based	Weighted context-based
%RMSE	5.4%	6.1%	6.3%

	Subgroup of subject 11-15		
SLE method	Single event -based	Highest context-based	Weighted context-based
%RMSE	6.9%	11.5%	3.6%

	All 15 subjects		
SLE method	Single event-based	Highest context-based	Weighted context-based
%RMSE	6.5%	7.9%	5.7%

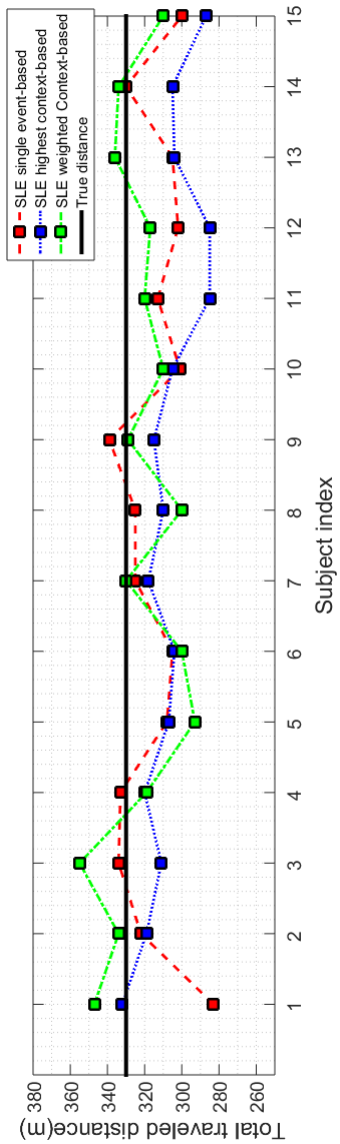


Figure 6.19: total final distances traveled by the subjects and computed for each considered SLE algorithm.

Chapter 7

Conclusion

This thesis has involved both position fixing and dead reckoning methods: in particular, advanced solutions have been proposed for each of these two methods.
Addressing to position fixing, a peer-to-peer cooperative GPS positioning technique has been demonstrated. The benefits and disadvantages of the cooperation between peers has been evaluated. In particular, the effect of time synchronization between the aiding and the aided GPS receivers, for both the procedures of acquisition and positioning, has been characterized. Two GPS software-defined receivers implemented in MATLAB and cooperating in outdoor-to-indoor (O2I) and outdoor-to-outdoor (O2O) scenarios, have been defined. The performance of the satellite signal acquisition procedure has been assessed by considering the number of acquired satellites and the computational load. Moreover, the performance of the positioning routine has been evaluated by examining the position accuracy and the Time-to-First Fix (TTFF).
In the O2I aiding scenario, the aided receiver needs to increase its sensitivity in order to acquire a sufficient number of visible satellites. This process determines an increment of the computational load in the acquisition procedure. The positioning results of the aided receiver have exhibited a better accuracy in the case of fine-time synchronization.
In the O2O aiding scenario, the aided receiver does not need to strongly increase its sensitivity, as in the case of the O2I scenario. Therefore, it can directly exploit the aiding information to reduce the TTFF. The positioning result is more accurate in the presence of fine-time synchronization than in

the case of coarse-time synchronization (as in the O2I scenario) , and the computational load of the positioning procedures is comparable to the ones in the O2I scenario.
Addressing to dead reckoning, a weighted context-based SLE algorithm has been demonstrated: the single step lengths determined as a linear combination of a constant, the step frequency and the specific force variance, are weighted by the pedestrian context probabilities. The proposed SLE algorithm is compared with other two SLE approaches: the highest context-based method, which considers the step lengths computed for the step mode corresponding to the highest probability context, and the single event-based method, which does not take the context probabilities into consideration, and determines the length of each step depending on the detected step mode.
The SLE algorithms are part of a PDR system which includes the step detection, the step mode classification and the context classification routines. The step detection aims to detect the step time boundaries and is based on continuous wavelet transform (CWT) analysis. The step mode classification algorithm aims to determine the step mode and compares three methods: DT, SVM, KNN. The context classification routine exploits the RVM method to determine the pedestrian context probabilities over the context time window. Moreover, a dataset of pedestrian activities and actions were collected. Fifteen subjects, which have been equipped with a waist-belt smartphone, traveled along a predefined path. Six step modes and pedestrian contexts have been considered: stationary, walking, walking sideways, climbing and descending stairs, and running.
The SVM method has exhibited a predictive accuracy of 90.5 % which results the best accuracy performance among the compared step mode classification methods. The RVM method used for context classification has achieved a predictive accuracy of 92.5 %. For both the SVM and the RVM algorithms, walking and climbing stairs are the most confused movements and produce the main contribution to the overall misclassification rate. The total distance traveled by the subjects has been determined for each SLE methods. The %RMSE has been computed by comparing the actual path distance with the total distances determined by the SLE algorithms. The weighted context-based SLE algorithm has exhibited a %RMSE of 5.7% across all subjects providing the best performance among the assessed SLE methods.
A continuous development of the navigation technologies and applications is envisaged in the next years. In future, both cooperative GNSS positioning

and context-aware PDR will be parts of a wider and integrated navigation system able to combine the concepts of context information, user cooperation, and multisensor navigation. The latter permits the definition of robust solutions by integrating different technologies and methods. On the other hand, the context determination becomes a crucial procedure to adapt different technologies to particular operational contexts. Finally, cooperation enables user to obtain information they cannot observe directly. The always growing interconnection between users can be exploited in future solutions of cooperative GNSS positioning to improve the navigation solution in harsh environment. Concerning the PDR systems, the robustness and integrity of the step length algorithm can be enhanced to achieve a more reliable performance over longer time and multiple contexts.

Appendix A

Publications

This research activity has led to several publications in international journals and conferences. These are summarized below.[1]

International Journals

1. E. D. Re, S. Morosi, L. S. Ronga, S. Jayousi, **Thesis Author**, "Flexible Heterogeneous Satellite-based Architecture for Enhanced Quality of Life Applications", *IEEE Communications Magazine*, vol. 53, pp. 186-193, 2015.
2. S. Morosi, **Thesis Author**, E. D. Re, "Peer-to-Peer Cooperation for GPS Positioning", *International Journal of Satellite Communications and Networking*, Wiley Online Library, 2016.
3. **Thesis Author**, S. Morosi, E. D. Re, "Daily Living Movement Recognition for Pedestrian Dead Reckoning Applications", *Mobile Information Systems, Hindawi*, vol. 2016, 2016.

International Conferences and Workshops

1. S. Morosi, E. D. Re, **Thesis Author**, "P2P Cooperative GPS Positioning with Fine/Coarse Time Assistance", in *Proc. of International Conference on Localization and GNSS (ICL-GNSS)*, 2013.
2. S. Morosi, E. D. Re, **Thesis Author**, "Cooperative GPS Positioning with Peer-to-Peer Time Assistance", in *Proc. of Wireless Communications, Vehicular Technology, Information Theory and Aerospace Electronic Systems (VITAE)*, Aalborg (Denmark), 2014.

[1] The author's bibliometric indices are the following: H-index = 3, total number of citations = 13 (source: Google Scholar on Month November, 2016).

3. **Thesis Author**, S. Morosi, E. D. Re "Daily Movement Recognition for Dead Reckoning Applications", in *Proc. International Conference on Indoor Positioning and Indoor Navigation (IPIN)*, Calgary (Canada), 2015.

National Conferences

1. S. Morosi, E. D. Re, and, **Thesis Author**, "Cooperative GPS Positioning with Peer-to-Peer Time Assistance", in *Annual meting GTTI*, Palermo (PL), Italy, 2014.

Bibliography

[1] "Location Based Services (LBS) and Real–Time Location Systems (RTLS) Market – Global Forecast to 2020," *marketsandmarkets.com*, vol. TC 2371, 2015.

[2] D. Alvarez, R. C. Gonzalez, and A. L. andd J. C. Alvarez, "Comparison of step length estimators from weareable accelerometer devices," *Proc. 28th Annual International Conference of the IEEE Engineering in Medicine and Biology Society (EMBS), New York, NY, USA, August-September*, pp. 5964–5967, 2006.

[3] A. Arafa, X. Jin, and R. Klukas, "A Differential Photosensor for Indoor Optical Wireless Positioning," *Proc. ION GNSS 2011*, pp. 1758–1763, 2011.

[4] C. Audoin and B. Guinot, "The Measurements of Time: Time, Frequency and the Atomic Clock," *Cambridge University Press*, 2001.

[5] Ayrulu-Erdem and B. Barshan, "Leg motion classification with artificial neural networks using wavelet-based features of gyroscope signals," *Sensors*, vol. 11, pp. 1721–1743, 2011.

[6] T. Bailey and H. D. Durrant-Whyte, "Simultaneous Localization and Mapping (SLAM): Part II," *IEEE Robotics and Automation Magazine*, 2006.

[7] R. Barnes, J. Winterbotton, and M. Dawson, "Internet Geolocation and Location-Based Services," *IEEE Communications Magazine*, vol. 49, no. 4, pp. 102–108, 2011.

[8] A. Bensky, "Wireless Positioning Technologies and Applications," *Artech House*, 2008.

[9] C. M. Bishop, "Pattern recognition and machine learning," *Company New York*, 2006.

[10] K. Borre, D. M. Akos, N. Bertelsen, P. Rinder, and S. H. Jensen, "A software-Defined GPS and Galileo Receiver: A single-Frequency Approach," *New York: Birkhäuser*, 2007.

[11] B. Butler and R. Verrall, "Precision Hybrid Inertial/Acoustic Navigation System for a Long-Range Autonomous Underwater Vehicle," *Navigation: JION*, vol. 48, no. 1, pp. 1–12, 2001.

[12] M. Caceres, F. Penna, H. Wymeersch, and R. Garello, "Hybrid Cooperative Positioning Based on Distributed Belief Propagation," *IEEE Journal on Selected Areas in Communications*, vol. 29, no. 10, 2011.

[13] M. Cowie, N. Wilkinson, and R. Powlesland, " Latest development of the TERPROM Digital Terrain System (DTS)," *Proc. Position, Location and Navigation Symposium, 2008 IEEE/ION*, 2008.

[14] P. Defraigne, P. Banerjee, and W. Lewandowski, "Time transfer through GPS," *Indian Journal of Radio and Space Physics*, 2007.

[15] F. V. Diggelen, "A-GPS: Assisted GPS, GNSS, and SBAS," *1st ed., Artech House*, 2009.

[16] F. Diggelen, "Method and Apparatus for Time Free Processing of GPS Signals," *United States Patent, Patent No: US 6,417,801*, July 9, 2002.

[17] F. Dovis, C. Chiasserini, and C. B. L. Musumeci, "Context-aware peer-to-peer and cooperative positioning," *International Conference on Localization and GNSS (ICL-GNSS), Turin*, 2014.

[18] H. Gao and P. D. Groves, "Context Determination for Adaptive Navigation using Multiple Sensors on a Smartphone," *Proc. ION GNSS+ 2016, Portland, Oregon, Sept. 12-16*, 2016.

[19] R. Garello, L. Presti, G. Corazza, and J. Samson, "Peer-to-Peer Cooperative Positioning – Part I: GNSS Aided Acquisition," *Inside GNSS*, 2012.

[20] A. Goldsmith, "Wireless Communication," *Cambridge University Press*, 2005.

[21] U. Government, "http://www.gps.gov/systems/gps/modernization/," *GPS Modernization*, 2016.

[22] P. Groves, "Principles of GNSS, Inertial, and Multisensor Integrated Navigation Systems," *2nd Edition, Artech House*, 2013.

[23] P. Groves, H. F. S. Martin, K. Voutsis, D. J. Walter, and L. Wang, "Context Detection, Categorization and Connectivity for Advanced Adaptive Integrated Navigation," *Proc ION GNSS 2013*, pp. 2704–2714, 2013.

[24] P. Gupta and T. Dallas, "Feature selection and activity recognition system using a single triaxial accelerometer," *IEEE Transactions on Biomedical Engineering*, vol. 61, no. 6, pp. 1780–1786, 2014.

[25] A. Harter, A. Hopper, P. Steggles, A. Ward, and P. Webster, "The anatomy of a context-aware application," *Proc. 5th annual ACM/IEEE international conference on Mobile computing and networking*, pp. 59–68, 1999.

[26] W. He and et al., "Recognition of human activities with wearable sensors," *Journal on Advances in Signal Processing*, vol. 12, pp. 704–714, 2012.

[27] N. Ho, P. H. Truong, and G. M. Jeong, "Step-Detection and Adaptive Step-Length Estimation for Pedestrian Dead-Reckoning at Various Walking Speeds Using a Smartphone," *Sensors*, vol. 16, 2016.

[28] J. K. Holmes, "Spread Spectrum Systems for GNSS and Wireless Communications," *Artech House*, 2007.

[29] J. Jahn, U. Batzer, J. Seitz, L. Patino-Studencka, and J. G. Boronat, "Comparison and Evaluation of Acceleration Based Step Length Estimators for Handheld Devices," *Proc. IPIN 2010, Zürich, Switzerland,15-17 September*, 2010.

[30] B. Jalving and K. Gade, "Positioning accuracy for the HUGIN detailed seabed mapping UUV," *Proc. OCEANS '98*, pp. 108–112, 1998.

[31] S. Jin, "Global navigation satellite systems, signal, theory and application," *Intech*, 2012.

[32] T. Judd, "A Personal Dead Reckoning Module," *Proc. ION GPS 1997, Kansas, MO, September*, pp. 47–51, 1997.

[33] A. Kalamandeen, A. Scannell, E. de Lara, A. Sheth, and A. LaMarca, "Ensemble: Cooperative Proximity-based Authentication," *MobiSys, San Francisco, California, USA*, 2010.

[34] E. D. Kaplan and C. J. Hegarty, "Understanding GPS," *2nd ed., Artech House*, 2005.

[35] J. Käppi, J. Syrjärinne, and J. Saarinen, "MEMS-IMU Based Pedestrian Navigator for Hand.held Devices," *Proc. ION GPS 2001, Salt Lake City, UT, September*, pp. 1369–1373, 2001.

[36] M. B. Kjærgaard, "Location-Based Services on Mobile Phones: Minimizing Power Consumption," *IEEE Pervasive Computing*, vol. 11, no. 1, pp. 67–73, 2012.

[37] M. Kose, O. D. Incel, and C. Ersoy, "Online Human Activity Recognition on Smart Phones," *Proc. 2nd International Workshop on Mobile Sensing, Beijing, China, April 16*, 2012.

[38] A. Küpper, "Location-Based Services: Fundamentals and Operation," *marketsandmarkets.com*, vol. TC 2371, 2005.

[39] Q. Ladetto, "On Foot Navigation: Continuous Step Calibration Using both Complementary Recursive Prediction and Adaptive Kalman Filtering," *Proc. ION GPS 2000, Salt Lake City, UT, September*, pp. 1735–1740, 1997.

[40] J. H. Lee, B. Shin, S. Lee, J. H. Kim, C. Kim, T. Lee, and J. Park, "Motion based Adaptive Step Length Estimation using Smartphone," *Proc. ISCE 2014*, 2014.

[41] L. H. Lee, B. Shin, C. Kim, laehun Kim, S. Lees, and T. Lee, "Real Time Adaptive Step Length Estimation for Smartphone User," *Proc. International Conference on Control, Automation and Systems (ICCAS)*, 2013.

[42] Y. Liu, S. Tian, G. Li, W. Dai, and J. Chang, "On the localizability of cooperative positioning: Two user model," *International Conference on Wireless Communications and Signal Processing (WCSP)*, 2014.

[43] D. Loh, S. Zihajehzadeh, R. Hoskinson, H. Abdollahi, and E. J. Park, "Pedestrian Dead Reckoning With Smartglasses and Smartwatch," *IEEE Sensors Journal*, vol. 16, no. 22, pp. 1421–1429, 2016.

[44] S. Mallat, "A Wavelet Tour of Signal Processing: The Sparse Way," *3rd Edition, Elsevier, Amsterdam, Netherlands,*, 2009.

[45] A. Mannini and A. M. Sabatini, "Machine learning methods for classifying human physical activity from on-body accelerometers," *Sensors*, vol. 10, no. 2, pp. 1154–1175, 2010.

[46] A. Martinelli, S. Morosi, and E. D. Re, "Daily Living Movement Recognition for Pedestrian Dead Reckoning Applications," *Mobile Information Systems*, vol. 2016, 2016.

[47] C. J. Mather, P. D. Groves, and M. R. Carter, "A Man Motion Navigation System Using High Sensitivity GPS, MEMS IMU and Auxiliary Sensors," *Proc. ION GNSS 2006, Fort Worth, TX, September*, pp. 2704–2714, 2006.

[48] P. Misra and P. Enge, "Global positioning system: Signals, measurements, and performance," *Revised 2nd ed., Ganga-Jamuna Press*, 2012.

[49] S. Morosi, S. Jayousi, E. Falletti, and G. Araniti, "Cooperative strategies in satellite assisted emergency services," *International Journal of Satellite Communications and Networking*, vol. 31, no. 3, pp. 141–156, 2013.

[50] S. Morosi, E. D. Re, and A. Martinelli, "P2P Cooperative GPS Positioning with Fine/Coarse Time Assistance," *International Conference on Localization and GNSS (ICL-GNSS), Turin*, 2013.

[51] S. Morosi, E. D. Re, and A. Martinelli, "Cooperative GPS Positioning with Peer-to-Peer Time Assistance," *Proc. 4th International Conference on Wireless Communications, Vehicular Technology, Information Theory and Aerospace and Electronic Systems (WVITAE), Aalborg, Denmark*, 2014.

[52] Navipedia, "http://www.navipedia.net/index.php/GLONASS," *European Space Agency*, 2016.

[53] T. Neaogoe, V. Cristea, and L. Banica, "Time transfer through GPS," *IEEE ISIE*, 2006.

[54] A. Norrdine, Z. Kasmi, and J. Blankenbach, "Step Detection for ZUPT-Aided Inertial Pedestrian Navigation System Using Foot-Mounted Permanent Magnet," *IEEE Sensors*, vol. 16, no. 17, pp. 6766–6773, 2016.

[55] L. Pepa, G. Marangoni, L. C. Matteo Di Nicola, F. Verdini, L. Spalazzi, and S. Longhi, "Real Time Step Length Estimation on Smartphone," *Proc. ICCE 2016*, 2016.

[56] M. Petovello and K. Muthuraman, "GNSS Solutions: Coarse Time Positioning," *Inside GNSS*, 2012.

[57] A. R. Pratama and H. R. Widyawan, "Smartphone-based pedestrian dead reckoning as an indoor positioning system," *Proc. International Conference on System Engineering and Technology (ICSET), Bandung, Indonesia, September*, 2012.

[58] L. L. Presti, D. Margaria, and J. Samson, " A novel Peer to Peer Acquisition Strategy Tailored to Galileo E1 Receiver," *53nd International Symposium ELMAR, Zadar, Croatia*, 2010.

[59] N. B. Priyantha, "The Cricket Indoor Location System," *PhD Thesis, Massachusetts Institute of Technology*, 2005.

[60] J. Qian, J. Maand, L. Xu, R. Ying, W. Yu, and P. Liu, "Investigating the use of MEMS based Wristworn IMU for Pedestrian Navigation Application," *Proc. ION GNSS+ 2013, Nashville, Tennessee, September 16-20*, pp. 1057–1064, 2013.

[61] J. Qian, L. Pei, R. Ying, X. Chen, D. Zou, P. Liu, and W. Yu, "Continuous Motion Recognition for Natural Pedestrian Dead Reckoning Using Smartphone Sensors," *Proc. ION GNSS+ 2014, Tampa, Florida, September 8-12*, pp. 1796–1801, 2014.

[62] E. D. Re, S. Morosi, , S. Jayousi, and C. Sacchi, "SALICE Satellite-Assisted LocalIzation and Communication systems for Emergency services," *1st International Conference on Wireless Communications, Vehicular Technology, Information Theory and Aerospace and Electronic Systems, (WVITAE)Aalborg, Denmark*, 2009.

[63] D. Robertson and R. Cipolla, " An Image-Based System for Urban Navigation," *Proc. BMVC 2004*, 2004.

[64] M. B. D. Rosario, S. J. Redmond, and N. H. Lovell, "Tracking the evolution of smartphone sensing for monitoring human movement," *Sensors*, vol. 15, pp. 18 901–18 933, 2015.

[65] S. H. Shin and C. G. Park, "Adaptive step length estimation algorithm using optimal parameters and movement status awareness," *Medical Engineering and Physics*, pp. 1064–1071, 2011.

[66] S. H. Shin, C. G. Park, J. W. Kim, H. S. Hong, and J. M. Lee, "Adaptive Step Length Estimation Algorithm Using Low-Cost MEMS Inertial Sensors," *Proc. IEEE Sensors Applications Symposium San Diego, California USA, 6-8 February*, pp. 1064–1071, 2007.

[67] J. V. Sickle, "GPS for Land Surveyors," *CRC Press Taylor and Francis Group*, 2016.

[68] M. Susi, D. Borio, , and G. Lachapelle, "Accelerometer signal features and classification algorithms for positioning applications," *Proc. International Technical Meeting of the Institute of Navigation (ION ITM),San Diego, USA*, pp. 158–169, 2011.

[69] M. Susi, V. Renaudin, and G. Lachapelle, "Motion Mode Recognition and Step Detection Algorithms for Mobile Phone Users," *IEEE Sensors Journal*, vol. 13, pp. 1539–1562, 2015.

[70] C. S. Toro and V. J. T. Roig, "Exploring Relevance Vector Machines for Faster Pedestrian Classification," *Proc. 6th Iberian Conference on Pattern Recognition and Image Analysis Madeira, Portugal, June 5-7*, vol. 7887, 2013.

[71] J. Torres-Solis, T. H. Falk, and T. Chau, "A review of indoor localization technologies towards navigational assistance for topographical disorientation," *Ambient Intelligence, intechopen.com*, 2010.

[72] R. Want, A. Hopper, V. Falcao, and J. Gibbons, "The Active Badge Location System," *ACM Transactions on Information Systems (TOIS)*, vol. 10, no. 1, pp. 91–102, 2011.

[73] Wikipedia, "https://en.wikipedia.org/wiki/GPS," *GPS signals*, 2016.

[74] N. Yazdi, F. Ayazi, and K. Najafi, "Micromachined inertial sensors," *Proc. IEEE*, vol. 86, no. 8, pp. 1640–1659, 1998.

[75] H. Zhang, W. Yuan, Q. Shen, T. Li, and H. Chang, "A handheld inertial pedestrian navigation system with accurate step modes and device poses recognition," *IEEE Sensors*, vol. 15, no. 3, pp. 1421–1429, 2015.

[76] S. Zhang, P. McCullagh, C. Nugent, , and H. Zheng, "Activity monitoring using a smart phone's accelerometer with hierarchical classification," *Proc. IEEE 6th International Conference on the Intelligent Environments (IE), Kuala Lumpur, Malaysia, July*, 2010.

[77] Y. Zhao, "Vehicle Location and Navigation Systems," *Artech House*, 1997.

[78] X. Zhoubing, F. Sottile, M. Spirito, and R. Garello, "Analysis of hybrid and cooperative positioning algorithms in urban canyon scenarios," *International Conference on Localization and GNSS (ICL-GNSS), Turin*, 2013.